# Numerical modelling of the dynamics of deep convective systems over Indian region using the Weather Research Forecast (WRF) model

Thesis submitted to the Cochin University of Science and Technology (CUSAT) in partial fulfilment of the requirements for the Degree of

DOCTOR OF PHILOSOPHY

in

ATMOSPHERIC SCIENCE

under the

**Faculty of Marine Sciences**

*by*

**SMITHA JOHN**

**(Reg. No.3321)**


Dept. of Atmospheric Sciences
Cochin University of Science and Technology (CUSAT)
Cochin - 682016, India

September 2019

# CERTIFICATE

This is to certify that the thesis entitled "**Numerical modelling of the dynamics of deep convective systems over Indian region using the Weather Research Forecast (WRF) Model**" is an authentic record of the research work done by Smitha John (Reg. No.3321) under my guidance and supervision at the Department of Atmospheric Sciences, Cochin University of Science and Technology, Cochin-16 and has not been included in any other thesis submitted previously for the award of any degree or diploma in any University or Institution.

Cochin-16
08.08.19

Dr. H S Ram Mohan
(Supervising Guide)
Professor (Retd)
Dept of Atmospheric Sciences
CUSAT

# DECLARATION

I hereby declare that the thesis entitled **"Numerical modelling of the dynamics of deep convective systems over Indian region using the Weather Research Forecast (WRF) Model"** is a genuine record of the research work carried out by me for the partial fulfilment of the degree of Doctor of Philosophy in Atmospheric Science at the Dept. of Atmospheric Sciences, Cochin University of Science & Technology (CUSAT) under the guidance of Dr H S Ram Mohan, Professor (Retd), Dept. of Atmospheric Sciences, CUSAT . The research work presented in this thesis has not been submitted earlier for the award of any degree/diploma of any University.

Smitha John

Cochin-16
08.08 2019

# *Acknowledgements*

*I wish to express my profound sense of gratitude, appreciation and sense of indebtness to Dr H S Ram Mohan for his valuable guidance, constant support and care throughout the period of my research work.*

*I am expressing my gratitude towards Dr K Mohan Kumar, Professor, Dept. of Atmospheric Sciences, CUSAT for his valuable suggestions and constant encouragement.*

*Also I am deeply indebted to Mr B Chakrapani, Assoc. Professor, Dept. of Atmospheric Sciences, CUSAT for introducing me into the world of Numerical Weather Prediction and Operational Weather Forecasting. Also I am grateful to him for his valuable suggestions, constant support and encouragement.*

*I am thankful to Dr K Satheesh, Head, Dept. of Atmospheric Sciences, CUSAT for the support and the facilities provided.*

*I also wish to express my sincere gratitude towards Dr.Rosamma Philip, Dean, Faculty of Marine Sciences, CUSAT for her support and encouragement.*

*I also wish to express my sincere thanks to Dr C A Babu, Professor, Dept. of Atmospheric Sciences, CUSAT for teaching me the dynamics of the atmosphere during my MTech which immensely helped me to understand and interpret the findings of my research work*

*I am also indebted to Mrs. S S Vaidya, J Sanjay and P. Mukhopadyay, Forecasting Research Division (FRD), IITM, Pune for introducing me into the world of mesoscale modelling using Advanced Research Prediction System (ARPS) and High Performance Computing Clusters.*

*I am deeply indebted to Dr C K Rajan, Retd. Professor, Dept. of Atmospheric Sciences for the guidance provided in the initial phase of my research career as JRF and SRF. Also I wish to thank him for his valuable suggestions, constant support and encouragement.*

*I am also indebted to Indian Space Research Organisation and Dept of Science & Technology for providing me the funding as well as infrastructure for carrying out High Performance Computations through various collaborative projects.*

*I also wish to express my sincere thanks to Dr. K R Santhosh, Retd. Professor, Dept. of Atmospheric Sciences and Dr Madhu V, Asst. Professor, Dept. of Atmospheric Sciences, Dr Abhilash, Asst. Professor, Dept. of Atmospheric Sciences for their constant support. I wish to express my gratitude to all other faculty at Dept. of Atmospheric Sciences, CUSAT for their support. I also wish to express my thanks to all the faculties of the various departments at School of Marine Sciences for their support and encouragement.*

*National Centre for Atmospheric Research (NCAR) is thankfully acknowledged for providing the Weather Research Forecasting (WRF) Model freely available to the research community. Indian Meteorological Department is thankfully acknowledged for the use of surface charts from IDWR and also for the satellite imagery and Doppler Radar Data. National*

*Centre for Environmental Prediction (NCEP) is also thankfully acknowledged for the FNL Operational Model Global Tropospheric Analysis dataset. I am also indebted to University of Wyoming, USA for providing upper air sounding data. NASA is thankfully acknowledged for providing TRMM precipitation data. EUMETSAT is thankfully acknowledged for providing the METEOSAT satellite imagery.*

*I wish to express my gratitude towards Dr. Sreedevi M G for her constant support. Also I wish to extend my sincere thanks to all the non-teaching staff of the Department. I also wish to express my thanks to my friends and all the research scholars of the Department for providing a friendly atmosphere in the institution.*

*I wish to thank the Principal and all the faculties of Toc H Institute of Science & Technology for providing a peaceful atmosphere which helped me immensely in the final phase of research. I wish to express my sincere thanks to Kerala Technological University (KTU) for providing PARAM supercomputing facility for carrying out the simulations in the final phase of research work.*

*I wish to express my heartfelt thanks to my parents Mr. John Thomas and Mrs. Susamma T V for their immense support, constant encouragement, care and prayers. Also I wish to express my heartfelt gratitude to the parents-in-law Mr .M. M. Pappachan and Ponnamma Pappachan for their immense support, care and prayers. I also wish to express my sincere thanks to my younger sister Ms. Saumya John for her encouragement, care and prayers.*

*I wish to express my sincere thanks to my loving husband Mr.Eby Pappachan for his immense support and care throughout the period of my research. I also wish to express special thanks to my lovely daughters Shreya Eby and Samaara Eby for their immense support, love and care throughout my research period.*

*Above all, I express my special and sincere thanks to God Almighty who made everything possible.*

***Smitha John***

# CONTENTS

# List of Tables

# List of Figures

# Chapter 1
# Introduction

Deep convective systems over tropics redistribute heat, moisture and momentum through the atmosphere and play a vital role in the global energy balance of the biosphere (Riehl and Malkus, 1958). The interaction between these deep convective systems and large-scale circulations determine the clouds, moisture, temperature and structure of the troposphere in tropical regions. The deep convection over tropical oceans occurs in cloud clusters consisting of many individual cumulonimbus towers (Martin and Karst, 1969; Martin and Suomi, 1972) and they are characterized by the enhanced vertical transport of energy and momentum, very strong self-organized flow fields, very complex microphysical transformations and stratospheric penetrations and rapid evolution and dissipation processes. Deep convective clouds are frequently observed to produce heavy rainfall and severe weather events such as gust fronts, flash floods, severe thunderstorms, tornadoes, squall lines, Mesoscale Convective Systems (MCSs) etc. These severe weather events are major threats to agriculture, aviation, space vehicle launch operations, damage to structure and loss of life.

The convective systems include

- Single cell thunderstorms
- Multicell thunderstorms
- Squall lines
- Supercell thunderstorms
- Mesoscale convective Systems(MCSs)
- Mesoscale convective complexes(MCCs)

Thunderstorms are elementary units of all the convective systems mentioned above and occur so frequently that they produce a large amount of rainfall in most tropical areas. Thunderstorms are Cumulonimbus (Cb) clouds of convective origin and high vertical extent that are capable of producing lightning and thunder. It develops mostly due to intense convection accompanied by heavy rain, lightning, thunder, hail storm, surface wind squall, down-burst and tornado. It is a meso-scale phenomena whose spatial extent ranges from a few kilometers to a few hundreds of kilometers and temporal extent ranges from a few hours to several hours. Multicell thunderstorms organise in the form of squall lines, accompanied with deep convection reaching 12-14 km in altitude sometimes penetrating upto the stratosphere. These intense convection spans a horizontal area exceeding 20,000 $km^2$ with their cold cirrus canopy even exceeding 100000 $km^2$ with a temporal extent of 6-12 hours. These gigantic convective system travel across several hundred kilometres in the form of squall lines (Tyagi et.al.,2012). During the pre-monsoon season of April and May, north India gets severe thunderstorms. In this season, Gangetic West Bengal and surrounding areas gets severe thunderstorms called Nor'westers, which is locally called KalBaisaki. The northwest India gets convective dust-storms called locally Andhi in this season. These severe weather events are major threat to agriculture, aviation, space vehicle launch operations, damage to structure and loss of life. The strong wind produced by the thunderstorm downdrafts after coming in contact with the earth's surface spreads out laterally and is known as downbursts. This is a real threat to aviation. Hence an accurate prediction of severe thunderstorms is essential for the society. The inherent nonlinearity in the dynamics and physics of thunderstorms as well as the smaller spatial and temporal scale of occurrence makes the understanding and prediction of thunderstorms as a challenging task to atmospheric scientists

(Orlanski,1975). However, a better understanding of the underlying physics and dynamics is very much required for the better prediction of the phenomena. Numerical modelling is one of the most sophisticated technique for the understanding and prediction of thunderstorms and it has made substantial advances in modelling convective clouds and MCSs (Hobbs,1991).

The conditions which are pre-requisite for the development of the thunderstorms are i) Conditional instability ii) Low level convergence iii) Advection of moisture at the lower level iv) Any source triggering convection by the vertical uplift of the parcel v) Upper level divergence.

Large scale processes are helping in developing a suitable thermodynamic structure which is required for the formation of the convective systems and mesoscale processes are mainly initiating convection leading to thunderstorms. Thus thunderstorms are produced as a result of the interaction between the synoptic scale flow and localized mesoscale forcing (Mukhopadhayay et.al, 2003). The lightning and thunder produced by thunderstorms occur only when large mass of liquid and frozen water have been carried up to such heights that the temperature is well below $-20^0$ C. Large masses of condensed water can be carried to great heights only if the updrafts are strong. Hence thunderstorms develop only when the lapse rate of temperature is steep through the deep layers of air. Thunderstorms, therefore occur in warm, humid and unstable air.

### 1.1 Structure of Thunderstorms

The lifecycle of thunderstorm passes through three phases (Byers and Braham, 1948). They are

i) Cumulus Stage which is the first stage of growth with updraft persisting throughout the cell. The updraft is strongest at the higher altitudes and increases in magnitude towards the ends of this stage. The converging

air feeds the updrafts not only from the surface but also from all levels through which the cell penetrates and this entrainment continues throughout all the stages. The cell contains liquid drops or frozen particles. The isotherms in the developing stage is higher than the environmental temperatures at all levels and the cloud air is buoyant and the cell contains updrafts throughout which the drops or ice particles are suspended. Fig.1.1 shows that the updraft is increasing with elevation. The cloud builds rapidly to heights and a large amount of cloud droplets, rain drops and snowflakes accumulate in the cloud. Eventually the amount of accumulated water becomes so large that the heavier elements cannot be supported by the updrafts. Liquid water then began to fall through the cloud.

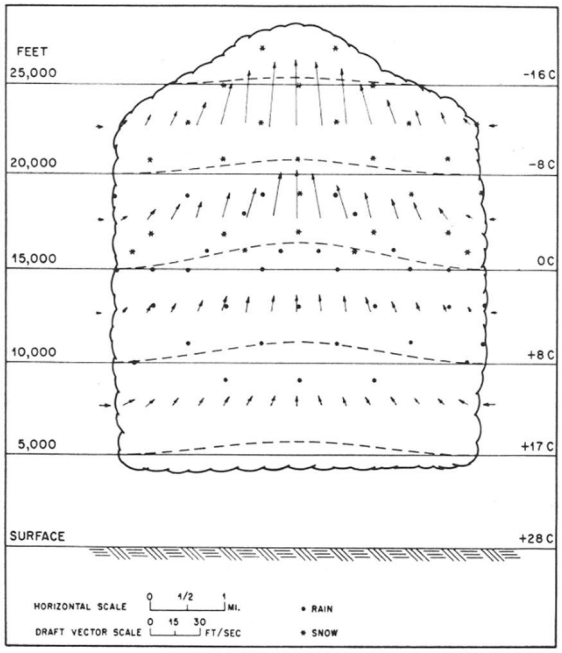


Fig.1.1: Circulation within a typical cell in the cumulus stage.
(Byers and Braham, 1948)

ii) Mature Stage is characterised by the presence of both the updrafts and the downdrafts which are magnified in the presence of wind shear in the troposphere. The mature stage begins when the first rain falls from the base of the clouds. This indicates that the particles that form the precipitation have increased to sufficient size to allow them to fall through the updraft. The frictional drag of these particles helps to change the updraft to a downdraft, the speed of which may be accelerated if the air is thermally unstable. Fig.1.2 shows that the updrafts and downdrafts exist side by side which is an important feature of the mature stage. The temperature in the downdraft are lower than the environmental temperature and in the updraft the temperature is higher than the environmental temperature. The greatest negative temperature anomalies are found in the lower levels and there exists a close association between updrafts and downdrafts. The downdrafts start at the level of initiation above or below the freezing level and later growing in vertical as well as horizontal extent. The updrafts also continue and often reaches the greatest strength in the early mature stage in upper part of the cloud system. The updraft speeds may locally exceed 25 m/s. Fig.1.2 reveals that the downdraft is usually not strong as the updraft and is most pronounced in the lower part of the cloud, although naturally weakening and spreading laterally near the ground. Horizontal divergence, rainy area and downdraft are found stronger at the surface. The mature stage represents the most intense period of thunderstorm in every aspect including electrical activity. If aeroplanes encounter the clouds in this stage, it will experience the most severe turbulence including the short, intense accelerations known as ‘gusts’ in aeronautics. Heavy rain and strong winds can be observed at the ground during this stage. If hail is present, it is most often found in this stage. The cloud may extend to more

than 20 km penetrating the tropopause. The maximum height reached for most of the thunderstorm varies between 12 to 15 km.

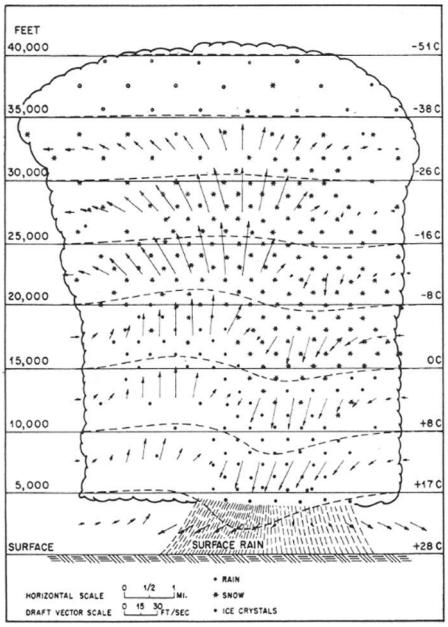


Fig.1.2: Circulation within a typical cell in a mature stage (Byers and Braham, 1948)

iii) Dissipating Stage or Anvil stage is the stage in which the the updraft disappears and the entire lower part of the cell contains gentle downdrafts. The upper part of the cell contains drafts of negligible velocities. Dissipation results from the fact that there is no longer updraft source of condensing water. As the updraft is cut off, the mass of water available to accelerate the descending air diminishes, so the downdraft also weakens. The entire cell is colder than the environment as long as the downdraft and the rain persist.

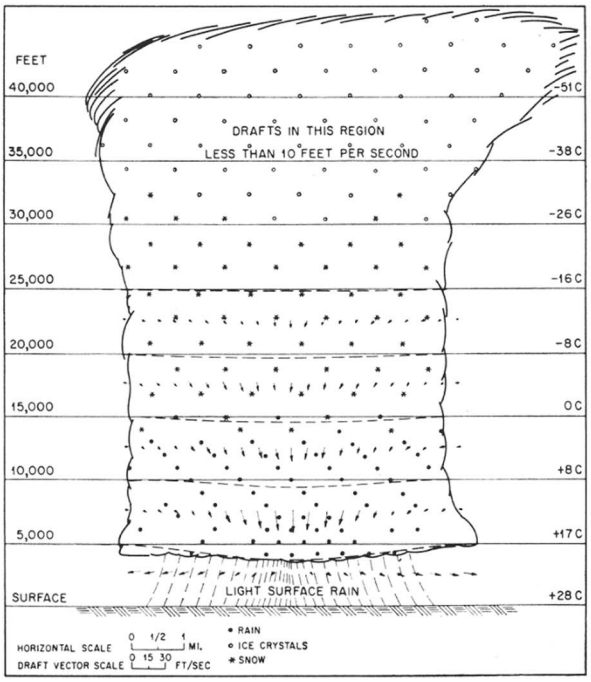


Fig.1.3: Circulation within a thunderstorm cell in dissipating or anvil stage (Byers and Braham, 1948)

The temperature within the cell is restored to a value approximately equal to that of the surroundings. Then complete dissipation occurs or only stratified clouds remain. All the surface signs of thunderstorm ultimately disappear.

## 1.2. Climatology of Thunderstorms

The average monthly and annual frequency of days of thunder for all Indian and neighbouring stations are given in the Climatological Tables of Observatories in India (IMD, 1953). Simultaneously, the World Meteorological Organisation (WMO) published the average frequencies of thunder in the WMO publication World distribution of thunderstorm days (WMO, 1953). These averages are based on data for a uniform period of 15 years. Rao and Raman (1961) studied monthly and annual frequency of

thunderstorm in India in the form of chart with brief description using 20 years of data and found the highest thunderstorm activity occurs over Assam, West Bengal, Jharkhand and Orissa. The statistics of Annual Average thunderstorms frequency over the area is 75 days/year. The diurnal variation of thunderstorm occurrence over India is studied by Raman and Raghavan (1961). The diurnal variation of thunderstorm for some selected observatories such as observatories at plain regions, hill observatories and coastal observatories are studied by Mukherjee and Sen (1983) inorder to understand the influence of different physical features. The thunderstorm occurrences at Agartala are studied by Gupta and Chorghade (1961) based on period of three years (1957-59). Location specific climatological studies are conducted by various researchers. [Viswanathan and Faria (1962), Krishnamurthy (1965), Awadesh Kumar (1992), Moid (1996), Indrani Kar and Bandopadhyay (1998), Santosh et al. (2001)]. The highest annual frequency of thunder in India was given as 60 days over northeast India in WMO publication (WMO, 1953). Subsequent study by Rao and Raman (1961) showed higher frequency of 75 days over northeast India, Bangladesh, West Bengal and adjoining areas with more than 100 days over northeastern parts of Assam.

Alvi and Punjabi (1966) studied the diurnal variation in squalls which usually accompany thunderstorms. They found that the annual frequency of thunderstorms over Northeast India, West Bengal, Bangladesh and adjoining Orissa as 75days/year. They also identified northeast Assam as the most thundery area in India with an average frequency exceeding 100days/year.

Tyagi (2007) studied the thunderstorm climatology over Indian region based on latest representative climatological data including 390 IMD observatories, 50 Indian Air Force (IAF) observatories, six Bangladesh

observatories, two Pakistan observatories and one each in Nepal and Sri Lanka. The study brought out a higher annual frequency of thunderstorms as compared to those given by earlier studies (80-100 days/year). The study also found that the highest annual frequency (more than 100-120 days/year) is observed over Assam and Sub Himalayan West Bengal in the east and Jammu region in the north. The lowest frequency (less than 5 days) is observed over Ladakh region. Gangetic West Bengal and Bangladesh record between 80 and 100 days of thunderstorm annually. The highest annual frequency (100-120 days) is observed over Assam and Sub-Himalayan West Bengal in the east and Jammu region in the north (Figure 1.4). The lowest frequency (less than 5 days) is observed over Ladakh region. Kerala records highest (80-100 days) thunderstorm frequency of thunderstorm over peninsula. With the onset of summer conditions, there is a significant increase in thunderstorm days over the east and northeast India especially in the month of April.

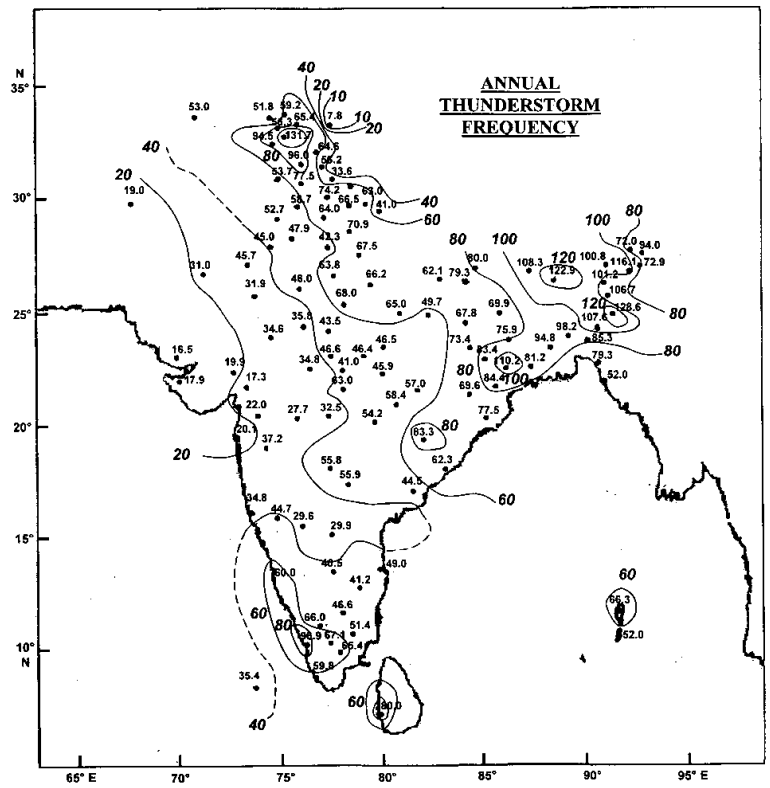


Fig 1.4: Annual Thunderstorm Frequency ( Tyagi, 2007)

Singh et.al. (2011) studied the thunderstorm climatology over northeast and adjoining east India and identified two different regions of occurrence of thunderstorms, including the maximum region of occurrence viz. east-west oriented region along the foothills of Himalayas and northwest to southeast oriented region from Sub Himalayan West Bengal to Tripura. They also found that there is an increasing trend in frequency of thunderstorms over some parts of south coastal Orissa and coastal West Bengal and a decreasing trend over some parts of north coastal Orissa, Mizoram, Tripura and Manipur.

The Weather Research and Forecasting (WRF) model is a numerical weather prediction (NWP) model and atmospheric simulation system designed for operational forecast as well as scientific weather research (Skamarock et al. 2008). The sensitivity of WRF Model to different microphysics parameterization schemes over South east India has been studied by Rajeevan et al.(2010). The sensitivity of WRF Model to different parameterization schemes over different regions of India are carried out by many scientists. [Mohan and Bhati (2011); Soni.et.al. (2014); Madala et al. (2014); Gunwani and Mohan (2017)]. Such studies are very useful but numerical simulation studies to understand the structure and evolution of severe thunderstorms over Indian region is very essential.

## 1.3 Objectives of the study

The main objectives of the present study are:

- **To understand the dynamics of deep convective systems over Indian region using Weather Research and Forecasting (WRF) Model.**
- **To identify the most suitable combination of cumulus and microphysics parameterization schemes for Indian region.**
- **To identify whether there exist any signatures/precursors in the atmosphere before the occurrence of a severe weather event.**
- **To study the structure and evolution of deep convective systems using WRF Model**

Many cumulonimbus clouds grow, develop and manifest as different types of severe weather systems. However, very few attempts have been done to understand the temporal and spatial evolution of clouds in tropics especially over Indian region. In order to understand the convective systems, case studies of different types of thunderstorms formed under different large scale environmental conditions have been studied.

## 1.4 Components of the thesis

The doctoral thesis comprises of seven chapters. Chapter 1 gives an introduction to deep convective systems and reviews the available scientific literature in the area of deep convection. A detailed overview of the deep convective systems as well as the main objectives and the relevance of the study are explained in this Chapter.

Chapter 2 gives the details of the Weather Research Forecast (WRF) Model. It also discusses the details of all the observational data as well as the details of the datasets used as the initial and lateral boundary conditions of the model. The details of various parameterization schemes are also included in this Chapter.

Chapter 3 describes the details of the experiments designed in order to understand the sensitivity of the WRF model to different cumulus and microphysics parameterization schemes. It also discusses the performance evaluation of the model with different combinations of parameterization schemes to enable identification of the best suitable combination of parameterization schemes for the study region. The WRF model was also run with different combinations of microphysics and cumulus parameterization schemes in order to select the most suitable combination of microphysics and cumulus dynamics. The detailed analysis of the model output identifies that

the Kain-Fritsch cumulus parameterization scheme and WSM-3 class microphysics scheme as the best suitable combination of parameterization schemes which can be used for the Indian region.

Chapter 4 provides the observational and modelling study of the genesis, structure and evolution of a supercell thunderstorm over Odisha. The event is simulated using WRF Model with a very high horizontal resolution of 1 km and a temporal resolution of 5 seconds in order to advance our theoretical understanding of the structure and dynamics of a supercell tornadic thunderstorm. The simulated output fields such as reflectivity, vertical velocity, vorticity etc are plotted for every 10 minutes with a horizontal resolution of 1 km: they clearly depict the spatial distribution and temporal evolution of clouds. The output parameters have been studied in order to understand the following aspects of the convective systems:

a) The genesis and growth of convective cells
b) The spatial distribution and vertical structure
c) The characteristics of updrafts and downdrafts
d) The direction of motion and speed of the movement of convective system
e) The life time of the convective system

Chapter 5 includes the simulation of two unusual heavy rainfall episodes over Southern Peninsula in March 2008. The two heavy rainfall episodes during 12-14 March 2008 and 19-22 March 2008 have been simulated using WRF Model: simulated parameters have been validated using IMD data and Satellite based Automatic Weather Station (AWS) data. The rainfall has been validated with Tropical Rainfall Measuring Mission (TRMM) 3B42V6 precipitation data and AWS data. The model could simulate the heavy rainfall episode during 12-14 March 2008 with good spatial and temporal accuracy. This study shows how a strong easterly wave could produce widespread

heavy rainfall with severe thunder activity. This simulation has enabled the study of the precipitation characteristics of thunderstorm cells embedded inside an easterly trough and an overlying westerly trough. The association of the mid-level westerly trough with low-level easterlies resulted in enhanced thunderstorm activity and heavy rainfall. The model also simulated the heavy rainfall episode during 19-22 March 2008 with good spatial and temporal accuracy. This event enabled the study of the widespread rainfall activity triggered by a low-pressure system over the Arabian sea and an associated cycir over Lakshadweep-Comorin area. These two simulations could successfully simulate the mesoscale features as well as precipitation characteristics of heavy rainfall episodes associated with two different synoptic scale systems. The presence of a highly active region vertically extending from 6 – 12 km about an hour before its manifestation as a heavy rainfall event is revealed in the simulation of these two events also but with a lesser magnitude when compared with supercell storm.

Chapter 6 discusses the modelling study of the structure and evolution of Extremely Severe Cyclonic Storm (ESCS) FANI during its advance through the Bay of Bengal during 30 April 2019 – 03 May 2019. The intensity, propagation and structure of the cyclone is studied using the model predicted values of reflectivity, sea level pressure, wind speed and direction, rainfall etc. The model predicted values have been validated with the observational data. The simulation clearly shows the eyewall and spiral band structure as well as the eye of the storm. The landfall characteristics of the cyclonic storm during its landfall in Odisha coast is also carried out by the simulation of vertical velocity, vorticity and reflectivity with a horizontal resolution of 1 km and a temporal resolution of 5 seconds. The study also shows the characteristics of the atmosphere above a tropical cyclone during its

movement over the sea towards the coast. The simulation could identify the highly active region of troposphere extending from 6 -12 km.

Chapter 7 includes the summary and conclusions of the study. The Chapter also includes suggestions for further studies in this area that can contribute to the nowcasting of severe weather events and thereby benefit many different sectors which includes aviation and disaster management.

References cited in the text are listed at the end of the Thesis in alphabetical order.

# Chapter 2

# An overview of the Weather Research Forecast (WRF) model and the datasets used

## 2.1 Introduction

Numerical modelling is one of the most sophisticated technique for the understanding and prediction of convective systems. Recent advances in observational and numerical modelling capabilities have greatly improved the tools used by atmospheric scientists to study mesoscale weather systems. This Chapter provides the details of the WRF model, its formulation, governing equations, physics and other modelling techniques. It also gives the details of the data sets utilized for the study.

The Weather Research and Forecasting (WRF) model is a numerical weather prediction (NWP) model and atmospheric simulation system designed for operational forecast as well as scientific weather research. The development of WRF is led by the Mesoscale and Microscale Meteorology (MMM) Division of National Center for Atmospheric Research(NCAR), National Center for Environmental Prediction (NCEP) of National Oceanic and Atmospheric Administration(NOAA) and Earth System Research Laboratory (ESRL)with partnerships at the Department of Defense's Air Force Weather Agency (AFWA) and Naval Research Laboratory (NRL), the Center for Analysis and Prediction of Storms (CAPS) at the University of Oklahoma, and the Federal Aviation Administration (FAA) in collaboration with universities and other government agencies in the US and overseas. WRF is found suitable for a wide range of applications: real-time NWP, data assimilation research, parameterized physics research, regional climate simulations, air quality modelling, atmosphere-ocean coupling, and idealized simulations.

## 2.2 The WRF Modelling System program components

The principal components of the WRF system are shown in Fig. 2.1. The WRF Software Framework (WSF) provides the infrastructure that accommodates the dynamics solvers, physics packages which interface with the solvers, programs for initialization, WRF-Var, and WRF-Chem. There are two dynamics solvers in the WSF: the Advanced Research WRF (ARW) solver (originally referred to as the Eulerian mass or "em" solver) developed primarily at NCAR, and the NMM (Nonhydrostatic Mesoscale Model) solver developed at NCEP.

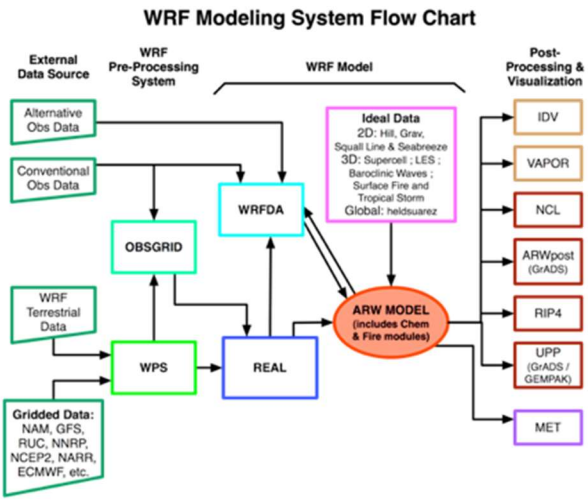


Fig.2.1 WRF Modelling System Flowchart

### 2.2.1.The WRF Pre-processing System (WPS)

WPS consists of three independent programs *geogrid, ungrib, and metgrid* whose collective role is to take terrestrial and meteorological data and converts the data for inputting into the ARW pre-processor program for real-data simulations. The program *geogrid* defines a model domain

including the projection type, location on the globe, number of grid points, nest locations, and grid distances and interpolates various static geographical data to the model grids. The program *ungrib* extracts meteorological fields from GRIB-formatted files; and the program *metgrid* horizontally interpolates the meteorological fields extracted by ungrib to the model grids defined by geogrid. The work of vertically interpolating meteorological fields to WRF eta levels is performed within the real program. The data flow diagram of WPS is shown in Fig.2.2.

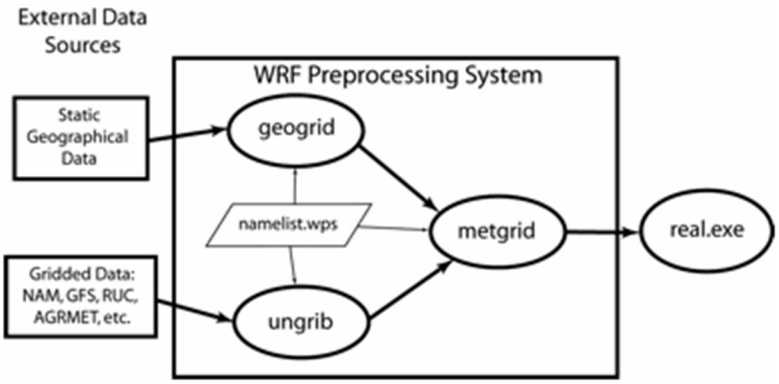


Fig.2.2 : Data flow diagram of WPS

The output data from WPS provides a complete 3-dimensional representation of the atmosphere on the selected model grid's horizontal staggering at the selected time slices, which is sent to the ARW pre-processor program for real-data cases. The input to the ARW real-data processor from WPS contains 3-dimensional fields of temperature, relative humidity and the horizontal components of momentum. The two-dimensional static terrestrial fields include albedo, Coriolis parameters, terrain elevation, vegetation/land-use type, land/water mask, map scale factors, map rotation angle, soil texture category, vegetation greenness fraction, annual mean temperature, and latitude/longitude. The 2-dimensional time-dependent fields from the external model, after processing by WPS, include surface pressure and sea-

level pressure, layers of soil temperature and soil moisture, snow depth, skin temperature, sea surface temperature etc.

### 2.2.2 WRF Variational Data Assimilation (WRF-Var)

WRF-Var can be used to ingest observations into the interpolated analyses created by WPS. It is optional and can also be used to update WRF model's initial condition when WRF model is run in cycling mode.

### 2.2.3 ARW Solver

### Governing Equations

The ARW solver integrates thefully compressible, nonhydrostatic Euler equations which are formulated in flux form using a terrain-following pressure coordinate in the vertical.The equations are cast in flux form using variables that have conservation properties, following the philosophy of (Ooyama, 1990). The ARW model equations and the time integration scheme are described in detail by (Skamarock et al., 2008; Skamarock and Klemp, 2008).The ARW equations are formulated using a terrain-following hydrostatic-pressure vertical coordinate(Laprise, 1992) denoted by η and defined as

$$\eta = \frac{(p_h - p_{ht})}{\mu} \quad \text{where} \quad \mu = (p_{hs} - p_{ht}). \tag{2.1}$$

where μ is the dry air mass per unit area within a model column, which is defined as $\mu = p_{hs} - p_{ht}$. The pressure variables $p_h$, $p_{ht}$, and $p_{hs}$ are the hydrostatic pressure of the dry atmosphere, the hydrostatic pressure of the dry atmosphere at the top of the model domain, and the hydrostatic pressure of the dry atmosphere at the surface, respectively. In this coordinate system the horizontal momentum equations and the thermodynamic equation are written as

$$\frac{\partial \mathrm{U}}{\partial \mathrm{t}} = -\frac{\partial U_u}{\partial \mathrm{x}} - \frac{\partial V_u}{\partial \mathrm{y}} - \frac{\partial \Omega_u}{\partial \eta} - \alpha\mu_d \frac{\partial \mathrm{p}}{\partial \mathrm{x}} - \frac{\alpha}{\alpha_d}\frac{\partial p}{\partial \eta}\frac{\partial \emptyset}{\partial x} + R_u + Q_u \quad (2.2)$$

$$\frac{\partial \mathrm{V}}{\partial \mathrm{t}} = -\frac{\partial U_V}{\partial \mathrm{x}} - \frac{\partial V_V}{\partial \mathrm{y}} - \frac{\partial \Omega_V}{\partial \eta} - \alpha\mu_d \frac{\partial \mathrm{p}}{\partial \mathrm{y}} - \frac{\alpha}{\alpha_d}\frac{\partial p}{\partial \eta}\frac{\partial \emptyset}{\partial y} + R_v + Q_v \quad (2.3)$$

$$\frac{\partial \mathrm{W}}{\partial \mathrm{t}} = -\frac{\partial U_w}{\partial \mathrm{x}} - \frac{\partial V_w}{\partial \mathrm{y}} - \frac{\partial \Omega_w}{\partial \eta} - g(\mu_d - \frac{\alpha}{\alpha_d}\frac{\partial p}{\partial \eta}) + R_w + Q_w \quad (2.4)$$

$$\frac{\partial \mu_d}{\partial \mathrm{t}} = -\frac{\partial \mathrm{U}}{\partial \mathrm{x}} - \frac{\partial \mathrm{V}}{\partial \mathrm{y}} - \frac{\partial \Omega}{\partial \eta} \quad (2.5)$$

$$\frac{\partial \Theta}{\partial \mathrm{t}} = -\frac{\partial U_\Theta}{\partial \mathrm{x}} - \frac{\partial V_\Theta}{\partial \mathrm{y}} - \frac{\partial \Omega_\Theta}{\partial \eta} + R_\Theta + Q_\Theta \quad (2.6)$$

$$\frac{\partial \mu_d q_j}{\partial \mathrm{t}} = -\frac{\partial \mathrm{U} q_j}{\partial \mathrm{x}} - \frac{\partial \mathrm{V} q_j}{\partial \mathrm{y}} - \frac{\partial \Omega q_j}{\partial \eta} + Rq_j + Qq_j \quad (2.7)$$

$$\frac{\partial \phi}{\partial \mathrm{t}} = -\mathrm{u}\frac{\partial \phi}{\partial \mathrm{x}} - \mathrm{v}\frac{\partial \phi}{\partial \mathrm{y}} - w\frac{\partial \phi}{\partial \eta} + gw \quad (2.8)$$

where t is time, x and y are the horizontal coordinates, p is pressure, φ is geopotential, α is the specific volume of air including moisture, $\alpha_d$ is the specific volume of dry air, u and v are the horizontal wind components in x and y direction, respectively, and V is the three-element wind vector (U, V, Ω) with Ω being the vertical velocity in η coordinates.

The diagnostic relations are

$$\frac{\partial \phi}{\partial \eta} = -\alpha_d \mu_d \quad (2.9)$$

$$p == \left(\frac{R_\mathrm{d}\Theta_\mathrm{m}}{p_0 \mu_d \alpha_d}\right)^{\gamma} \quad (2.10)$$

$$\Theta_m = \Theta\left[1 + \frac{R}{R_\mathrm{d}} q_v\right] \quad (2.11)$$

$$u = \frac{dx}{dt}, \quad v = \frac{dy}{dt}, \quad w = \frac{dz}{dt}, \quad \omega = \frac{d\eta}{dt}, U = \mu u, \quad V = \mu v, W = \mu w$$

$\Omega = \mu\omega$ , $\gamma = c_{p/c_v}$ denotes the ratio of heat capacities for dry air

$R_d$ is the gas constant for dry air

$p_0$ is the reference pressure (typically $10^5$ Pa)

Θ is the potential temperature

For real-case simulations some of the tendency terms in the model code are coupled to map-scale factors. Variables U, V, Ω and Θ are thus defined as U = μu, V = μv, Ω = μ ∂η ∂t, and Θ = μθ. The prognostic variables include velocity components, u and v in cartesian coordinate, vertical velocity w, perturbation potential temperature, perturbation geopotential, and perturbation surface pressure of dry air. Optionally, turbulent kinetic energy and any number of scalars such as water vapor mixing ratio, rain/snow mixing ratio, cloud water/ice mixing ratio, and chemical species and tracers.

**Model discretization**

*Temporal discretization*

The ARW solver uses a time-split integration scheme. The slow or low-frequency meteorologically significant modes are integrated using a third-order Runge-Kutta (RK3) time integration scheme and the high-frequency acoustic modes are integrated over smaller time steps to maintain numerical stability. The horizontally propagating acoustic modes are integrated using a forward-backward time integration scheme, and vertically propagating acoustic modes and buoyancy oscillations are integrated using a vertically implicit scheme using the acoustic time step. The time-split integration is similar to that first developed by Klemp and Wilhelmson (1978) and analyzed by Skamarock and Klemp (1992). The time-split RK3 scheme is described in general terms in Wicker and Skamarock (2002).

*Spatial Discretization*

The spatial discretization in the ARW solver uses Arakawa-C grid staggering for the variables where the normal velocities are staggered one-half grid length from the thermodynamic variables. The points where Θ is located is taken as mass points and the locations at which u, v and w are defined as u points, v points and ω points. The diagnostic variables p and α are computed at mass points. The vertical grid length is specified in the initialization. η decreases monotonically between the surface ($\eta = 1$) and the model top ($\eta = 0$). The grid lengths dx and dy are constants in the model formulation and the changes in physical grid lengths associated with the various projections to the sphere are accounted using the map factors. The spatial discretization for the ARW solver is defined by using these grid and variable definitions. The model has $2^{nd}$ to $6^{th}$ order advection options in horizontal and vertical.

***Map projections***

The ARW solver currently supports four projections to the sphere— the Lambert conformal, polar stereographic, Mercator, and latitude-longitude projections. These projections are described in (Haltiner and Williams,1980).

***Turbulent Mixing and Model Filters***

A number of formulations for turbulent mixing and filtering are available in the ARW solver. A few of them such as divergence damping, external-mode filtering, vertically implicit acoustic step off-centering etc are required for numerical reasons. The divergence damping is used to filter acoustic modes from the solution and polar filtering is used to reduce the timestep restriction arising from the converging gridlines of the latitude-longitude grid. Other filters are meant to represent sub-grid scale turbulence processes that cannot be resolved on the chosen grid. These filters remove

energy from the solution and are formulated in part on turbulence theory and observations, or represent energy sink terms in some approximation to the Euler equation.

### *Initial Conditions*

The ARW may be run with user-defined initial conditions for idealized simulations. For real-data cases ARW may be run using interpolated data from either an external analysis or forecast. The programs that generate the specific initial conditions for the selected idealized or real data case provide the ARW with input data that is on the correct horizontal and vertical staggering; hydrostatically balanced reference state and perturbation fields and the metadata specifying such information as the date, grid physical characteristics, and projection details. The initial conditions for the real-data cases are pre-processed through a separate package called the WRF Pre-processing System (WPS).The output from WPS is passed to the real-data pre-processor in the ARW- program 'real' which generates initial and lateral boundary conditions.

### *Digital Filtering Initialization*

ARW provides a digital filtering initialization (DFI) to remove noise, which results from imbalances between mass and wind fields, from the model initial state. DFI is applied to the output of the real pre-processor before the model simulation begins. DFI is applied to the analysis produced by the WRF-Var system if data assimilation is performed using WRF-Var. rather than the output of program real. any noise is assumed as of higher frequency than meteorologically significant modes, DFI attempts to remove the noise by filtering all oscillations above a specified cut-off frequency. Accordingly, the filters in the ARW DFI are low-pass digital filters, which are applied to time series of model fields; the initialized model state is the output of the filter

at some prescribed time, e.g., the analysis time. Time series of model states are generated through combinations of adiabatic, backward integration and diabatic, forward integration in the model by choosing DFI scheme determining the specific combination of integrations. Three DFI schemes are present. They are digital filter launch (DFL; Lynch and Huang, 1994), diabatic DFI (DDFI; Huang and Lynch, 1993), and twice DFI (TDFI; Lynch and Huang,1994)

### *Boundary Conditions*

Lateral boundary condition options that are suitable for idealized flows and a specified lateral boundary condition for real-data simulations is available in ARW. For nesting, all fine domains use the nest time-dependent lateral boundary condition where the outer row and column of the fine grid is specified from the parent domain. Primarily for real-data cases, the specified boundary condition is also referred to as a relaxation, or nudging, boundary condition. There are two uses of the specified boundaries in the ARW: one for the outer-most coarse grid and the other for the time-dependent boundaries supplied to a nested grid. The specified lateral boundary conditions for the nest are automatically selected for all of the fine grids, even if the coarse grid is using combinations of the symmetry, periodic, or open options. If the specified lateral boundary condition is selected for the coarse grid, then all four grid sides (west, east, north, and south) use specified lateral conditions. However, in tropical channel mode, where the domain wraps completely around the equator, it is possible to combine specified boundary conditions with periodic conditions in the x direction.

### 2.2.4 Post-processing & Visualization tools

A large number of visualization tools are available to display WRF model data. WRF have graphical tools such as NCL**,** RIP4**,** ARW post**,** VAPOR **e**tc

**NCL**

NCL (the NCAR Command Language) is a very powerful scripting language which has many advantages over the traditional NCAR Graphics codes that use Fortran or C.

**ARWpost**

The ARW post package reads in WRF model output netcdf files and creates GrADS readable output files.

**RIP4**

RIP, which stands for Read/Interpolate/Plot, is a Fortran program that utilizes the NCAR Graphics System Plot Package Simulator suite of plotting routines for creating plots from mesoscale model output. RIP is capable of producing horizontal or vertical cross section plots of scalar fields (contours) or vector fields (barbs or arrows), vertical profiles and soundings, and trajectories.

**VAPOR**

VAPOR is the Visualization and Analysis Platform for Ocean, Atmosphere, and Solar Researchersdeveloped at NCAR to provide interactive visualization and analysis of numerically simulated fluid dynamics.

**IDV**

Unidata's Integrated Data Viewer (IDV) is a multiplatform visualization and analysis tool for interdisciplinary geoscience data. The IDV brings together the ability to display and work with a wide range of data including satellite imagery, gridded data, observations and radar data, all within a unified interface.

## 2.3 Model Physics

The physics incorporated in the WRF Model can be categorized into five. They are

(1) **Microphysics**

**(2) Cumulus parameterization**

**(3) Planetary Boundary Layer (PBL) physics**

**(4) Surface Physics**

**(5) Atmospheric Radiation physics**

A brief overview of all these five categories of physics is very essential for the understanding the physical mechanisms responsible for the development of atmospheric systems. It is also very much required for the proper choice of parameterization schemes during the model integration..A knowledge of the physics schemes and its assumptions can provide a good insight in to the physical processes happen during model integration. Hence a brief description of each category is given below.

### **2.3.1**. **Microphysics**

Microphysics includes explicitly resolved water vapor, cloud, and precipitation processes. The model is general enough to accommodate any number of mass mixing-ratio variables, and otherquantities such as number concentrations. The different microphysics schemes available in WRF are as follows:

a) Kessler Scheme
b) Purdue Lin scheme
c) WRF Single-Moment 3-class (WSM3) scheme
d) WSM5 scheme
e) WSM6 scheme

f) Eta Grid-scale Cloud and Precipitation (2001) scheme or Eta Ferrier scheme
g) Thompson et al. scheme
h) Goddard Cumulus Ensemble Model scheme
i) Morrison et al. 2-Moment scheme

The details of each schemes are as follows:

a) Kessler scheme

Kessler scheme (Kessler, 1969) is a simple warm cloud scheme that includes water vapor, cloud water, and rain. The microphysical processes included are: the production, fall, and evaporation of rain; the accretion and autoconversion of cloud water; and the production of cloud water from condensation.

b) Purdue Lin scheme (Lin et al. scheme)

This scheme includes six classes of hydrometeors: water vapor, cloud water, rain, cloud ice, snow, and graupel. All parameterization production terms are based on (Lin et al.,1983; Rutledge and Hobbs,1984) with some modifications, including saturation adjustment following (Tao et al., 1989) and ice sedimentation. This is a relatively sophisticated microphysics scheme in WRF, and it is most suitable for use in research studies. The scheme is taken from the Purdue cloud model, and the details can be found in (Chen and Sun,2002).

c) WRF Single-Moment 3-class (WSM3) scheme

The WRF single-moment microphysics scheme is a simple efficient scheme with ice and snow processes and suitable for mesoscale grid sizes. This scheme includes ice sedimentation and other new ice-phase parameterizations (Hong et al., 2004). The diagnostic relation based on ice

mass content is included in this scheme and this makes it different from other schemes. The freezing/melting processes are computed during the fall-term sub-steps to increase accuracy in the vertical heating profile of these processes. The WSM3 scheme predicts three categories of hydrometeors: vapor, cloud water/ice, and rain/snow, which is a so-called simple-ice scheme. It assumes cloud water and rain for temperatures above freezing and cloud ice and snow for temperatures below freezing and the details of assumptions are included (Dudhia, 1989). This scheme is computationally efficient for the inclusion of ice processes, but lacks supercooled water and gradual melting rates.

d) WSM5 scheme

The WSM5 scheme is similar to the WSM3 simple ice scheme. However, vapor, rain, snow, cloud ice, and cloud water are held in five different arrays. Thus, it allows supercooled water to exist, and a gradual melting of snow falling below the melting layer (Hong et al.,2004; Hong and Lim, 2006). As with WSM6, the saturation adjustment follows (Dudhia,1989) and (Hong et al.,1998) in separately treating ice and water saturation processes, rather than a combined saturation such as the Purdue Lin (above) and Goddard (Tao et al., 1989) schemes. This scheme is efficient in intermediate grids between the mesoscale and cloud-resolving grids.

e) WSM6 scheme

The six-class scheme extends the WSM5 scheme to include graupel and its associated processes. Some of the graupel-related terms follow Lin et al. (1983), but its ice-phase behavior is much different (Hong et al., 2004). A new method for representing mixed-phase particle fall speeds for the snow and graupel particles by assigning a single fallspeed to both that is weighted by the mixing ratios, and applying that fallspeed to both sedimentation and

accretion processes are introduced (Dudhia et al., 2008). The behavior of the WSM3, WSM5 and WSM6 schemes differ little for coarser mesoscale grids, but they work much differently on cloud-resolving grids. Of the three WSM schemes, the WSM6 scheme is the most suitable for cloud-resolving grids, considering the efficiency and theoretical backgrounds (Hong and Lim, 2006).

f) Eta Grid-scale Cloud and Precipitation (2001) scheme (EGCP01 or the Eta Ferrier scheme)

This scheme predicts changes in water vapor and condensate in the forms of cloud water, rain, cloud ice, and precipitation ice (snow/graupel/sleet). The individual hydrometeor fields are combined into total condensate and it is the water vapor and total condensate that are advected in the model. Local storage arrays retain first-guess information that extract contributions of cloud water, rain, cloud ice, and precipitation ice of variable density in the form of snow, graupel, or sleet. The density of precipitation ice is estimated from a local array that stores information on the total growth of ice by vapor deposition and accretion of liquid water. Sedimentation is treated by partitioning the time averaged flux of precipitation into a grid box between local storage in the box and fall out through the bottom of the box. This approach, together with modifications in the treatment of rapid microphysical processes, permits large time steps to be used with stable results. The mean size of precipitation ice is assumed to be a function of temperature following the observational results of (Ryan,1996). Mixed-phase processes are now considered at temperatures warmer than -30◦C (previously -10◦C), whereas ice saturation is assumed for cloudy conditions at colder temperatures.

g) Thompson et al. scheme [Thompson et al.,2004)]

This scheme is a new bulk microphysical parameterization (BMP) scheme which incorporates a large number of improvements to physical processes and employs many techniques in sophisticated spectral/bin schemes. The assumed snow size distribution depends on both ice water content and temperature and is represented as a sum of exponential and gamma distributions. The snow assumes a non-spherical shape with a bulk density that varies inversely with diameteras found in observations and in contrast to nearly all other BMPs that assume spherical snow with constant density. The features include non-spherical, variable density snow and size distribution matching observations, generalized gamma distribution shape for each hydrometeor species, y-intercept of rain depends on rain mixing ratio and whether apparent source is melted ice, y-intercept of graupel depends on graupel mixing ratio, and a more accurate saturation adjustment scheme. It also includes variable gamma distribution shape parameter for cloud water droplets based on observations, look-up table for transferring cloud ice into snow category, look-up table for freezing of water drops, improved vapor deposition/sublimation and evaporation, variable collection efficiency for rain, snow, and graupel collecting cloud droplets, improved rain collecting snow and graupel.

h) Goddard Cumulus Ensemble Model scheme

The Goddard Cumulus Ensemble (GCE) models (Tao and Simpson, 1993) one-moment bulk microphysical schemes are mainly based on Lin et al. (1983) with additional processes from (Rutledge and Hobbs,1984). The Goddard microphysics schemes have several modifications which includes an option to choose either graupel or hail as the third class of ice (McCumber et

al., 1991). Graupel has a relatively low density and a high intercept value (i.e., more numerous small particles). In contrast, hail has a relative high density and a low intercept value (i.e., more numerous large particles). These differences can affect not only the description of the hydrometeor population and formation of the anvil-stratiform region but also the relative importance of the microphysical-dynamical-radiative processes. It also contains new saturation techniques which are basically designed to ensure that super saturation (sub-saturation) cannot exist at a grid point that is clear (cloudy). All microphysical processes that do not involve melting, evaporation or sublimation are calculated based on one thermodynamic state. This ensures that all of these processes are treated equally. The sum of all sink processes associated with one species will not exceed its mass which ensures that the water budget will be balanced in the microphysical calculations. The Goddard microphysics has a third option, which is equivalent to a two-ice (2ICE) scheme having only cloud ice and snow. This option may be needed for coarse resolution simulations (i.e., > 5 km grid size). The two-class ice scheme could be applied for winter and frontal convection.

i) Morrison et al. 2-Moment scheme

This scheme is based on the two-moment bulk microphysics scheme (Morrison et al.,2005,2008) and (Morrison and Pinto, 2006). Six species of water are included: vapor, cloud droplets, cloud ice, rain, snow, and graupel/hail. Number concentrations and mixing ratios of cloud ice, rain, snow, and graupel/hail, and mixing ratios of cloud droplets and water vapor are the prognostic variables. The prediction of two-moments (i.e., both number concentration and mixing ratio) allows for a more robust treatment of the particle size distributions, which acts as a key for calculating the

microphysical process rates and cloud/precipitation evolution. Several liquid, ice, and mixed-phase processes are included.

### 2.3.2 Cumulus parameterization

Cumulus parameterization schemes are responsible for the sub-grid-scale effects of convective and/or shallow clouds. The schemes are intended to represent vertical fluxes due to unresolved updrafts and downdrafts and compensating motion outside the clouds. They operate only on individual columns where the scheme is triggered and provide vertical heating and moistening profiles. Some schemes additionally provide cloud and precipitation field tendencies in the column, and future schemes may provide momentum tendencies due to convective transport of momentum. The schemes all provide the convective component of surface rainfall. Cumulus parameterizations are theoretically only valid for coarser grid sizes, (e.g., greater than 10 km), where they are necessary to properly release latent heat on a realistic time scale in the convective columns. While the assumptions about the convective eddies being entirely sub-grid-scale break down for finer grid sizes, sometimes these schemes have been found to be helpful in triggering convection in 5–10 km grid applications.

The cumulus parameterization schemes in WRF are

a) Kain-Fritsch scheme
b) Betts-Miller-Janjic scheme
c) Grell-Devenyi ensemble scheme
d) Grell-3 scheme.

The details of each schemes are as follows:

a) Kain-Fritsch scheme(KF)

Kain- Fritsch scheme utilizes a simple cloud model with moist updrafts and downdrafts, including the effects of detrainment, entrainment, and relatively simple microphysics. A number of modifications have been introduced in theKain- Fritsch scheme over the last decade or so.It differs from the original KF scheme in the following way: a minimum entrainment rate is imposed to suppress widespread convection in marginally unstable, relatively dry environments. Shallow (non precipitating) convection is allowed for any updraft that does not reach minimum cloud depth for precipitating clouds; this minimum depth varies as a function of cloud-base temperature. The entrainment rate is allowed to vary as a function of low-level convergence. Downdraft source layer is the entire 150 – 200 mb deep layer just above cloud base and they detrain over a fairly deep layer below cloud base but is no longer related to vertical wind shear. Downdraft mass flux is estimated as a function of the relative humidity and stability just above cloud base.The modified version of the Kain-Fritsch scheme (Kain, 2004) is based on (Kain and Fritsch,1990) and Kain and Fritsch,1993), but has been modified based on testing within the Eta model.

b) Betts-Miller-Janjic(BMJ) scheme

The Betts-Miller-Janjic (BMJ) scheme (Janjic, 1994, 2000) was derived from the Betts-Miller (BM) convective adjustment scheme (Betts, 1986; Betts and Miller, 1986). However, the BMJ scheme differs from the Betts-Miller scheme in several important aspects. The deep convection profiles and the relaxation time are variable and depend on the cloud efficiency, a nondimensional parameter that characterizes the convective regime (Janjic, 1994). The cloud efficiency depends on the entropy change, precipitation, and mean temperature of the cloud. The shallow convection moisture profile is derived from the requirement that the entropy change be small and nonnegative (Janjic, 1994). The BMJ scheme has been optimized over years

of operational application at NCEP, so that, in addition to the described conceptual differences, many details and/or parameter values differ from those recommended in Betts (1986) and Betts and Miller (1986). Recently, attempts have been made to refine the scheme for higher horizontal resolutions, primarily through modifications of the triggering mechanism. A floor value for the entropy change in the cloud is set up below which the deep convection is not triggered. The ascending particle mixes with the environment while searching for the cloud top and the work of the buoyancy force on the ascending particle is required to exceed a prescribed positive threshold.

c) Grell-Devenyi (GD) ensemble scheme

This is an ensemble cumulus scheme in which multiple cumulus schemes and variants are run within each grid box and then the results are averaged to give the feedback to the model. In principle, the averaging can be weighted to optimize the scheme, but the default is an equal weight. The schemes are all mass-flux type schemes, but with differing updraft and downdraft entrainment and detrainment parameters, and precipitation efficiencies. These differences in static control are combined with differences in dynamic control, which is the method of determining cloud mass flux. The dynamic control closures are based on convective available potential energy (CAPE or cloud work function), low-level vertical velocity, or moisture convergence. Those based on CAPE either balance the rate of change of CAPE or relax the CAPE to a climatological value, or remove the CAPE in a convective time scale. The moisture convergence closure balances the cloud rainfall to the integrated vertical advectionof moisture. Another control is the trigger, where the maximum cap strength that permits convection can be varied. These controls typically provide ensembles of 144 members (Grell and Devenyi,2002).

d) Grell-3(G3) scheme

The Grell-3 scheme is also based on an ensemble mean approach shares a lot in common with the Grell-Devenyi scheme but the quasi-equilibrium approach is no longer included among the ensemble members. The scheme is distinguished from other cumulus schemes by allowing subsidence effects to be spread to neighbouring grid columns, making the method more suitable to grid sizes less than 10 km, while it can also be used at larger grid sizes where subsidence occurs within the same grid column as the updraft.

### 2.3.3 Planetary Boundary Layer (PBL) physics

The planetary boundary layer (PBL) is responsible for vertical sub-grid-scale fluxes due to eddy transports in the whole atmospheric column, not just the boundary layer. Thus, when a PBL scheme is activated, explicit vertical diffusion is de-activated with the assumption that the PBL scheme will handle this process. The surface fluxes are provided by the surface layer and land-surface schemes. The PBL schemes determine the flux profiles within the well-mixed boundary layer and the stable layer, and thus provide atmospheric tendencies of temperature, moisture (including clouds), and horizontal momentum in the entire atmospheric column. Most PBL schemes consider dry mixing, but can also include saturation effects in the vertical stability that determines the mixing. The schemes are one-dimensional, and assume that there is a clear scale separation between sub-grid eddies and resolved eddies. This assumption will become less clear at grid sizes below a few hundred meters, where boundary layer eddies may start to be resolved, and in these situations the scheme should be replaced by a fully three-dimensional local sub-grid turbulence scheme such as the TKE diffusion scheme.

The different PBL schemes available in WRF are

a) Medium Range Forecast Model (MRF) PBL

This PBL scheme employs a so-called counter-gradient flux for heat and moisture in unstable conditions. It uses enhanced verticalflux coefficients in the PBL, and the PBL height is determined from a critical bulk Richardson number. It handles vertical diffusion with an implicit local scheme, and it is based on local Ri in the free atmosphere (Hong and Pan,1996).

b) Yonsei University (YSU) PBL

The Yonsei University PBL (Hong et al., 2006) is the next generation of the MRF PBL. An explicit treatment of the entrainment layer at the PBL top is added to the MRF PBL (Hong and Pan, 1996) and this scheme uses the counter gradient terms to represent fluxes due to non-local gradients. The entrainment is made proportional to the surface buoyancy flux (Noh et al., 2003). The PBL top is defined using a critical bulk Richardson number of zero and so is effectively dependent on the buoyancy profile in which the PBL top is defined at the maximum entrainment layer. A smaller magnitude of the counter-gradient mixing in the YSU PBL produces a well-mixed boundary-layer profile, whereas there is a pronounced over-stable structure in the upper part of the mixed layer in the case of the MRF PBL. Details are available in Hong et al. ,2006, including the analysis of the interaction between the boundary layer and precipitation physics. An enhanced stable boundary-layer diffusion algorithm (Hong, 2007) is also devised and it allows deeper mixing in windier conditions.

c) Mellor-Yamada-Janjic (MYJ) PBL

This parameterization of turbulence in the PBL and in the free atmosphere represents a non singular implementation of the Mellor-Yamada

Level 2.5 turbulence closure model (Mellor and Yamada, 1982) through the full range of atmospheric turbulent regimes(Janjic, 1990, 1996, 2002)

d) Asymmetrical Convective Model version 2 (ACM2) PBL

ACM2 can simulate rapid upward transport in buoyant plumes and local shear induced turbulent diffusion. The partitioning between the local and nonlocal transport components is derived from the fraction of non-local heat flux according to the model of Holtslag and Boville (1993). The ACM2 is particularly well suited for consistent PBL transport of any atmospheric quantity including both meteorological (u, v,θ, qv) and chemical trace species.

### 2.3.4. Land-Surface Model physics

The land-surface models (LSMs) use atmospheric information from the surface layer scheme, radiative forcing from the radiation scheme, and precipitation forcing from the microphysics and convective schemes, together with internal information on the land's state variables and land-surface properties, to provide heat and moisture fluxes over land points and sea-ice points. These fluxes provide a lower boundary condition for the vertical transport done in the PBL schemes. The land-surface models have various degrees of sophistication in dealing with thermal and moisture fluxes in multiple layers of the soil and also may handle vegetation, root, and canopy effects and surface snow-cover prediction. The land surface model provides no tendencies, but does update the land's state variables which include the ground (skin) temperature, soil temperature profile, soil moisture profile, snow cover, and possibly canopy properties.

The LSMs are

a) 5-layer thermal diffusion LSM

This simple LSM is based on the MM5 5-layer soil temperature model. Layers are 1, 2, 4, 8, and 16 cm thick. Below these layers, the temperature is fixed at a deep-layer average. The energy budget includes radiation, sensible, and latent heat flux. It also allows for a snow-cover flag, but the snow cover is fixed in time. Soil moisture is also fixed with a landuse and season-dependent constant value, and there are no explicit vegetation effects.

b) Noah LSM

This is a 4-layer soil temperature and moisture model with canopy moisture and snow cover prediction. The layer thicknesses are 10, 30, 60 and 100 cm (adding to 2 meters) from the top down. It includes root zone, evapotranspiration, soil drainage, and runoff, taking into account vegetation categories, monthly vegetation fraction, and soil texture. The scheme provides sensible and latent heat fluxes to the boundary-layer scheme. The Noah LSM additionally predicts soil ice, and fractional snow cover effects, has an improved urban treatment, and considers surface emissivity properties.

c) Rapid Update Cycle (RUC) Model LSM

The RUC LSM has a multi-level soil model (6 levels is default, could be 9 or more) with higher resolution in the top part of soil domain (0, 5, 20, 40, 160, 300 cm is default). The soil model solves heat diffusion and Richards moisture transfer equations, and in the cold season takes into account phase changes of soil water (Smirnova et al., 1997, 2000). The RUC LSM also has a multi-layer snow model with changing snow density, refreezing liquid water percolating through the snow pack, snow depth and temperature dependent albedo, melting algorithms applied at both snow-atmosphere interface and snow-soil interface, and simple parameterization of fractional snow cover with possibility of grid averaged skin temperature going above freezing. It also includes vegetation effects and canopy water. The RUC LSM has a layer

approach to the solution of energy and moisture budgets. The layer spans the ground surface and includes half of the first atmospheric layer and half of the top soil layer with the corresponding properties (density, heat capacity, etc.) The residual of the incoming fluxes (net radiation, latent and sensible heat fluxes, soil heat flux, precipitation contribution into heat storage, etc.) modify the heat storage of this layer. An implicit technique is applied to the solution of these equations. Prognostic variables include soil temperature, volumetric liquid, frozen and total soil moisture contents, surface and sub-surface runoff, canopy moisture, evapotranspiration, latent, sensible and soil heat fluxes, heat of snow-water phase change, skin temperature, snow depth and density, and snow temperature.

d) Pleim-Xiu LSM

The PX LSM (Pleim and Xiu, 1995; Xiu and Pleim, 2001), originally based on the ISBA model Noilhan and Planton (1989), includes a 2-layer force-restore soil temperature and moisture model. The top layer is taken to be 1 cm thick, and the lower layer is 99 cm. The PX LSM features three pathways for moisture fluxes: evapotranspiration, soil evaporation, and evaporation from wet canopies. Evapotranspiration is controlled by bulk stomatal resistance that is dependent on root zone soil moisture, photosynthetically active radiation, air temperature, and the relative humidity at the leaf surface. Grid aggregate vegetation and soil parameters are derived from fractional coverages of land use categories and soil texture types. There are two indirect nudging schemes that correct biases in 2-m air temperature and RH by dynamic adjustment of soil moisture (Pleim and Xiu, 2003) and deep soil temperature (Pleim and Gilliam, 2008).

e) Urban Canopy Model(UCM)

In UCM, all the urban effects in the vertical are assumed to be subgrid scale meaning that the urban processes are occurring below the lowest model

level. The urban canopy model includes parameterization of street canyons to represent the urban geometry, shadowing from building and radiation reflection, an exponential wind profile in the canopy layer ,multilayer heat equation from roof wall and road surfaces. The urban canopy model estimates the surface temperature and heat fluxes from the roof, wall and road surface. It also calculates the momentum exchange between the urban surface and the atmosphere. If they are available, the UCM can take three different densities of urban development using special land-use categories. An anthropogenic heating diurnal cycle is added as an option.

f) Ocean Mixed-Layer Model

This model is designed for hurricane modeling in order to simulate the cooling of the ocean underneath hurricanes. The ocean mixed-layer model is based on that of Pollard et al. (1973). Each column is independently coupled to the local atmospheric column, so the model is one-dimensional. The ocean part consists of a time-varying layer, representing the variable-depth mixed layer over a fixed layer acting as a reservoir of cooler water with a specified thermal lapse rate. In the mixed layer, the prognostic variables are its depth, vector horizontal current, and mean temperature taken to be the sea-surface temperature (SST). The hurricane winds drive the current, which in turn leads to mixing at the base of the mixed layer when the Richardson number becomes low enough. This mixing deepens and cools the mixed layer, and hence the cooler sea-surface temperature impacts the heat and moisture fluxes at the surface, and has a negative feedback on hurricane intensity.

Surface Layer parameterization

The surface layer schemes calculate friction velocities and exchange coefficients that enable the calculation of surface heat and moisture fluxes by the land-surface models and surface stress in the planetary boundary layer

scheme. The surface fluxes and surface diagnostic fields are computed in the surface layer scheme itself over water surfaces. The schemes provide only the stability-dependent information about the surface layer for the land-surface and PBL schemes but no tendencies. Each surface layer option is tied to particular boundary-layer option, but in the future more options may become available. The schemes are:

a) MM5 similarity: This scheme uses stability functions to compute surface exchange coefficients for heat, moisture, and momentum(Paulson (1970), Dyer and Hicks (1970), and Webb (1970)). A convective velocity is used to enhance surface fluxes of heat and moisture(Beljaars (1994)). No thermal roughness length parameterization is included in the current version of this scheme.

b)The Eta surface layer scheme (Janjic, 1996, 2002)

This scheme is based on similarity theory (Monin and Obukhov, 1954) and it includes parameterizations of a viscous sub-layer. Over water surfaces, the viscous sub-layer is parameterized explicitly following Janjic (1994). Over land, the effects of the viscous sub-layer are taken into account through variable roughness height fortemperature and humidity (Zilitinkevich (1995).This surface layer scheme must be run in conjunction with the Eta (Mellor-Yamada-Janjic) PBL scheme, and is therefore sometimes referred to as the MYJ surface scheme.

c)The Pleim-Xiu (PX)surface layer scheme (Pleim, 2006)

This scheme is based on similarity theory and includes parameterizations of a viscous sub-layer in the form of a quasi-laminar boundary layer resistance accounting for differences in the diffusivity of heat, water vapor, and trace chemical species. The surface layer similarity functions are estimated by analytical approximations from state variables.

### 2.3.5. Atmospheric Radiation Schemes

The atmospheric heating due to radiative flux divergence and surface downward longwave and shortwave radiation for the ground heat budget is provided to the model using the radiation schemes. The infrared or thermal radiation absorbed and emitted by gases and surfaces are included as longwave radiation. The surface emissivity which depends upon land-use type, as well as the ground (skin) temperature is utilised in the determination of upward longwave radiative flux from the ground. The visible and surrounding wavelengths that make up the solar spectrum is included as shortwave radiation and it includes absorption, reflection, and scattering in the atmosphere and at surfaces. The upward flux is the reflection due to surface albedo for shortwave radiation. The radiation responds to model-predicted cloud and water vapor distributions, as well as specified carbon dioxide, ozone, and trace gas concentrations within the atmosphere.

a) Rapid Radiative Transfer Model (RRTM) Longwave radiation scheme

This scheme is a spectral-band scheme using the correlated-k method(Mlawer et al., 1997). The longwave processes due to water vapor, ozone, CO2, and trace gases as well as accounting for cloud optical depth is accurately represented by using pre-set tables.

b) Eta Geophysical Fluid Dynamics Laboratory (GFDL) Longwave radiation scheme

This longwave radiation scheme from GFDL follows the simplified exchange method with calculation over spectral bands associated with carbon dioxide, water vapor, and ozone(Fels and Schwarzkopf, 1975; Schwarzkopf and Fels, 1991). The transmission coeffcients for carbon dioxide(Schwarzkopf and Fels, 1985), a water vapor continuum(Roberts et al. ,1976), and the effects of water vapor-carbon dioxide overlap and of a

Voigt line-shape correction are included in this scheme. The Rodger's formulation is adopted for ozone absorption (Rodgers, 1968) and it is assumed that the clouds are randomly overlapped and is implemented to conduct comparisons with the operational Eta model.

c) CAM Longwave radiation scheme

This scheme is a spectral-band scheme used in the NCAR Community Atmosphere Model (CAM 3.0) for climate simulations. It interacts with resolved clouds and cloud fractions, and is documented in Collins et al. (2004)and has the potential to handle several trace gases.

d) Eta Geophysical Fluid Dynamics Laboratory (GFDL) Shortwave radiation scheme

This shortwave radiation is a GFDL version of the Lacis and Hansen (1974) parameterization. The effects of atmospheric water vapor, ozone (Lacis and Hansen, 1974), and carbon dioxide (Sasamori et al., 1972) are employed. A daylight-mean cosine solar zenith angle over the time interval is used for shortwave calculations it is assumed that the clouds are randomly overlapped.

e) MM5 (Dudhia) Shortwave radiation scheme

This scheme (Dudhia ,1989)has a simple downward integration of solar flux, accounting for clear-air scattering, water vapor absorption (Lacis and Hansen, 1974), and cloud albedo and absorption. The look-up tables for clouds (Stephens,1978) is used in this scheme and an option to account for terrain slope and shadowing effects on the surface solar flux.

f) Goddard Shortwave radiation scheme

This scheme considers diffuse and direct solar radiation components in a two-stream approach that accounts for scattered and reflected components

and has a total of 11 spectral bands. The several available climatological profiles for ozone is also included. (Chou and Suarez ,1994).

g) CAM Shortwave radiation scheme

This spectral-band scheme can handle optical properties of several aerosol types and trace gases. The cloud fractions and overlap assumptions in unsaturated regionsis used in this scheme and includes a monthly zonal ozone climatology (Collins et al., 2004). The CAM radiation scheme have a ozone distribution that varies during the simulation according to monthly zonal-mean climatological data and hence suitable for regional climate simulations.

## 2.4 Datasets used

The datasets utilised for the study includes

- NCEP FNL Operational Model Global Tropospheric Analyses Data
- NCEP Global Forecast System (GFS) Forecast data
- MetSat-1 /KALPANA Satellite Imagery
- Meteosat Satellite Imagery [Indian Ocean Data Coverage (IODC)]
- Satellite based Automatic Weather Station(AWSs) data
- TRMM 3B42 daily merged rainfall data
- USGS 30 sec global topographical data and vegetation data
- Doppler Weather Radar (DWR) data
- IMD Rainfall data

The details of each dataset are as follows:

1. **NCEP FNL Operational Model Global Tropospheric Analyses Data**

The initial and lateral boundary conditions for the model run was taken from the NCEP FNL (Final) Operational Global Analysis data. These data were

prepared operationally every six hours ($1^0$ x $1^0$grids). This product was from the Global Data Assimilation System (GDAS), which has been continuously collecting observational data from the Global Telecommunications System (GTS), and other sources, for many analyses. The FNLs were made with the same model which NCEP uses in the Global Forecast System (GFS), but the FNLs were prepared about an hour or so after the initialization of GFS. The FNLs were delayed so that more observational data can be ingested. The analyses were available on the surface and also at 26 mandatory (and other pressure) levels vertically extending from 1000 millibars to 10 millibars. It was also available for the surface boundary layer and at some sigma layers, the tropopause and a few others. The parameters include sea level pressure, sea surface temperature, relative humidity, temperature, geopotential height, surface pressure, soil values, ice cover, u and v winds, vertical motion, vorticity and ozone.

2. **NCEP Global Forecast System (GFS) Forecast data**

If the model is run in operational mode, then the initial and lateral boundary conditions for the model run is taken from NCEP GFS data. The run given for Cyclone AILA has been carried out to check the predictive capacity of the identified schemes. Hence in Chapter 3, the initial and boundary conditions for the model run were provided with NCEP GFS data. This dataset was a collection of various NCEP GFS data used by NCAR's researchers. It consists of periods of GFS spectral coefficients (in binary format) and flux terms (in GRIB format), as well as their transformed, gridded NetCDF files of various spatial resolutions, T382, T254, T170 and T62. The variables include air temperature, geopotential height, humidity, upper air temperature, upper level winds etc.

3. **MetSat-1 /KALPANA Satellite Imagery**

MetSat-1 is ISRO's first dedicated GEO weather satellite project built by ISRO and it is renamed to Kalpana-1 to honour Kalpana Chawla, NASA astronaut. The satellite imagery provides valuable information as well as observational evidence for the occurrence of the event. With the help of the three Indian meteorological satellites: Kalpana-1, INSAT-3A and INSAT-3D, IMD is able to monitor several phenomena like cyclones, western disturbances, thunderstorms, etc., and provide early warnings to the affected areas. This imagery is utilised in this study of weather systems.

**4. Meteosat Satellite Imagery[Indian Ocean Data Coverage (IODC)]**

The Meteosat VISSR(IODC) imagery centered at 57 $^0$E was utilised for the study of heavy rainfall over Cochin and Peninsular India. These images are updated every six hours from the data provided by Europe's Meteorological Satellite Organization (EUMETSAT) by National Oceanic and Atmospheric Administration (NOAA).

**5. Satellite based Automatic Weather Station (AWSs) data**

Fifty-eight satellite based Automatic Weather Stations were installed over Kerala region as part of an ISRO-CUSAT collaborative project. The dataset includes hourly data of temperature, pressure, wind speed, wind direction , humidity and rainfall. The data was available for the period 2007-2009. Hence the case studies during that period have been compared with AWS data.

**6. USGS 30 sec global topographical data and vegetation data**

The United States Geological Survey(USGS) Global dataset with 30 sec horizontal resolution were used to create terrain/topography and landuse/vegetation fields for the model run. This is a global dataset which comprises the land use, vegetation type, vegetation fraction, albedo,

topographic heights and other variables and are provided at various resolutions. The dataset with the highest resolution of 30 seconds (approximately 1 km) have been used for the model run.

## 7. TRMM 3B42 daily merged rainfall data

The Tropical Rainfall Measuring Mission (TRMM) is a joint mission of NASA and the Japan Aerospace Exploration Agency launched in 1997 to study rainfall for weather and climate research. TRMM was a research satellite designed to improve our knowledge about the spatial and temporal distribution and variability of precipitation within the tropics as part of the water cycle in the current climate system. TRMM satellite covered the tropical and sub-tropical regions of the Earth and provided important information on rainfall and its associated heat release that drives the global atmospheric circulation. TRMM provided important precipitation information using several space-borne instruments in coordination with other satellites in NASA's Earth Observing System inorder to increase our understanding of the interactions between water vapor, clouds and precipitation. TRMM 3B42 daily merged rainfall data have been used for validating the model simulated rainfall. The output of TRMM Algorithm 3B42 is incorporated in this dataset to produce Tropical Rainfall Measuring Mission (TRMM) merged high quality (HQ)/infrared (IR) precipitation and root-mean-square (RMS) precipitation-error estimates.

## 8. Doppler Weather Radar (DWR) data

The three base products available from DWRs are Reflectivity(Z),radial velocity(V) and Spectrum width(ω).The maximum reflectivity, Max(Z) provides the distribution parameters in three dimensional spaces. Hence they were utilised in the study of weather systems.

## 9. India Meteorological Department(IMD) data

IMD have set a large number of raingauges at various parts of the country. The model simulated rainfall values were validated with IMD rainfall data. The IMD wind analysis at different vertical levels has been utilised for this research work.

# Chapter 3

# Numerical simulation of convective systems and their sensitivity to WRF microphysics and cumulus parameterization schemes

## 3.1 Introduction

Heavy rainfall events have been increasing in recent years over peninsular India, east and north-east India (Guhathakurtha et.al., 2011) and they are projected to increase further in the future under a warming climate(Milly et al., 2002 ; Ali and Mishra, 2018). The flash floods resulting from heavy spells have a huge impact on human life and economy. Recently, India has witnessed a large number of heavy rainfall events which resulted in huge loss of life and property especially Kerala during August 2018 and August 2019.Hence location specific accurate forecasts are very important in various disciplines. Numerical modelling is the most sophisticated technique in predicting severe weather events.

The WRF model is widely used for the prediction of weather events but found to be very sensitive to different parameterization schemes and hence it is very important to identify suitable parameterization schemes for the Indian region. Hence, in this study, the WRF model was run with different combinations of microphysics and cumulus parameterization schemes in order to identify the most suitable combination of microphysics and cumulus dynamics for peninsular India especially over Kerala.

## 3.2 Case Description

A severe convection event occurred over Cochin on 8th April 2010 with severe thunder, lightning and rainfall. The event manifested as heavy rainfall over Cochin during 1000UTC- 1200 UTC as per the satellite-based Automated Weather Station (AWS) data. The satellite imagery (Meteosat) of 1200 UTC of 8th April 2010 also confirmed the occurrence of the event. Fig.3.1 -Fig. 3.3 show the satellite imagery of 0600 UTC ,1200 UTC and 1800UTC of 8th April 2010 respectively.

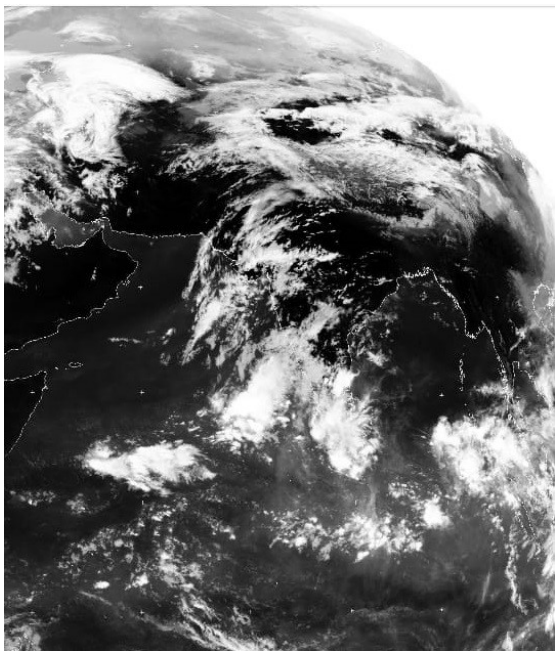

Fig.3.1: Meteosat VISSR satellite imagery of at 0600 UTC of 8th April 2010 showing deep convection over Cochin

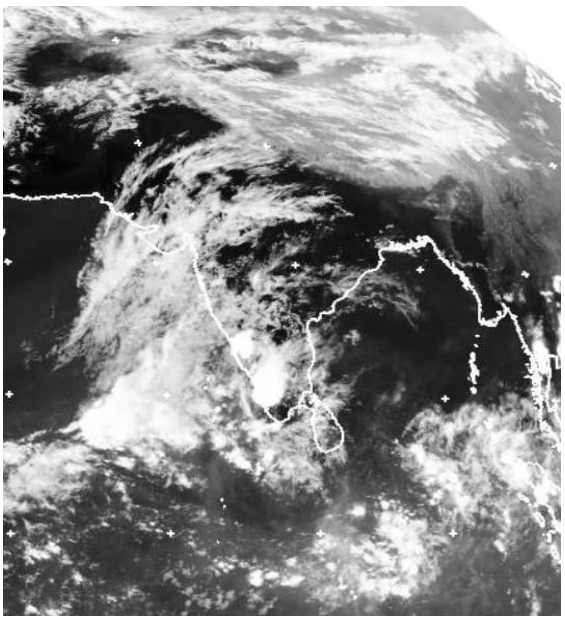

Fig.3.2: Meteosat VISSR satellite imagery of at 1200 UTC of 8th April 2010 showing deep convection over Cochin

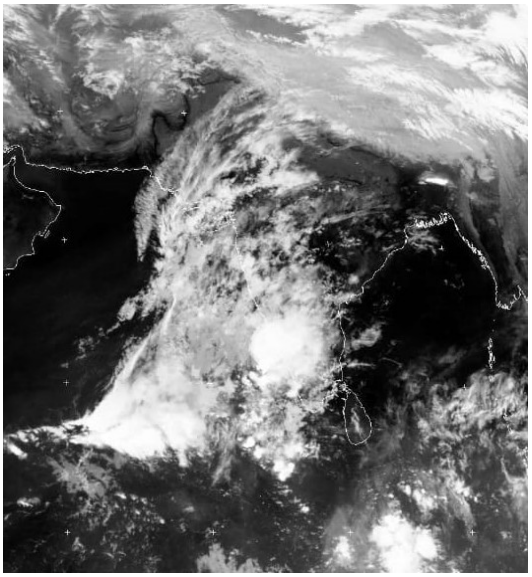

Fig.3.3: Meteosat VISSR satellite imagery of at 1800 UTC of 8th April 2010 showing deep convection over Cochin

### 3.3. Methodology and Experimental design

Four experiments have been carried out with different combinations of cumulus schemes and microphysics. The combination of parameterization schemes chosen for each experiment is given in Table 3.1.

| Expt. No. | Expt. Name | Cumulus Scheme | Microphysics |
|---|---|---|---|
| 1 | BMJ-WSM3 | Betts- Miller-Janjic scheme | WSM 3-class simple ice scheme |
| 2 | GD-WSM3 | Grell-Devenyi ensemble scheme | WSM 3-class simple ice scheme |
| 3 | KF-WSM3 | Kain-Fritsch Scheme (KF) | WSM 3-class simple ice scheme |
| 4 | BMJ-Ferrier | Betts-Miller-Janjic scheme | Ferrier(New Eta) scheme |

Table 3.1: Cumulus and microphysics parameterization schemes used in each experiment.

The above four experiments have been carried out using the WRF model with nested domains with a horizontal resolution of 90 km in the outer domain, 30 km in the middle domain and 10 km in the innermost domain. Two-way nesting technique was employed. The three-nested domains set up by the WPS program for the study is shown in Fig 3.4. The outer domain is referred as D1, the middle domain as D2 and the innermost domain as D3. The outer domain ranges from $60^0$ E -$98^0$ E and $10^0$ S – $30^0$ N, the middle domain ranges from $70^0$ E - $85^0$ E and $0^0$ – $20^0$ N, the innermost domain ranges from $74.5^0$ E - $79^0$ E and $7^0$ N– $13^0$ N.

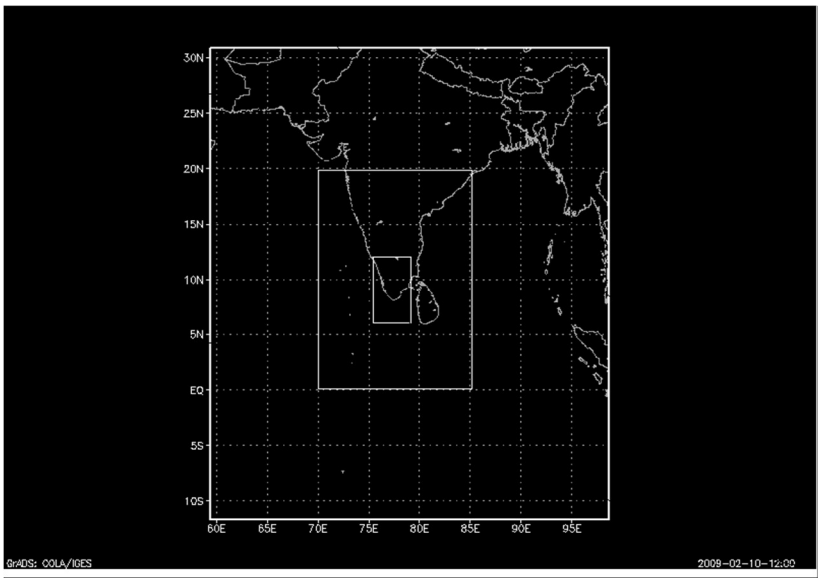


Fig.3.4: Two-way nested domains configured for the simulation.

The model was run using three different cumulus parameterization schemes, the Kain-Fritsch (new Eta) scheme, Grell-Devenyi ensemble scheme, Betts-Miller-Janjic scheme for cumulus parameterization with WSM3 class simple ice scheme for microphysics and Yonsei University (YSU) scheme for the boundary layer parameterization, Rapid Radiative Transfer Model (RRTM) for long wave radiation and Dudhia scheme for short wave radiation.The model was also run with Betts-Miller-Janjic cumulus parameterization scheme and Ferrier(New Eta) scheme.The grid staggering was the Arakawa C-grid. The model used the Runge-Kutta $2^{nd}$ and $3^{rd}$ order time integration schemes, and $2^{nd}$ to $6^{th}$ order advection schemes in both the horizontal and vertical. It used a time-split small step for acoustic and gravity-wave modes.

Ten more experiments were designed for a smaller domain with a higher horizontal resolution of 10 km in order to study the sensitivity of cumulus and microphysics parameterizations. The sensitivity of the WRF model to various combinations of cumulus and microphysics

parameterization schemes in simulating a heavy rainfall event over Cochin on 8th April 2010 was carried out by conducting ten different experiments. The cumulus and microphysics parameterization schemes used in the experiments are summarized in Table 3.2. The model simulated reflectivity for every experiment is plotted in Fig.3.5– Fig. 3.8.

| Expt. No. | Expt. Name | Cumulus Scheme | Microphysics |
|---|---|---|---|
| 1 | KF-WSM3 | Kain-Fritsch Scheme (KF) | WSM 3-class simple ice scheme |
| 2 | BMJ-WSM3 | Betts-Miller-Janjic (BM) Scheme | WSM 3-class simple ice scheme |
| 3 | BMJ-Ferrier | Betts-Miller-Janjic (BMJ) Scheme | Ferrier(New Eta) scheme |
| 4 | BMJ-Kessler | Betts-Miller-Janjic (BMJ) Scheme | Kessler scheme |
| 5 | BMJ-Lin | Betts-Miller-Janjic (BMJ) Scheme | Lin et. al scheme |
| 6 | BMJ-Thompson | Betts-Miller-Janjic (BMJ) Scheme | Thompson graupel scheme |
| 7 | GD-WSM3 | Grell-Devenyiensemble scheme (GD) | WSM 3-class simple ice scheme |
| 8 | G3-Kessler | New Grell Scheme (G3) | Kessler |
| 9 | G3-Lin | New Grell Scheme (G3) | Lin et. al scheme |
| 10 | G3-WSM3 | New Grell Scheme (G3) | WSM 3-class simple ice scheme |

Table 3.2: Cumulus and Microphysics parameterization schemes used in the simulation of experiments

## 3.4 Data and Methodology

The initial and lateral boundary conditions for the model run was taken from the Final (FNL) Operational Global Tropospheric Analyses of National Centre for Environmental Prediction (NCEP) on $1^0$ x $1^0$ grids prepared operationally every six hours. This FNL dataset is developed from the Global Data Assimilation System (GDAS), which continuously collects observational data from the Global Telecommunications System (GTS) and other sources. The United States Geological Survey (USGS) global dataset with 30 sec horizontal resolution were used to create terrain/topography and landuse/vegetation fields. The model output was validated using TRMM 3B42 precipitation data ($0.25^0$x$0.25^0$) and Satellite based Automatic Weather Stations (AWSs) data.

## 3.5 Results and Discussions

The WRF model output was analysed for each experiment. The WRF simulated reflectivity was plotted for every 3 hour interval inorder to understand whether these four combination of parameterization schemes could capture the convective weather event that occurred on $8^{th}$ April 2010.The experiment name and the scheme details are summarised in Table 3.1.

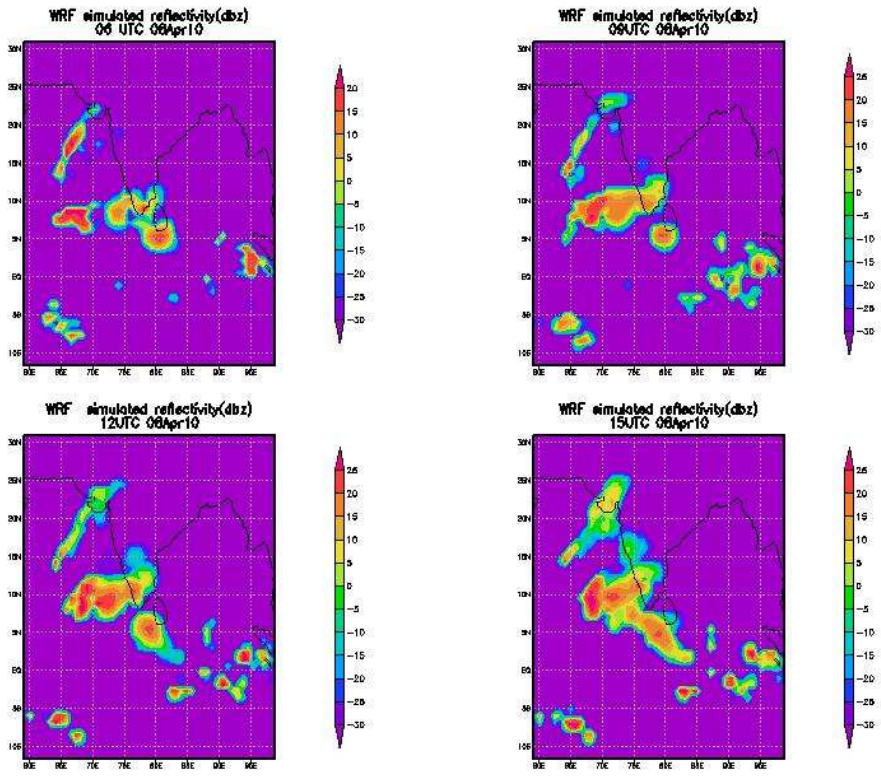


***Fig 3.5: WRF simulated reflectivity for the experiment BMJ-WSM3 from 06UTC-15UTC of 08April 2010***

The WRF simulated reflectivity for the experiment BMJ-WSM3 from 06UTC-15UTC of 08April 2010 is given in fig. 3.5. The reflectivity analysis reveals that the BMJ-WSM3 experiment could capture the severe convection and is in good agreement with satellite imagery.

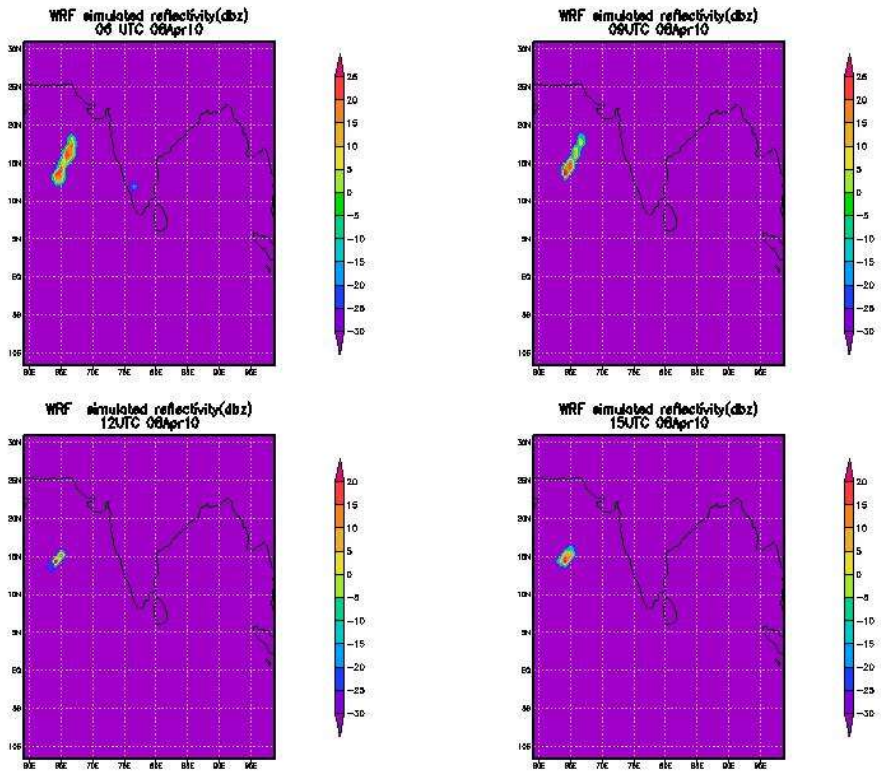


***Fig 3.6: WRF simulated reflectivity for the experiment GD-WSM3 from 06UTC-15UTC of 08 April 2010***

WRF simulated reflectivity for the experiment GD-WSM3 from 06UTC-15UTC of 08 April 2010 is plotted in Fig.3.6. The reflectivity analysis clearly shows that the combination of Grell-Devenyi cumulus scheme and WSM3 microphysics (GD-WSM3) scheme couldn't capture the convective weather event.

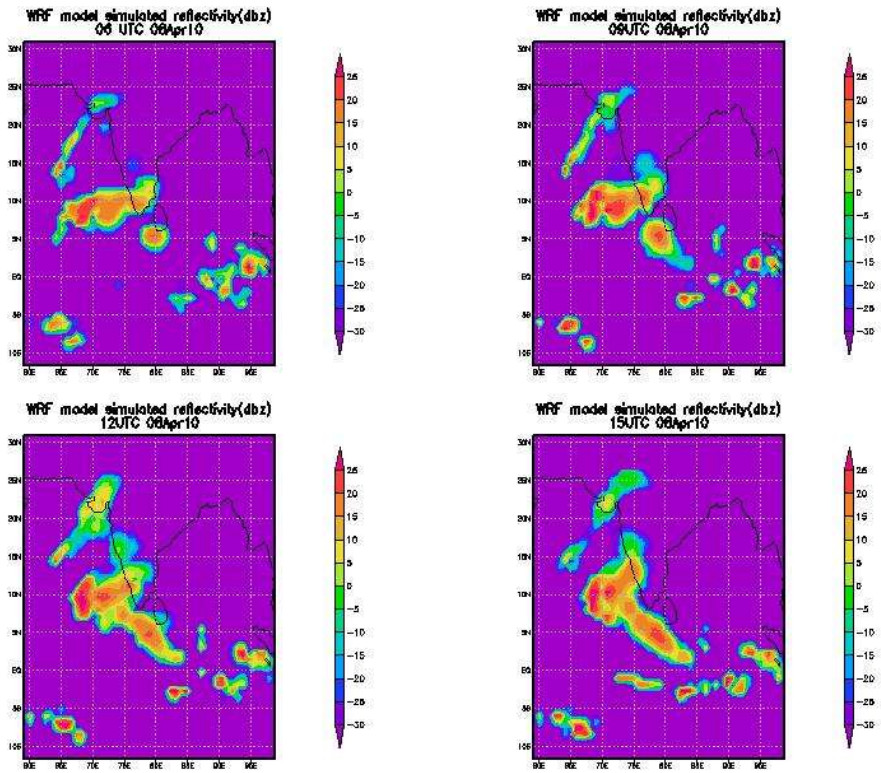


***Fig. 3.7: WRF simulated reflectivity for the experiment KF-WSM3 from 06UTC-15UTC of 08April 2010***

WRF simulated reflectivity for the experiment KF-WSM3 from 06UTC-15UTC of 08April 2010 is plotted in fig.3.7. The analysis of the simulated output shows that a combination of Kain Fritsch cumulus scheme and WSM3 microphysics (KF-WSM3) scheme could simulate the convective event very well and it agrees with the satellite imagery very well.

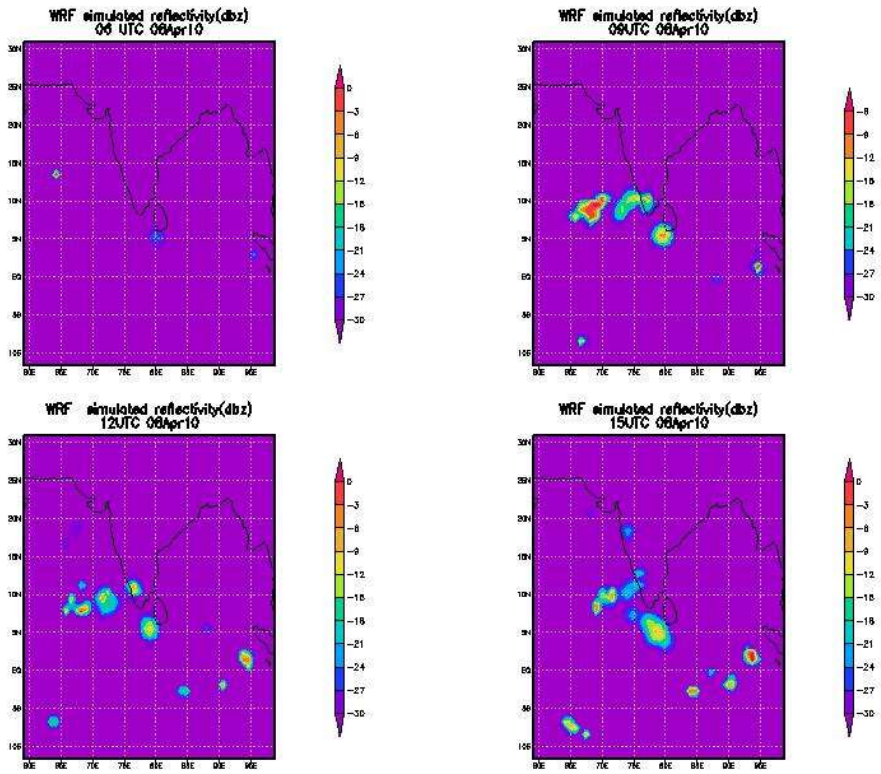


***Fig. 3.8: WRF simulated reflectivity for the experiment BMJ- Ferrier from 06UTC-15UTC of 08April2010***

WRF simulated reflectivity for the experiment BMJ-Ferrier from 06UTC-15UTC of 08April 2010 is plotted in Fig.3.8. The figure clearly shows that the combination of Betts-Miller-Janjic cumulus scheme and Ferrier (new Eta) microphysics (BMJ-Ferrier) couldn't capture the development of convective clouds. The analysis of the model output of the first four experiments reveals that only two experiments KF-WSM3 and BMJ-WSM3 could capture the convection.

To identify the suitable combination of parameterization schemes another ten experiments are carried out with a higher horizontal resolution of 10 km. The name of the experiments and combination of schemes selected for each experiment is given in Table 3.2.The model was run with different combinations of cumulus and microphysics parameterizations inorder to identify the best combination of parameterization schemes. The WRF model simulated rainfall was plotted in Fig.3.9 – Fig 3.11. The model output has been analysed and it is seen that the KF-WSM3 could simulate the rainfall with good accuracy and matches with the observed TRMM precipitation. The convection is also very well captured in the experiment KF-WSM3. BMJ-WSM3 experiment could capture the convection but couldn't simulate the spatial distribution of rainfall. The experiment BMJ-Ferrier under-predicted the rainfall while the experiment BMJ-Kessler couldn't predict the rainfall. The experiment BMJ-Lin and BMJ-Thompson under-predicted the rainfall. The experiments GD-WSM3 and G3-Kessler couldn't simulate the spatial distribution of rainfall and the values are over-predicted. The experiments G3-Lin couldn't simulate the spatial distribution of rainfall and the experiment G3-WSM3 could simulate the spatial distribution of rainfall fairly well but over-predicted the magnitude.

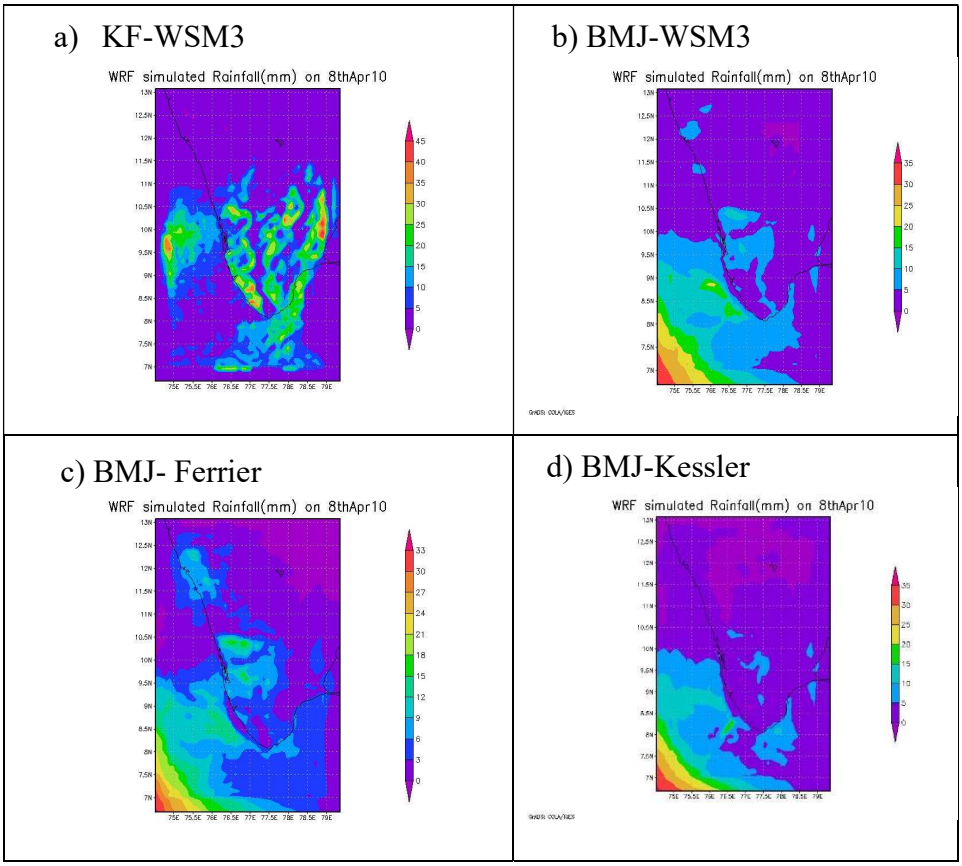


***Fig. 3.9: WRF simulated rainfall(mm) for the experiment a) KF-WSM3 b) BMJ- WSM3 c) BMJ-Ferrier d) BMJ-Kessler of 08April 2010***

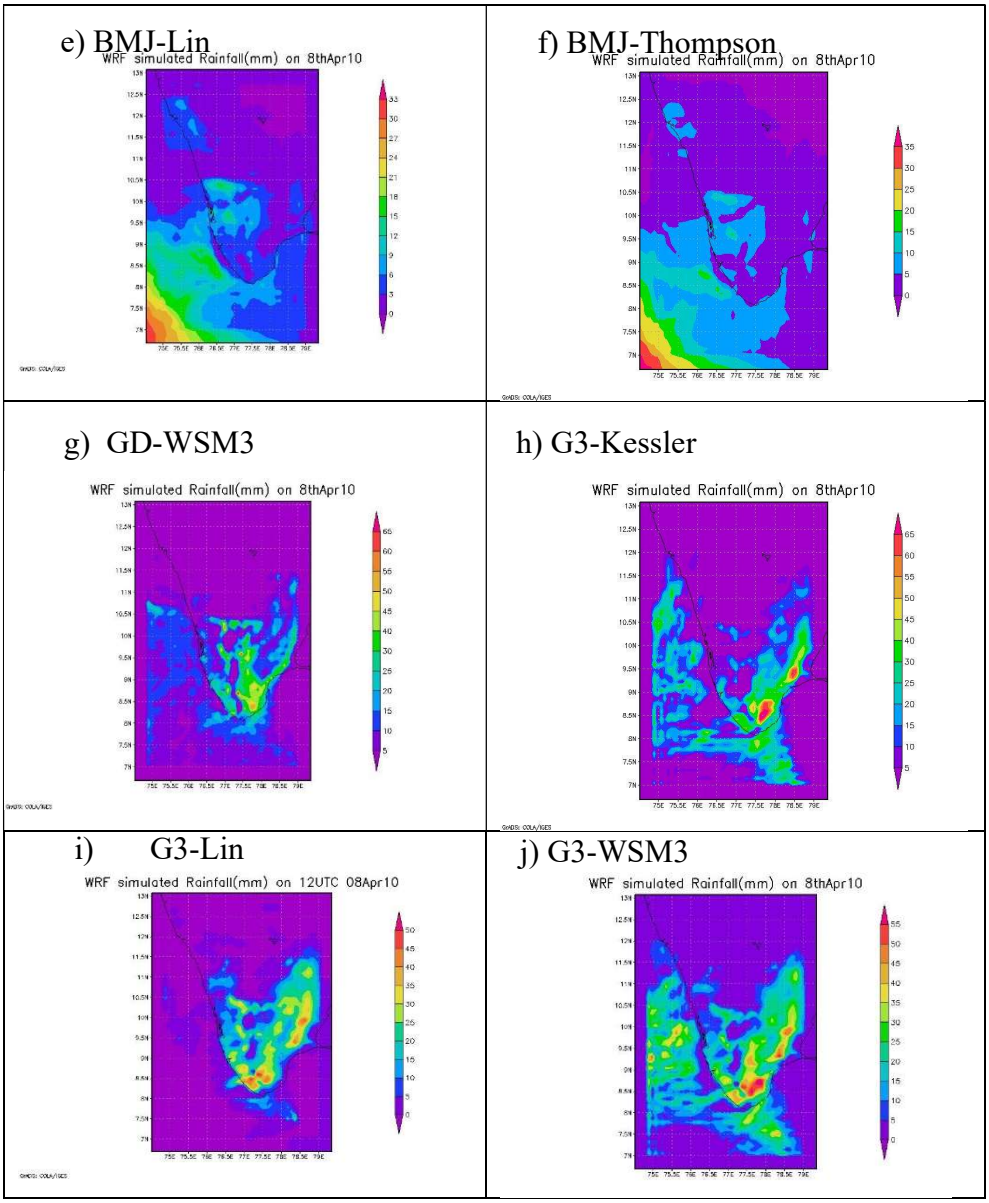


***Fig. 3.10: WRF simulated rainfall(mm) for the experiment e) BMJ-Lin f) BMJ- Thompson g) GD-WSM3 h) G3-Kessleri) G3-Lin and j) G3-WSM3 of 08April 2010***

The model output was validated using TRMM 3B42 daily precipitation data (0.25 deg x 0.25 deg). The TRMM precipitation data was plotted in

Fig.3.11 and compared with model output: it is seen that the KF-WSM3 experiment brought out the best performance when compared with TRMM data.

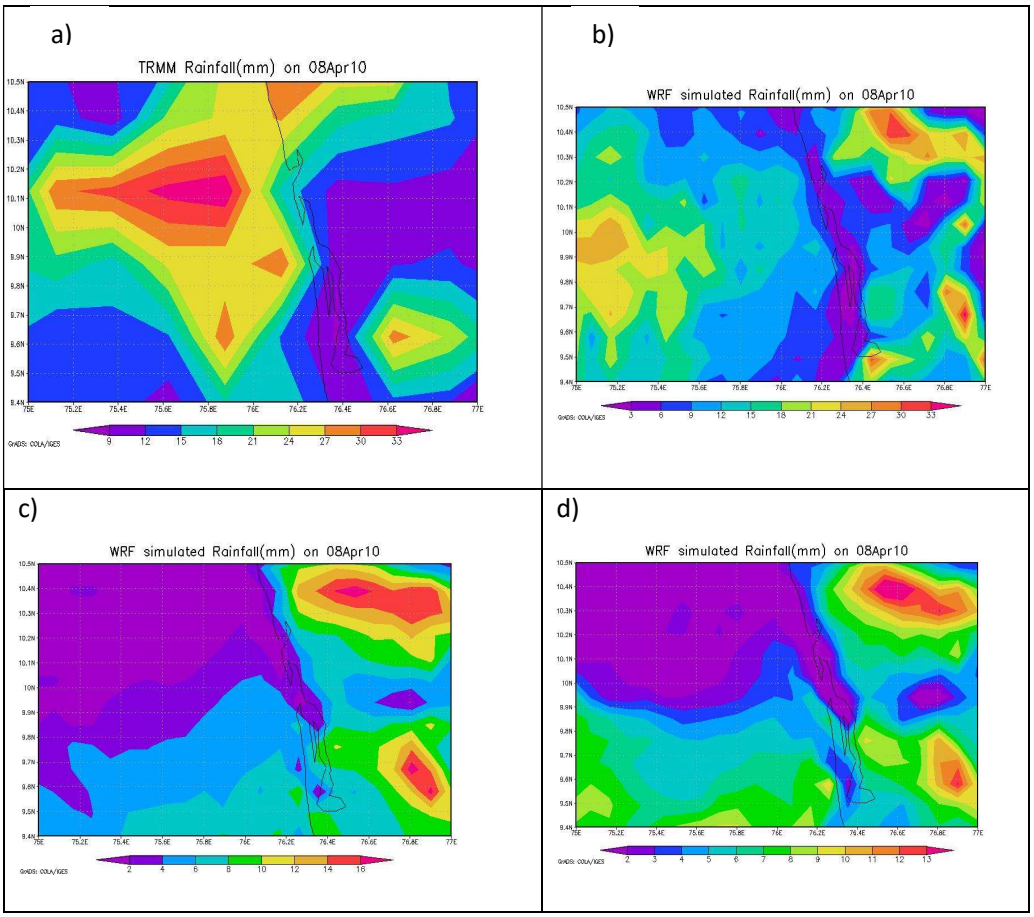


***Fig. 3.11: a) TRMM Rainfall (mm) b) WRF simulated rainfall for the experiment KF-WSM3 c) BMJ-Ferrier d)BMJ -WSM3 of 08April 2010***

Simulation of three more cases was conducted using WRF model in order to validate the best performance of this combination of Kain Fritsch cumulus parameterization scheme and WSM3 microphysics scheme.

## *Case 1: 18th April 2009*

The model could bring out the mesoscale rainfall variations within a district with good accuracy when it was run with Kain-Fritsch cumulus parameterization scheme and WSM 3 class simple ice microphysics scheme [Fig.3.12]. The model rainfall is compared with AWSs data and is in good agreement with the observed values.

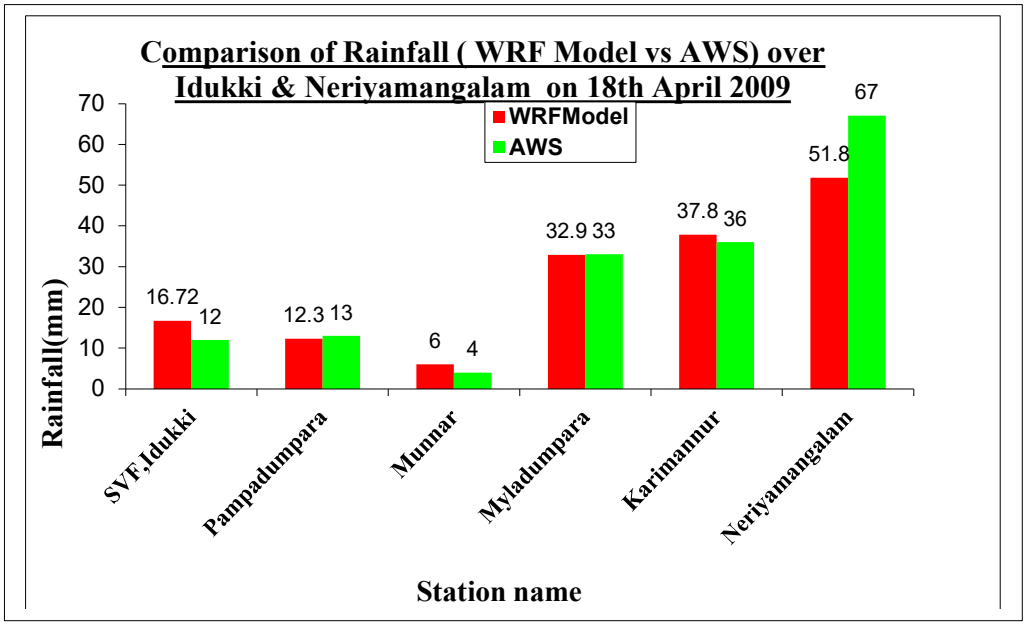


Fig.3.12: Comparison of WRF model simulated rainfall with AWS recorded rainfall on 18th April 2009

## *ii) Case 2: 5th May 2009*

The WRF model was run with the combination of Kain-Fritsch cumulus parameterization scheme and WSM-3 class simple ice scheme and the model output was compared with AWS rainfall for the 4 districts of northern Kerala [Kannur, Kozhikode, Wayanad and Idukki] on 5th May 2009 and the comparison is given in Fig.3.13.The analysis clearly shows that the model output matches well with the AWS observations.

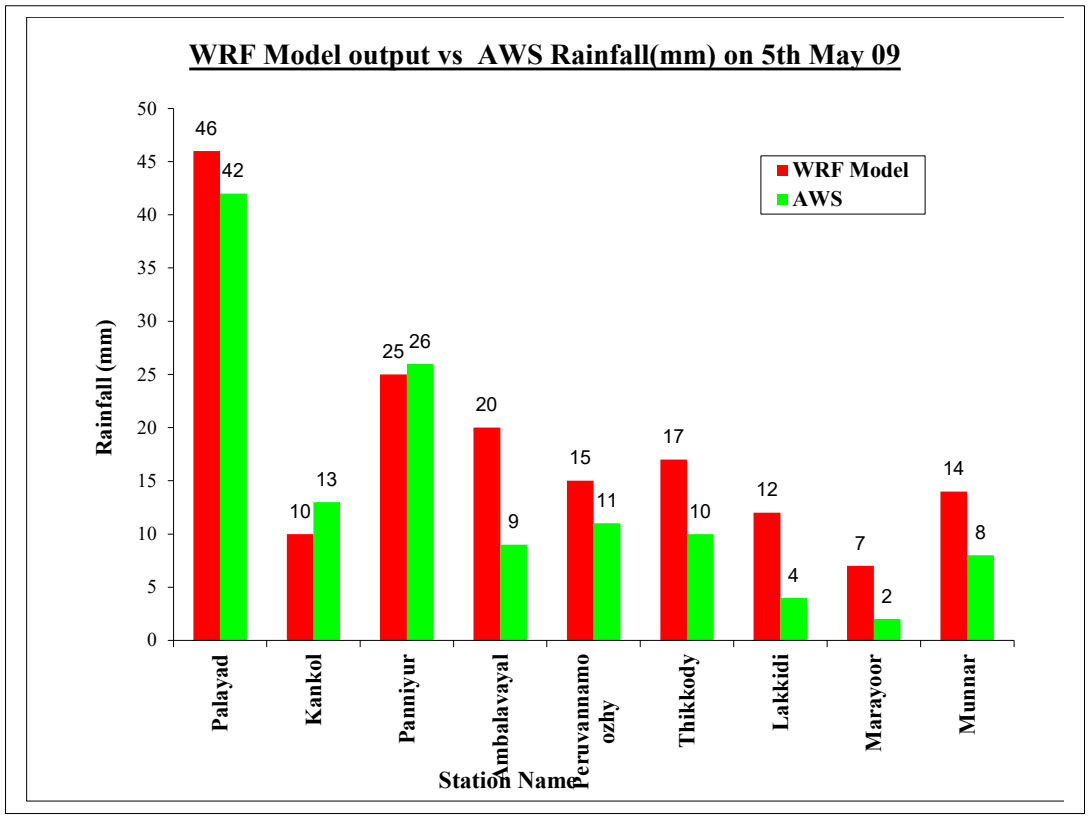


Fig.3.13: Comparison of WRF model simulated rainfall with AWS recorded rainfall on 5th May 2009

The results are in good agreement with the observational data(AWS data) which shows that the combination of Kain-Fritsch cumulus scheme and WSM 3-class simple ice scheme could successfully simulate severe convective events. The model rainfall data is again validated by comparing with IMD observations (Fig.3.14a) and they are also in good agreement with each other. The satellite imagery of 18th April 2009 and 5th May 2009 is shown in Fig.3.14 b.

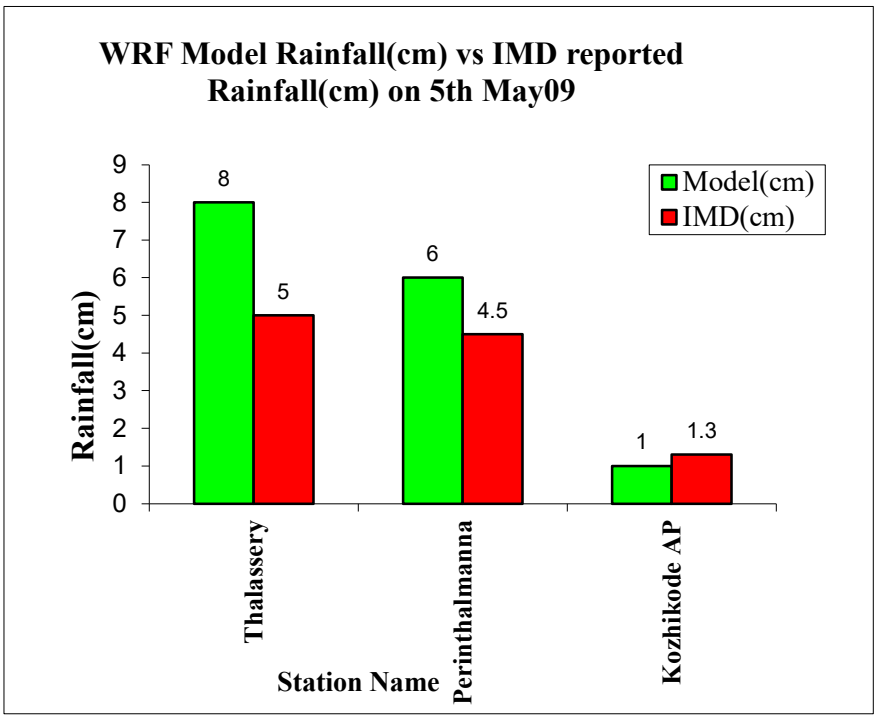


Fig.3.14 a: Comparison of WRF model simulated rainfall with IMD recorded rainfall on 5th May 2009

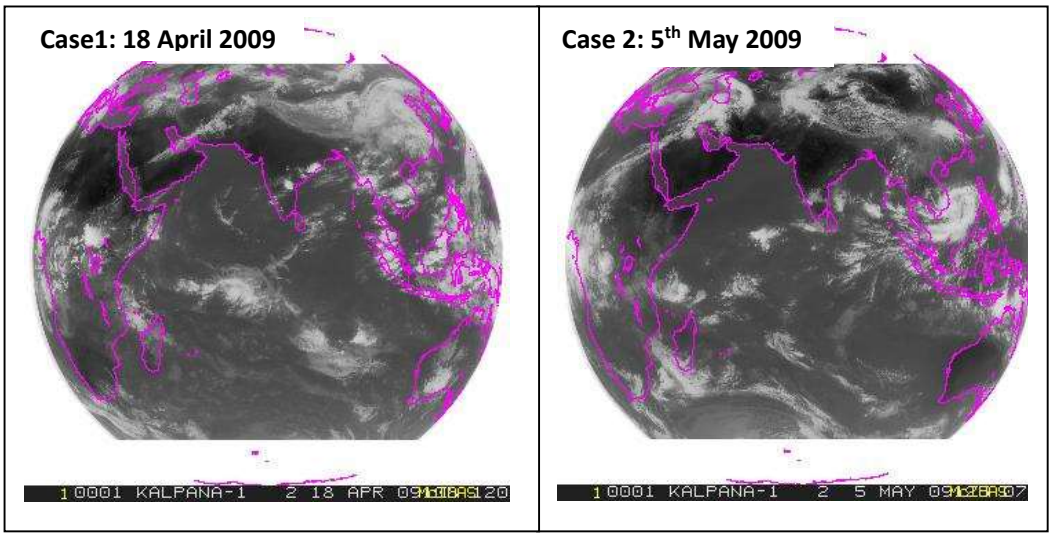


Fig.3.14 b: Satellite imagery of 18th April 2009 and 5th May 2009

**iii)** ***Case 3: Cyclone AILA (23rd May09-25th May 09)***

Another experiment was carried out to check whether the identified best combination of cumulus and microphysics schemes can be used for the prediction of large scale systems over Indian ocean especially Bay of Bengal. ***Cyclone AILA*** which hit West Bengal on 06Z of 25th May 09 was selected for the study. The satellite imagery of 06Z 25th May 09 is shown in Fig.3.14c. The model was initialized with NCEP GFS data to understand the predictability of severe weather events. The WRF model was run with a higher horizontal resolution of 5 km.

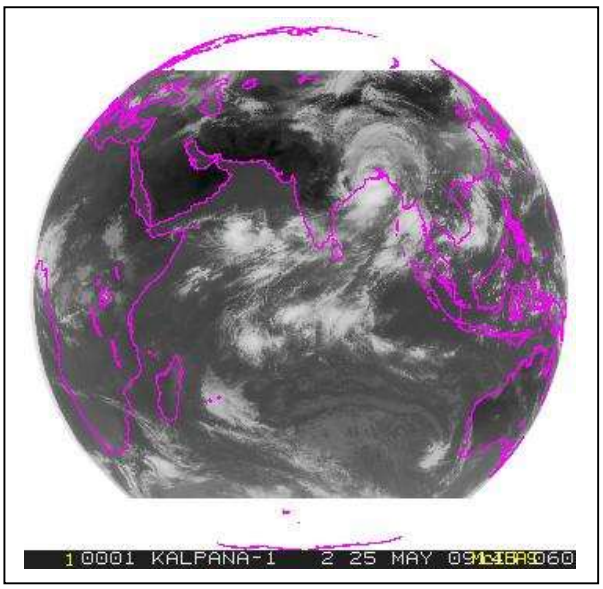


Fig.3.14c : Satellite imagery of 06Z 25May 09

The model predicted Mean Sea Level Pressure (MSLP) and surface wind for 06Z 25May 09 with the initial condition of 00Z 22May 09 is shown in Fig.3.17 and it can be seen that the central pressure is around 975 hPa with

a wind speed of 100 km/hr. As per reports, the lowest pressure recorded was 974 hPa and the wind speed was 100 km/hr. So the model predicted pressure drop and the wind speed are in very good agreement with the observations. The model could perfectly predict the track of the Cyclone as well as the location of landfall accurately. The plots of predicted MSLP are given in Fig. 3.15- Fig.3.17. The model predicted rainfall for the three days are plotted and compared with TRMM Multi-Satellite Precipitation Analysis data and is given in Fig.3.18 – Fig 3.20. The model predicted 850hPa wind is plotted in Fig.3.21- Fig. 3.23.

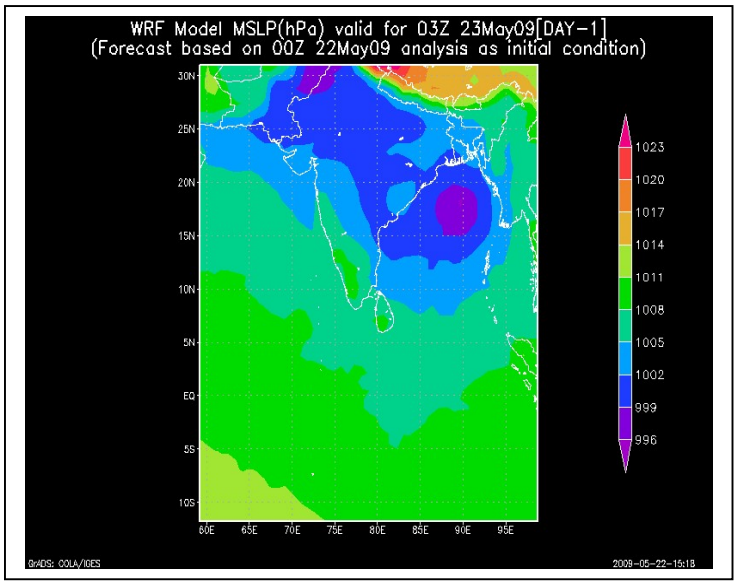


Fig 3.15: WRF model predicted Mean Sea Level Pressure (MSLP) valid for 03Z23May 09

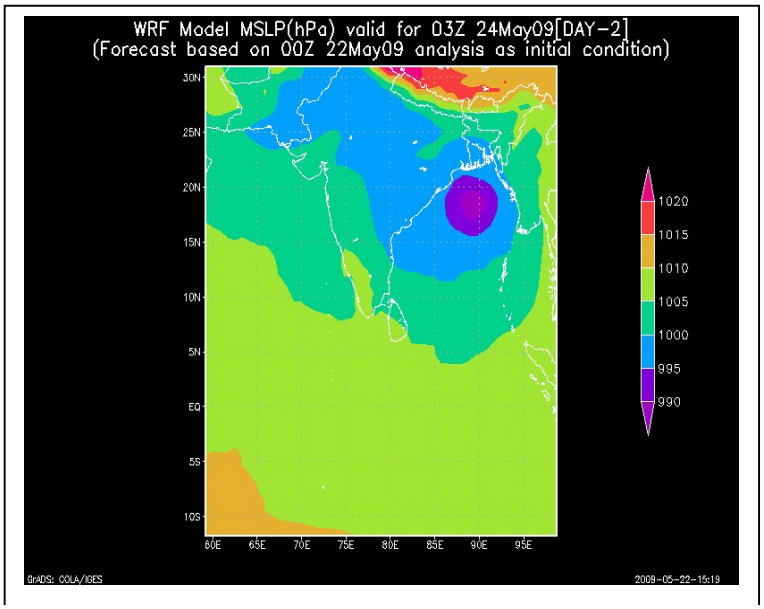


Fig 3.16: WRF model predicted Mean Sea Level Pressure (MSLP) valid for 03Z24May 09

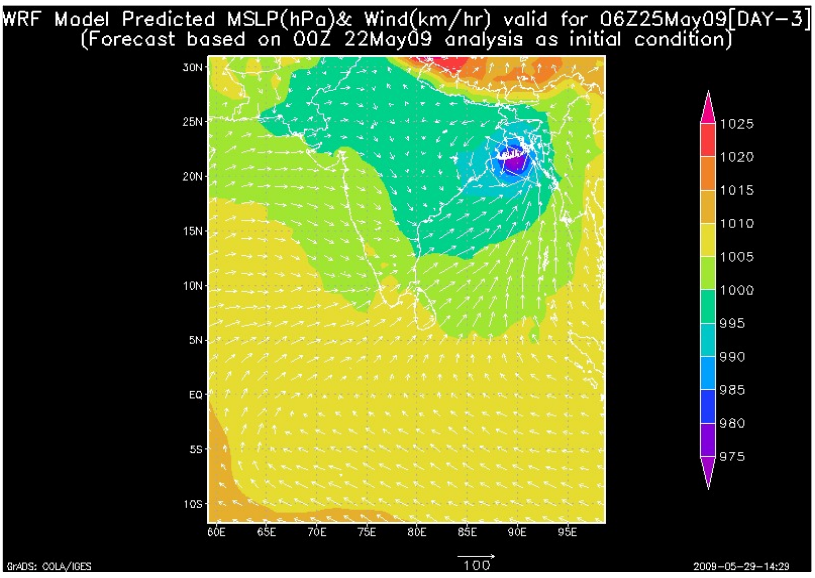


Fig 3.17: WRF model predicted Mean Sea Level Pressure (MSLP) and wind valid for 06Z25May 09

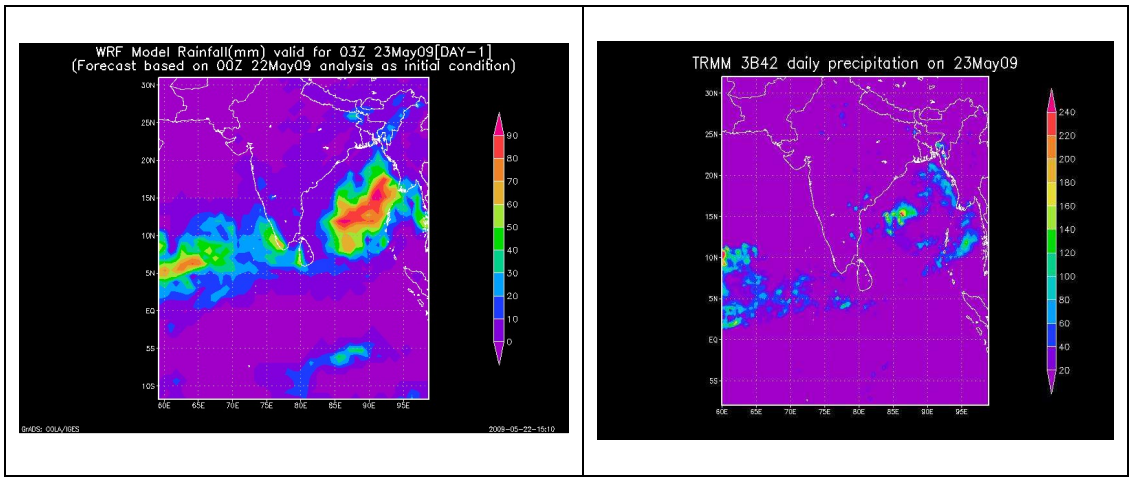


Fig 3.18: WRF model predicted rainfall (mm) vs TRMM rainfall of 23May 09

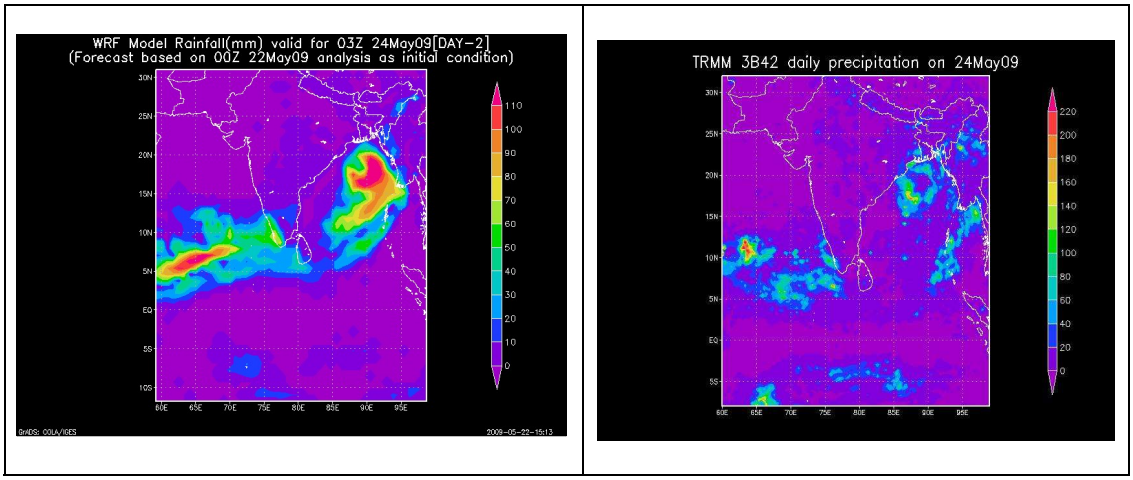


Fig 3.19: WRF model predicted rainfall (mm) vs TRMM rainfall of 24May 09

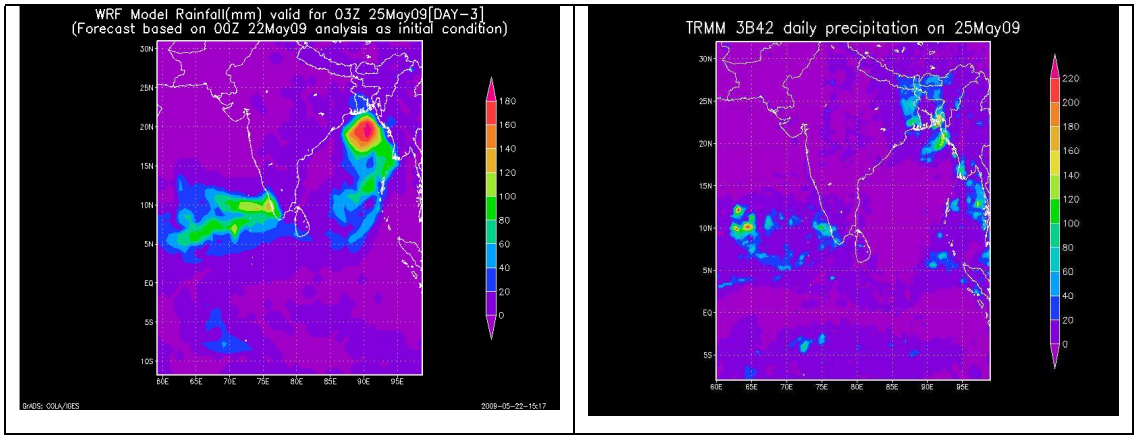


Fig 3.20: WRF model predicted rainfall (mm) vs TRMM rainfall of 25 May 09

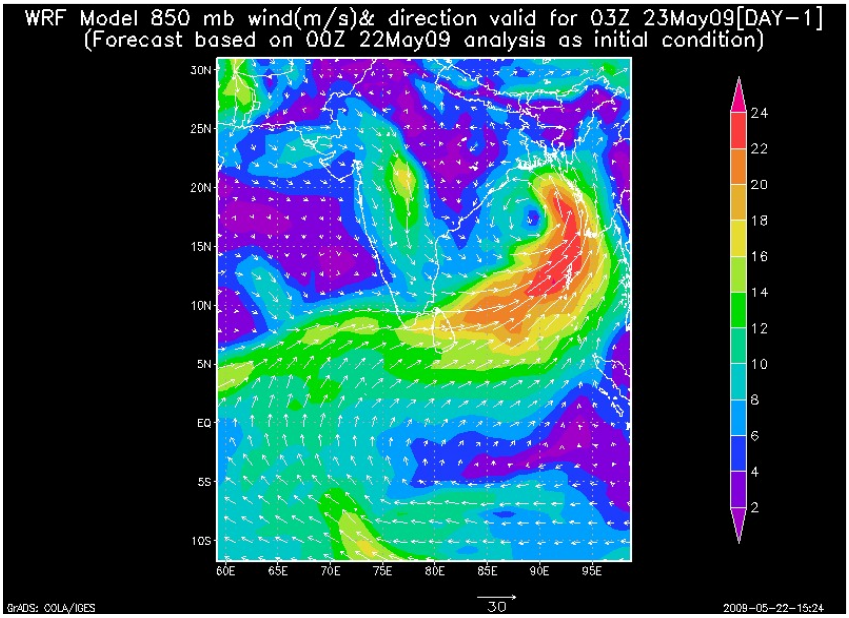


Fig 3.21: WRF model predicted 850 mb wind (m/s) valid for 03Z23May 09

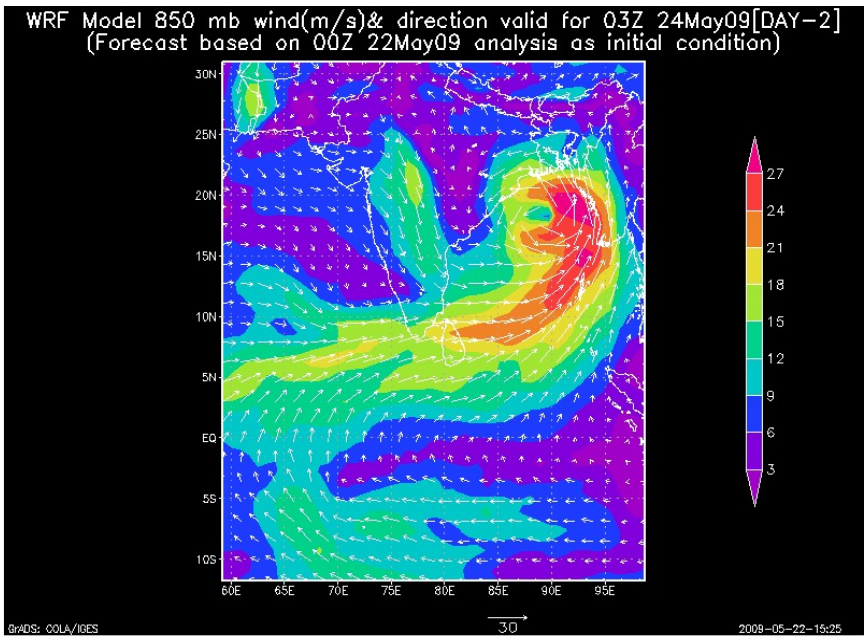


Fig 3.22: WRF model predicted 850 mb wind (m/s) valid for 03Z24May 09

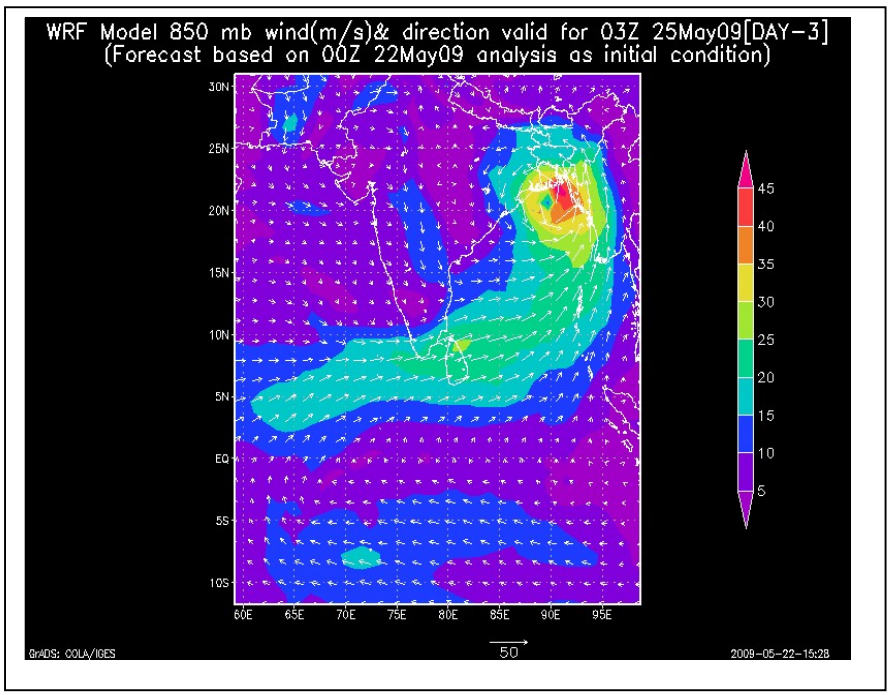


Fig 3.23: WRF model predicted 850 mb wind (m/s) valid for 03Z25May09

## 3.6 Conclusion/Summary

The WRF model was run with different combinations of cumulus and microphysics parameterization schemes in order to identify the best suitable combination of parameterization schemes. The study could identify the combination of Kain-Fritsch cumulus parameterization scheme and WSM 3-class simple ice microphysics scheme as the best suitable parameterization scheme for the prediction of weather systems over Indian region. After identifying the best combination of parameterization schemes, the model was run for different events over Indian region and validated the results with TRMM 3B42 daily precipitation data and AWS data. The model results are in good agreement with the observations. Again the model was run with a higher horizontal resolution of 5 km in order to check the predictability of the identified combination of parameterization schemes. ***Cyclone AILA*** which hit West Bengal on 06Z of 25$^{th}$ May 09 was selected for the model run. The model was initialized with 00UTC 22 May2009 NCEP Global Forecast (GFS) data and integrated for 72 hours. The model predicted wind and MSLP are in good agreement with the observations and the model could predict the event with good accuracy 3 days ahead.

WRF model with a fine horizontal resolution (5 km) and the combination of Kain-Fritsch cumulus parameterization scheme and WSM 3-class simple ice microphysics scheme could predict the occurrence of Cyclone AILA three days ahead with very good accuracy. Hence the study concludes that the identified combination of parameterization schemes are the best combination for the prediction as well as understanding of mesoscale as well as large scale systems over the Indian region.

# Chapter 4

# Observational and modelling study of the structure, evolution and propagation of a supercell tornadic thunderstorm over Odisha.

The observational and modelling study of the dynamics of a severe tornadic thunderstorm that occurred over Odisha on 31 March 2009 is presented in this Chapter.

## 4.1 Case description and Overview

A tornado accompanied with thunderstorm, rainfall and hailstorm affected Rajakanika block of Kendrapara district of Odisha in the afternoon of 31st March 2009. This tornadic thunderstorm occurred on 31 March 2009 affected 14 villages of Rajakanika block of Kendrapara district in Odisha. Fig.4.1 shows the tornado affected villages of Kendrapara district. This was one of the severe tornadoes occurred over Indian region which caused immense devastation to life and property. The special features of this tornado are as follows. (i) It was embedded in a thunder squall line. (ii) According to Doppler Weather Radar (DWR), Kolkata, the convective cloud cluster moved from north-northwest to south-southeast during its genesis, growth and mature stage like a Norwester. It is almost supported by the orientation of the area affected by the tornado. (iii) The convection developed after 1430 hrs IST and dissipated over the sea by 1730 hrs IST with a life period of less than three hours. The tornado survived for about 10 minutes, hitting ground at 1640 hrs IST, according to eye witnesses.

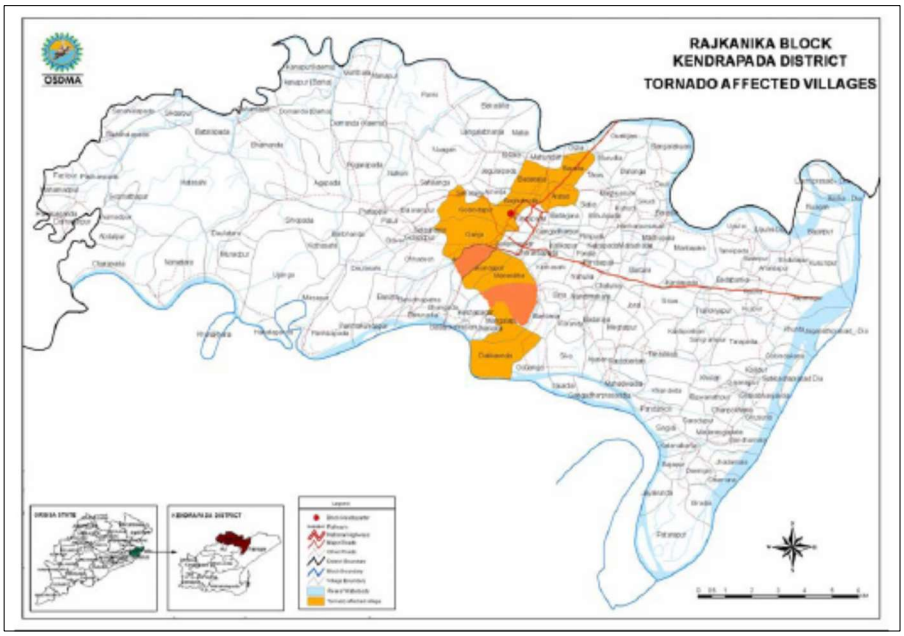


Fig. 4.1: Tornado affected villages of Kendrapara district of Orissa

## 4.2 Synoptic situation (as per IMD observations)

A well-marked trough of low-pressure area with associated upper air trough in lower levels from Jharkhand to Rayalaseema across interior Odisha coupled with strong pressure gradient towards the east and upper tropospheric divergence over the region at 0530 hrs 1ST of 31st March, 2009 was the synoptic system leading to the tornado in the afternoon. The pressure departure from normal at 0830 hrs IST was about -4 hPa near the tornado site. Considering the stream line analyses at 0530 hrs IST of 31st March 2009, an upper air trough ran from Jharkhand to Rayalaseema across interior Odisha and Telangana at 0.9 km above mean sea level. There was an anti-cyclonic circulation in this level over west central Bay of Bengal off Andhra Pradesh coast. It led to moisture incursion over the region in lower levels. At 700 hPa level, the trough extended from Bihar to north Odisha. Similar trough also

prevailed in mid-tropospheric level. All these indicated that there was strong horizontal positive vorticity over the region. The upper tropospheric wind pattern at 300 hPa level indicated that there was a deep upper tropospheric westerly trough to the left of the tornado site at 00 UTC of 31st Mar 2009 and hence the tornado site was associated with upper tropospheric divergence in the wind field

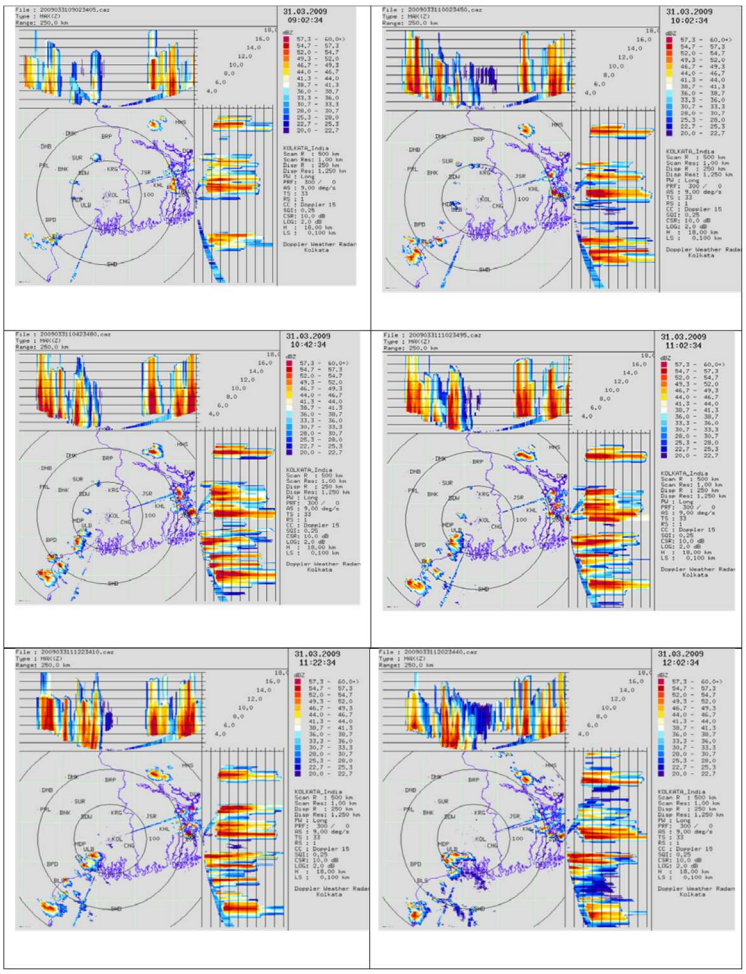

Fig. 4.2: The Doppler Weather Radar (DWR) imageries of Kolkata from 0900Z - 1200Z 31March 2009

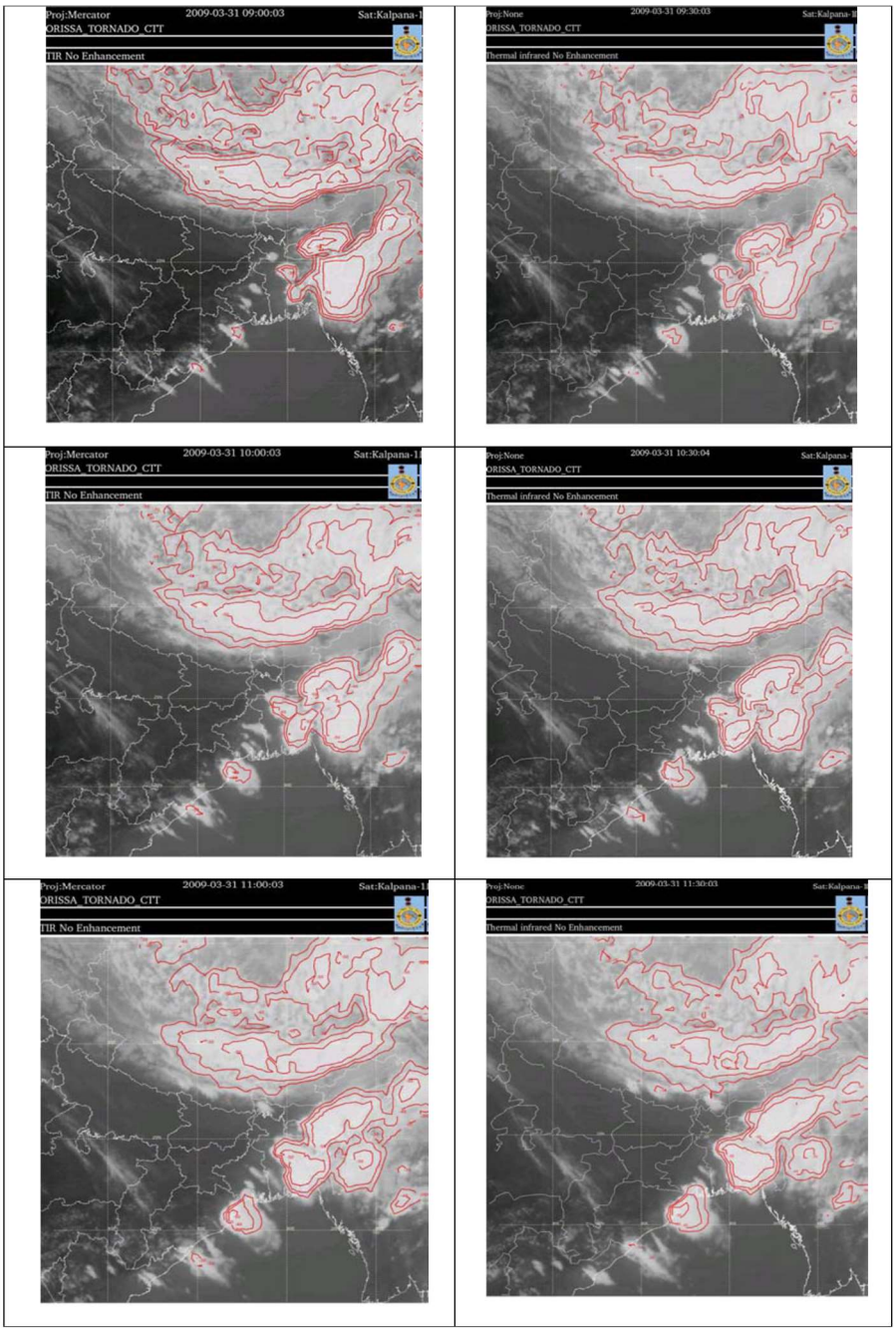


Fig.4.3: Half hourly INSAT IR imageries embedded with cloud top temperature ($^0$C) contours over east and northeast India during 0900 to 1100 UTC of 31st March 2009

Fig.4.2 shows the Doppler Weather Radar (DWR) imageries of Kolkata from 0900Z - 1200Z 31March 2009. According to these imageries, a severe thunderstorm was formed during 1530 to 1730 hrs IST over the tornado site. The height of the cumulonimbus cloud was about 14 km and the reflectivity was exceeding 55 dBz. The half hourly INSAT IR imageries embedded with cloud top temperature ($^0$C) contours over east and northeast India during 0900 to 1100 UTC of 31st March 2009 is shown in Fig.4.3. These imageries indicate that the convective cloud cluster moved from northwest to southeast and dissipated over the sea off Kendrapara coast. The imageries further indicate that there was a squall line with a number of embedded convective cloud clusters distributed from northeast to southwest across north-eastern states, Bangladesh, Gangetic West Bengal and coastal Odisha. There were two major convective cloud clusters, viz., over the tornado site and neighbourhood and over eastern Bangladesh and neighbourhood. This kind of distribution of convection was in well agreement with the synoptic situation. The convection was lying in the same orientation as the trough in lower levels. However, the convection lay to the eastern side of the trough.

### 4.3 Experimental setup and Model configuration

In this study, the Weather Research Forecast (WRF) model is run with three nested domains with a horizontal resolution of 9 km in the outer domain, 3 km in the middle domain and 1 km in the innermost domain. The simulation domain set up by the WPS program for a tornadic thunderstorm over Odisha on 31 March 2009 is shown in fig 3.4. The first domain is referred as D1, the second domain as D2 and the third domain as D3.

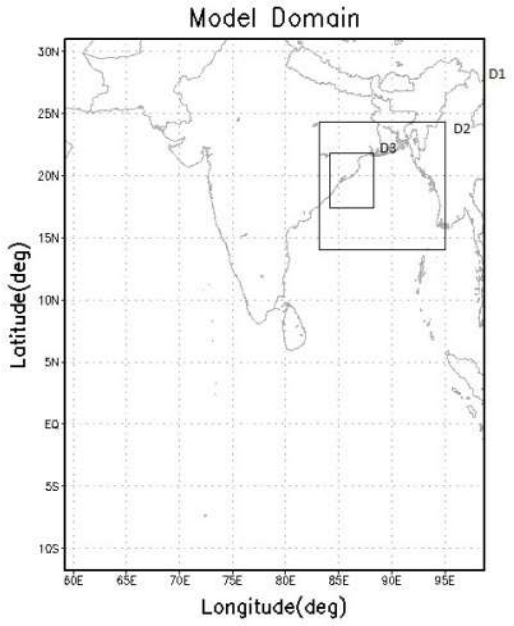


Fig.4.4: Two-way nested domains configured for the simulation of a severe tornadic thunderstorm occurred over Orissa on 31 March 2009. D1, D2, D3 refers to the first, second and third domain.

Two-way nesting technique with three domains are selected for simulating this event with a horizontal resolution of 1 km for the innermost domain. The model is run using the Kain-Fritsch (new Eta) scheme for cumulus parameterization (Kain and Fritsch 1993), Yonsei University (YSU) scheme for the boundary layer parameterization (Hong et al. 2006; Hong 2010), WSM 3 class simple ice scheme for microphysics (Hong et al. 2004) and Rapid Radiative Transfer Model (RRTM) for long wave radiation (Mlawer et al. 1997) and Dudhia scheme for short wave radiation (Dudhia 1989). The grid staggering is the Arakawa C-grid. The model used the Runge-Kutta 2$^{nd}$ and 3$^{rd}$ order time integration schemes, and 2$^{nd}$ to 6$^{th}$ order advection schemes in both the horizontal and vertical. It uses a time-split small step for acoustic and gravity-wave modes.

## 4.4 Data used

The initial and lateral boundary conditions for the model run was taken from the Final (FNL) Operational Global Tropospheric Analyses of National Centre for Environmental Prediction (NCEP) on $1^0$ x $1^0$ grids prepared operationally every six hours. This FNL dataset is developed from the Global Data Assimilation System (GDAS), which continuously collects observational data from the Global Telecommunications System (GTS) and other sources. The United States Geological Survey (USGS) Global dataset with 30 sec horizontal resolution were used to create terrain/topography and landuse/vegetation fields. Half hourly INSAT IR imageries (KALPANA-1) embedded with cloud top temperature ($^0$C) contours over east and northeast India as well as the composite reflectivity imageries from Doppler Weather Data, Kolkata of India Meteorological Department (IMD) were also utilised in this study to observe the occurrence and evolution of this event.

## 4.5 Results and Discussion

The observational and modelling study of a severe tornadic thunderstorm that occurred over Odisha on 31 March 2009 was carried out. This event affected 14 villages of Rajakanika block of Kendrapara district on 31March 2009. The model could simulate the event with a reasonable degree of accuracy both spatially and temporally. The present study has been carried out in order to understand the structure and evolution of a severe tornadic thunderstorm as well as the changes occurring in the atmosphere during a severe thunderstorm.

The genesis and growth of cells, their horizontal distribution, vertical structure, direction of motion and speed of their movement, time of dissipation etc are well studied through the simulated output fields such as

reflectivity, vertical velocity, vorticity etc and they are clearly depicting the spatial distribution and temporal evolution of clouds. The dynamical changes occurring in the atmosphere especially prior and during the event are analysed and plotted for a better understanding of the phenomenon.

### *Structure and evolution of the convective system*

### *a) Reflectivity analysis*

The model simulated longitude-wise vertical cross-section of reflectivity and u-w wind for every 10 minutes have been plotted and shown in Fig.4.5 to Fig .4.7. The model simulated reflectivity reveals that a convective system consisting of two cells were formed at 0840 UTC. The convective system extended up to 8 km in the vertical with a horizontal span of 25 km by 0900 UTC. The cells merged and became more organized by 0920 UTC. The system started propagating towards east by 0930 UTC and reached a vertical extent of 11 km by 1000 UTC: the convective system reached its mature stage by 1030 UTC. A new cell was generated to the westward side of the main convective system by 1040 UTC. The generated cell started growing and reached up to the middle troposphere by 1050 UTC and a severe tornado was generated at the location of the new cell by 1100 UTC. The WRF simulated reflectivity (dBz) and wind (m/s) at different vertical levels is plotted in Fig.4.8. The horizontal reflectivity at 1000 UTC is plotted for 8 different vertical levels ie, at 1.5 km, 2 km, 3 km, 5.5 km, 6 km, 7 km, 8 km and 10 km. The reflectivity profile at different levels reveals the vertical extent of the convective system as well as the spatial distribution of cloud cover in each vertical level thereby providing an overall distribution of the convective system in the troposphere. The horizontal winds are plotted for all these levels and and it is seen that horizontal winds of speed greater than 50 m/s existed from 8 km to 10 km. A horizontal wind of speed greater than 30 m/s

is observed between 6 - 7 km. The WRF simulated vertical cross-section of reflectivity (plotted for every 10 minutes) with a horizontal resolution of 1 km clearly shows the evolution of the system from 0830Z-1100Z.

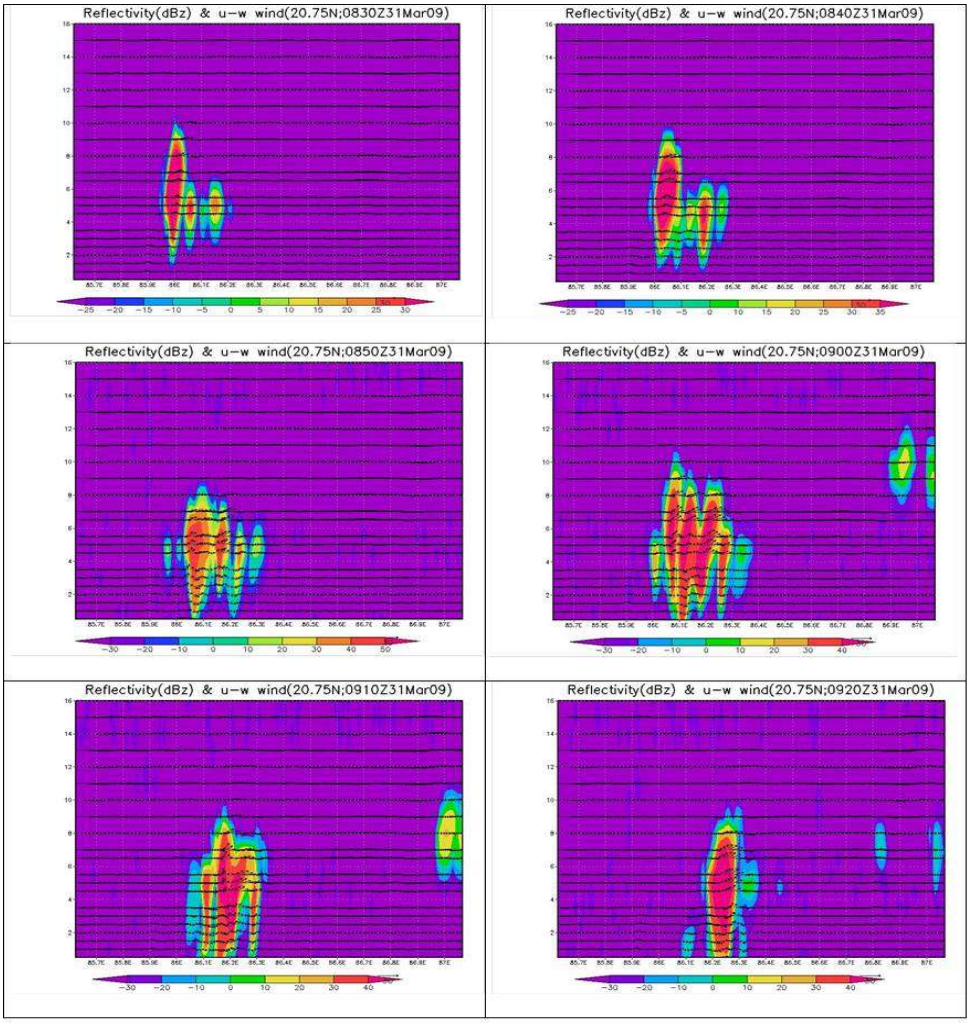


Fig. 4.5: WRF simulated longitude-wise vertical cross-section of reflectivity and u-w wind from 0830 UTC– 0920 UTC

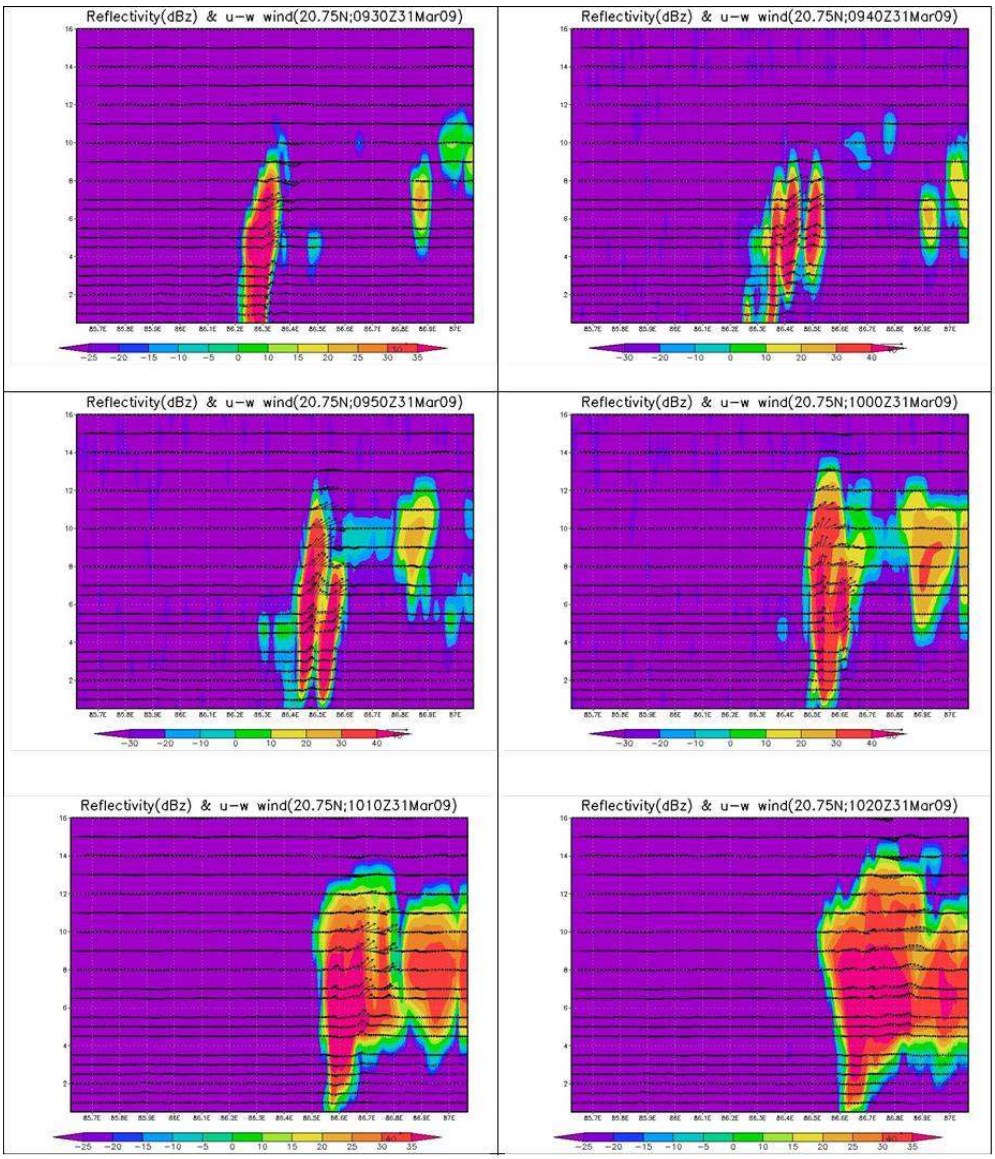


Fig 4.6: WRF simulated longitude-wise vertical cross-section of reflectivity and u-w wind from 0930 UTC – 1020 UTC

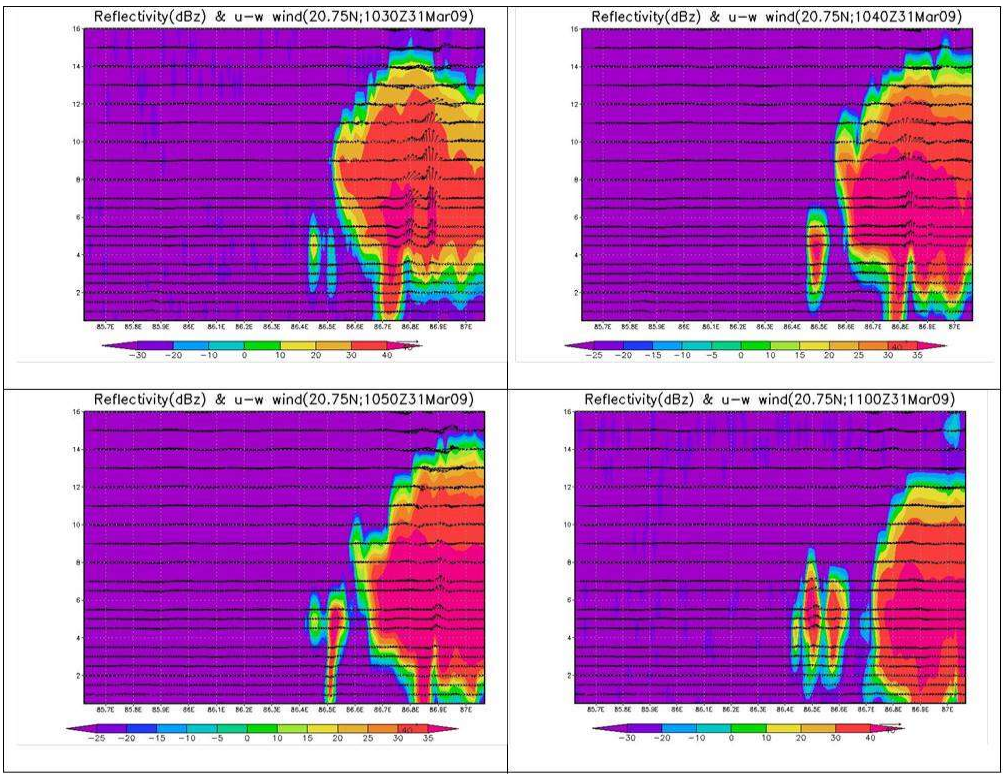


Fig. 4.7: WRF simulated longitude-wise vertical cross-section of reflectivity and u-w wind from 1030 UTC – 1100UTC

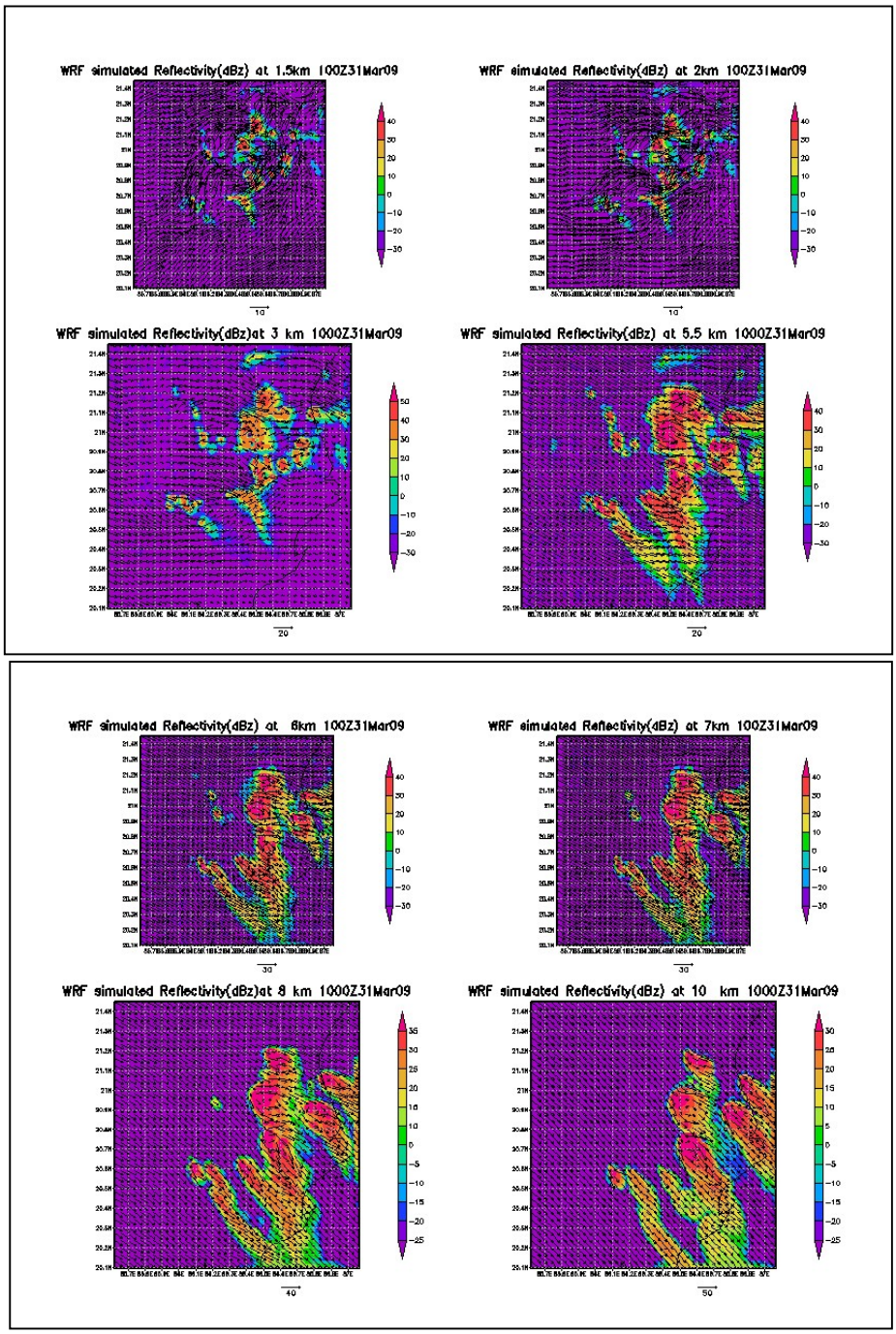


Fig. 4.8: WRF simulated reflectivity(dBz) and wind(m/s) at different vertical levels

### *b) Vorticity analysis*

The WRF simulated latitude-wise vertical cross-section of vorticity is plotted and analysed (Fig.4.9). Two positive vorticity centres exceeding a vertical vorticity of 0.01 $s^{-1}$ are observed at 1000 UTC which were centred at 20.75 N and 20.90 N and the positive vorticity region extends vertically from 6 km to 12.5 km. A very high positive vorticity of 0.01 $s^{-1}$ observed during the evolution of the thunderstorm at 1000Z indicating a mesocyclone formation : this is a unique characteristic of a supercell. A strong negative vorticity of - 0.01 $s^{-1}$ is observed from 3.5 km to 7 km which is centred at 20.8 N. A double vortex is formed from 6.5 km to 12.5 km with its convective core at 11 km.

The WRF simulated longitude-wise vertical cross-section of vorticity is plotted (Fig.4.10) and it is observed that a strong positive vorticity of 0.01 $s^{-1}$ extending from 6 km - 10 km in the vertical and is centred at 86.5 E and a strong negative vorticity of -0.01 $s^{-1}$ is observed at the eastward side of positive vorticity region which extends from 7 km -11 km in the vertical and centered at 86.55 E. The analysis of model simulated vorticity in the mid and upper troposphere clearly shows the presence of a double vortex circulation. The presence of mesocyclonic rotation clearly characterizes a supercell and it is playing a vital role in the evolution and structure of a supercell thunderstorm.

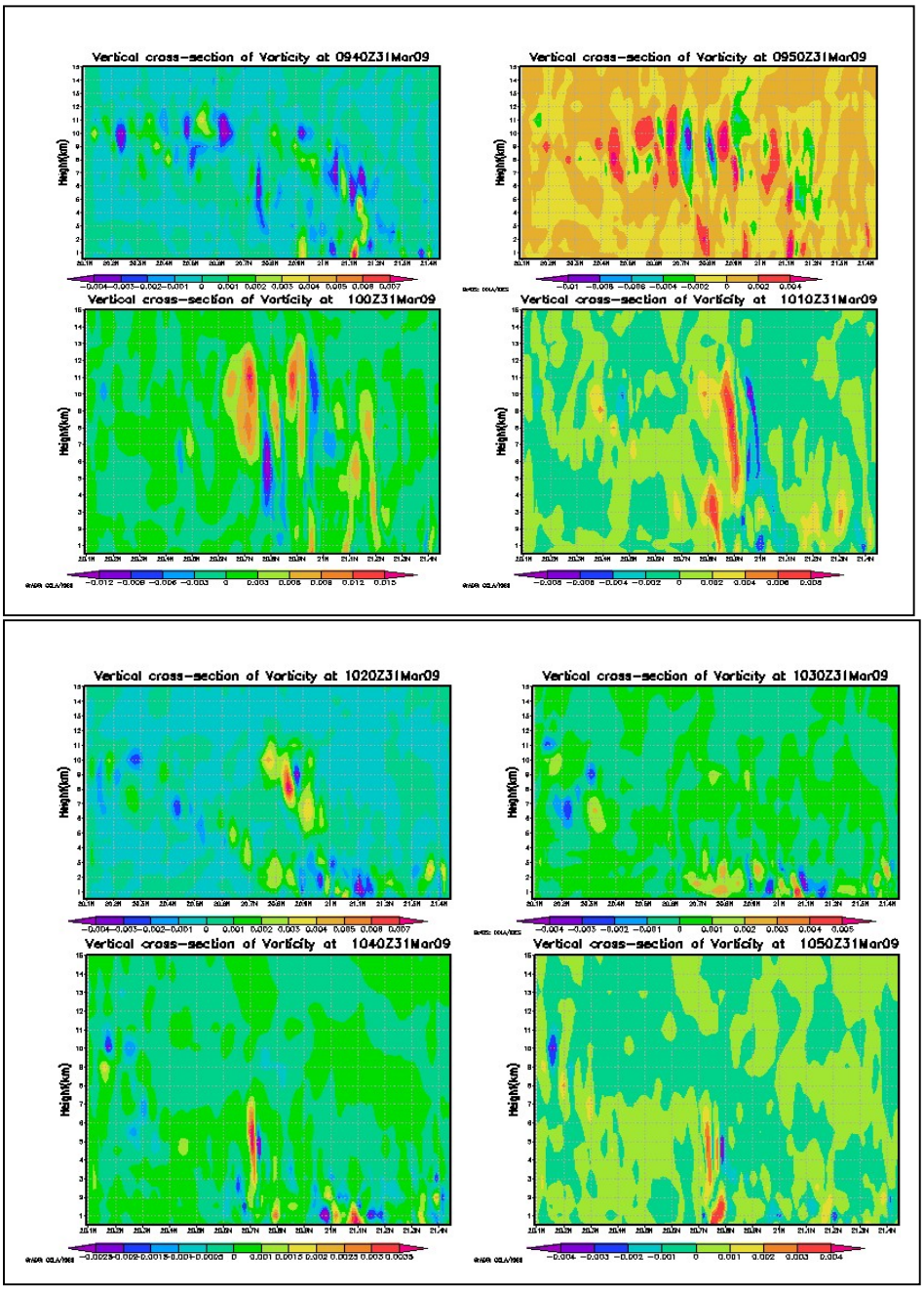


Fig.4.9 : WRF simulated latitude-wise vertical cross-section of vorticity from 0940UTC – 1050UTC

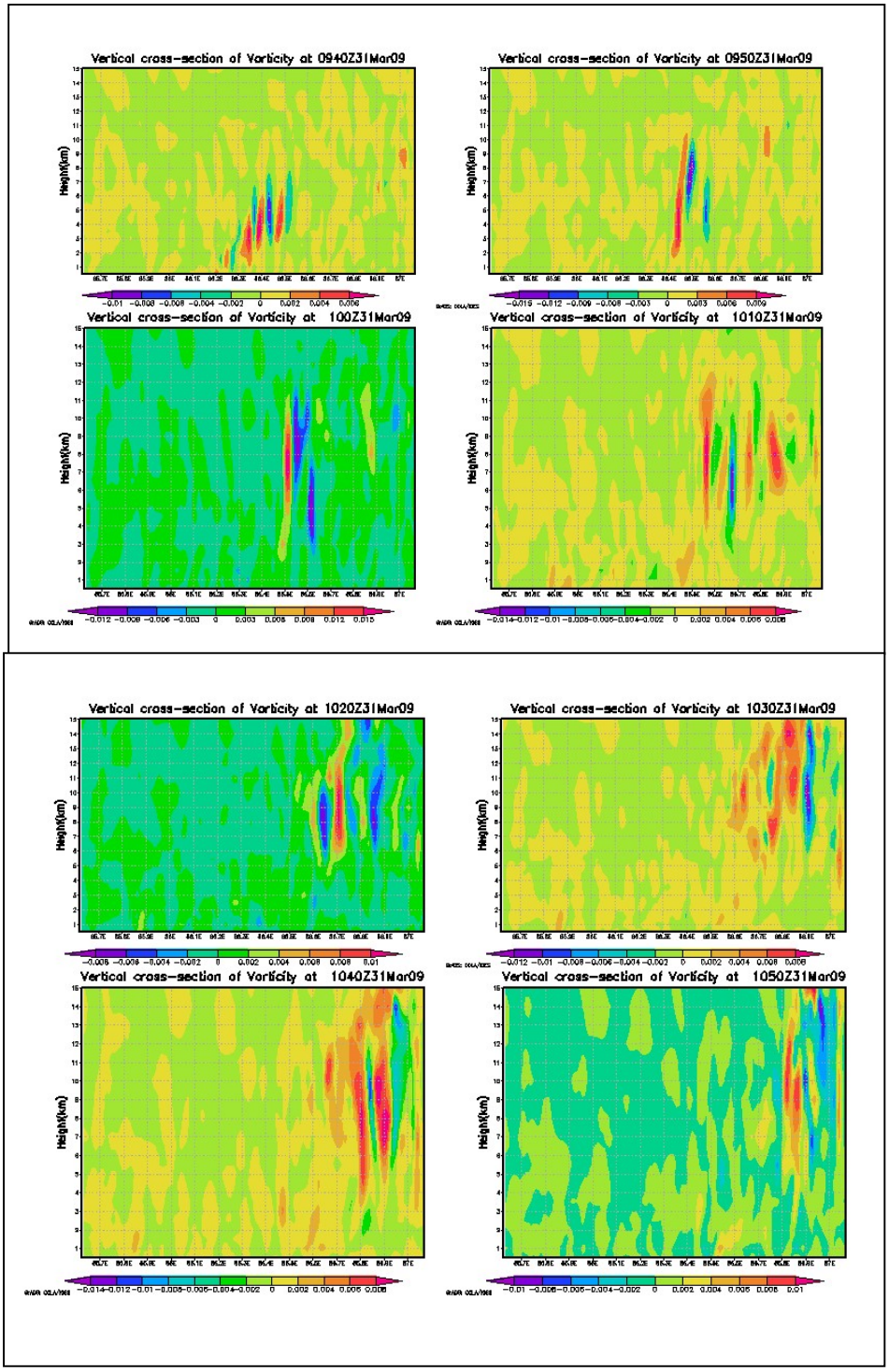
Vertical cross-section of Vorticity at 0940Z31Mar09
Vertical cross-section of Vorticity at 0950Z31Mar09
Vertical cross-section of Vorticity at 100Z31Mar09
Vertical cross-section of Vorticity at 1010Z31Mar09
Vertical cross-section of Vorticity at 1020Z31Mar09
Vertical cross-section of Vorticity at 1030Z31Mar09
Vertical cross-section of Vorticity at 1040Z31Mar09
Vertical cross-section of Vorticity at 1050Z31Mar09
Height(km)

### *c) Vertical velocity analysis*

The WRF simulated longitude wise distribution of vertical velocity during the the event has been plotted (Fig.4.11-4.12a,b). The updraft, downdraft as well as temporal evolution of vertical velocity are studied. By 0940 Z, a vertical velocity of 10-16 m/s is found at a height of 4-8 km at $86.4^0$E and it increased upto 15-27 m/s vertically extending the system upto 10.5 km at $86.5^0$E by 0950Z. A very high vertical velocity of 30 m/s is observed at a height level extending from 7.5 km to 10 km at $86.5^0$E at 1000Z and after 10 minutes the system shows an eastward propagation with its upward motion centered at $86.7^0$E at a height level extending from 4 -10.5 km. A positive vertical velocity of 20-25 m/s is observed at $86.9^0$E vertically extending from 7-11 km and a negative vertical velocity of -10 m/s is observed at $86.85^0$E at a vertical level between 13-16 km which shows the co-existence of updrafts and downdrafts. The temporal evolution of vertical velocity, reflectivity (dBz) and wind (m/s) at $20.75^0$N; $86.52^0$E is plotted in fig 4.13. The reflectivity at 1000 GMT shows the vertical extent of the convective system from 1.5 km - 11.5 km with a high vertical velocity of 30 m/s at 9 km above mean sea level. A vertical velocity of 25 m/s exists between 7 km -11 km.

WRF simulated reflectivity and u-w wind at $20.75^0$N at 1030Z 31Mar09 are plotted in Fig 4.14 which clearly shows the vertical structure, updraft and downdraft of a mature thunderstorm. Vertically integrated liquid water (VIL) during the event is plotted in order to understand the intrinsic dynamics of the convective clouds. Fig. 4.15 shows the VIL mixing ratio at 10Z31Mar2009. The temporal evolution of wind at various levels (Time-height cross-section) is plotted. Fig. 4.16 shows the time-height cross-section at 0900Z-1130Z 31 Mar2009. A change in wind speed and direction is observed at 1000Z in the upper troposphere extending from 6 km -12 km. A

cyclonic rotation can also be seen from the surface upto 2 km at 1100Z which corresponds to the time of occurrence of the tornado.

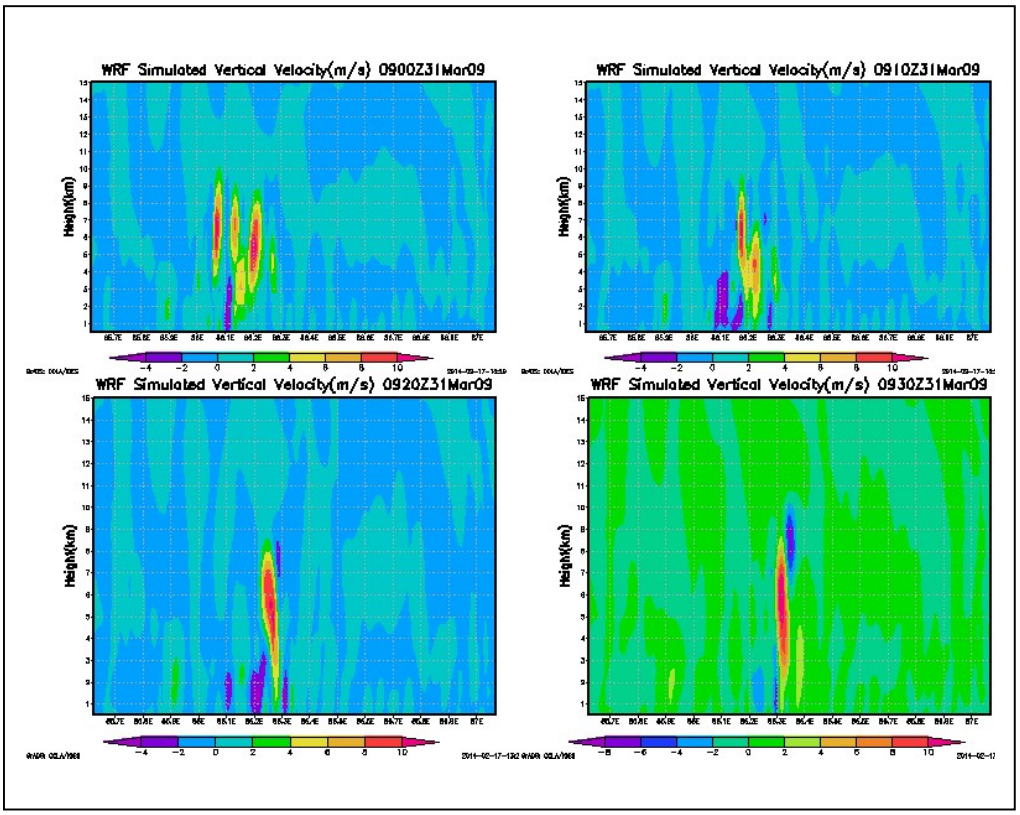


Fig.4.11 : WRF simulated longitude-wise vertical velocity from 0900UTC-0930UTC

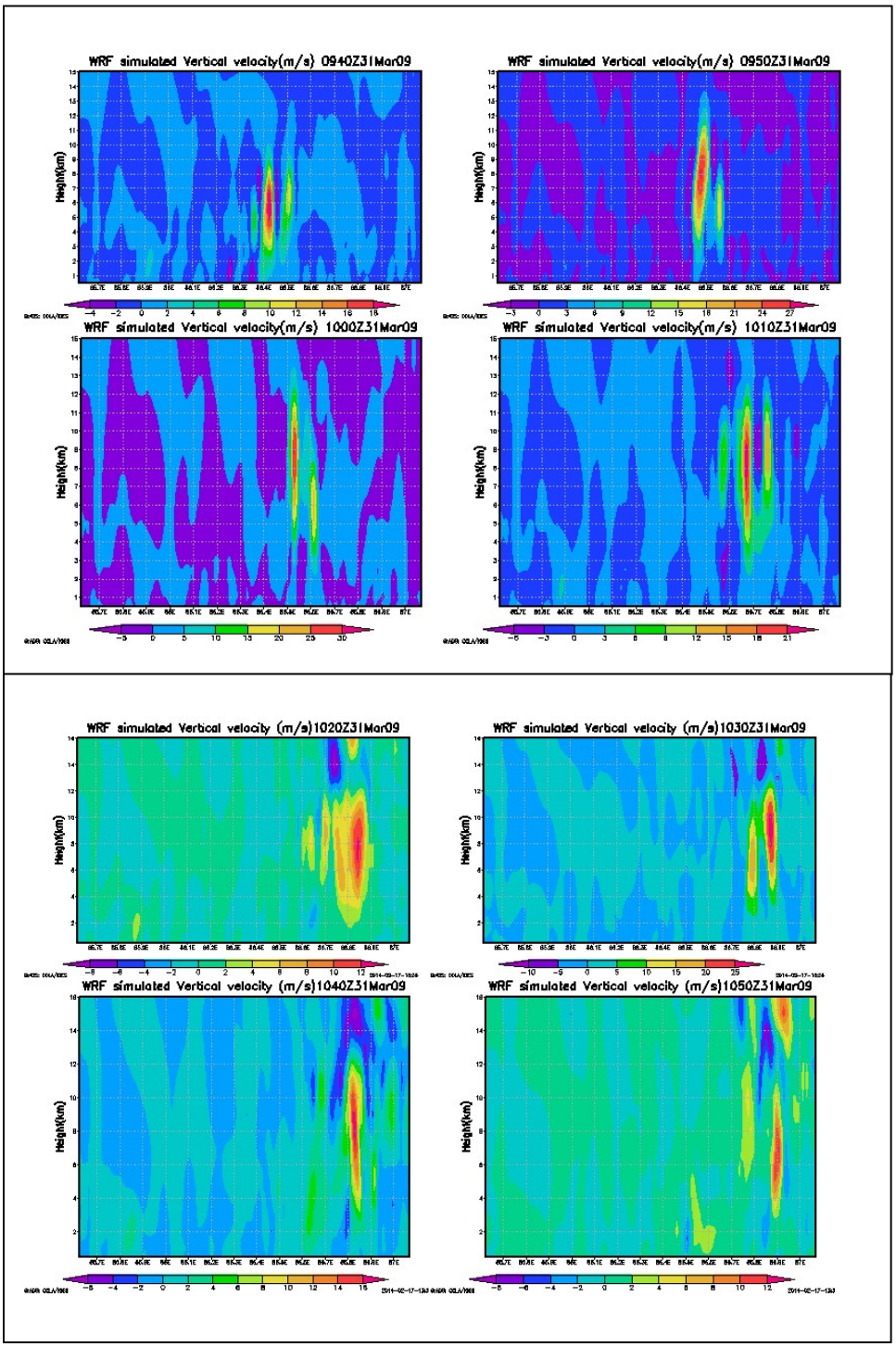


Fig.4.12a: WRF simulated longitude-wise vertical velocity from 0940Z – 1010Z

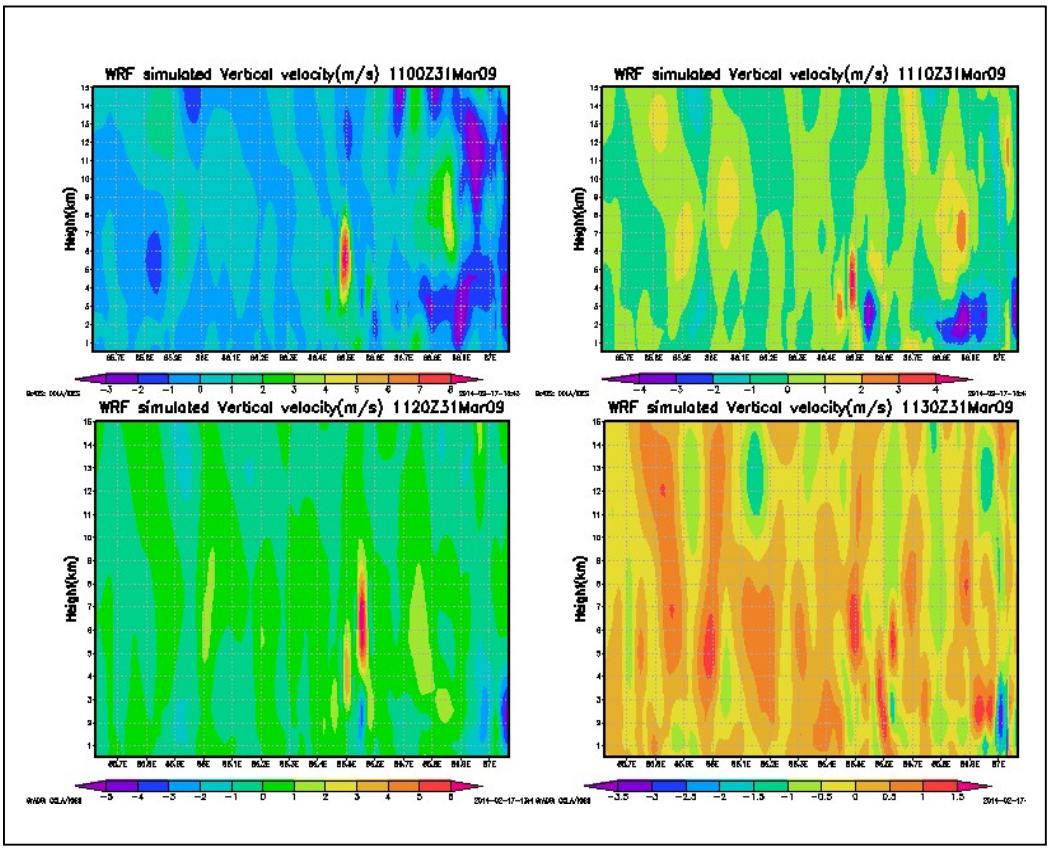


Fig. 4.12b: WRF simulated longitude-wise vertical velocity from 1020Z – 1130Z

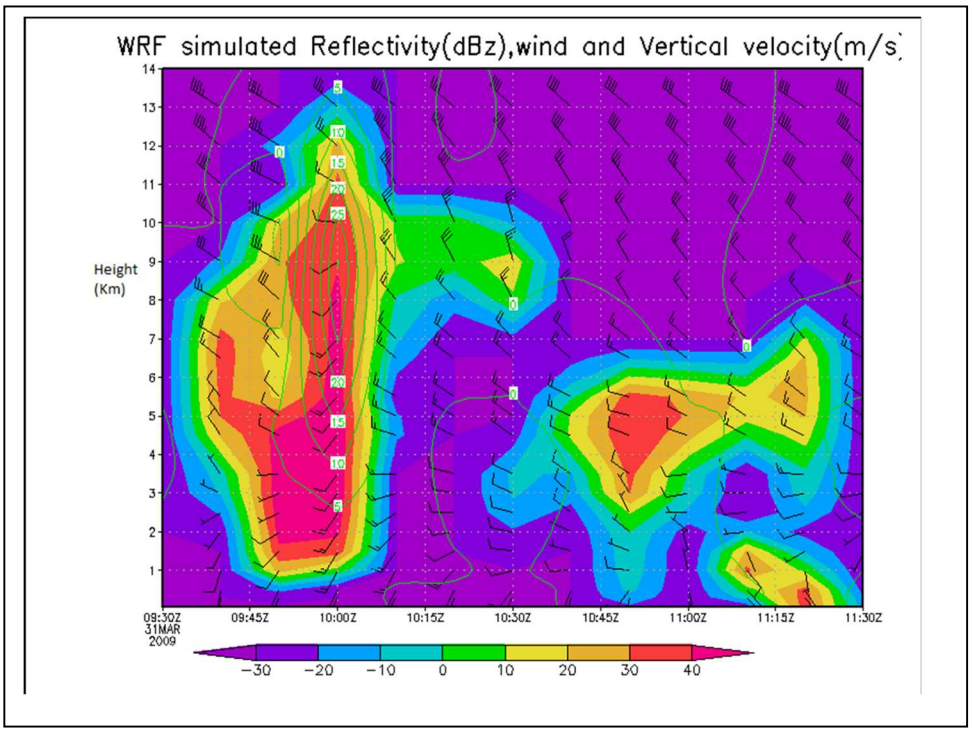


Fig. 4.13: WRF simulated temporal evolution of reflectivity(dBz), wind and vertical velocity(m/s) at 20.75N;86.52 E

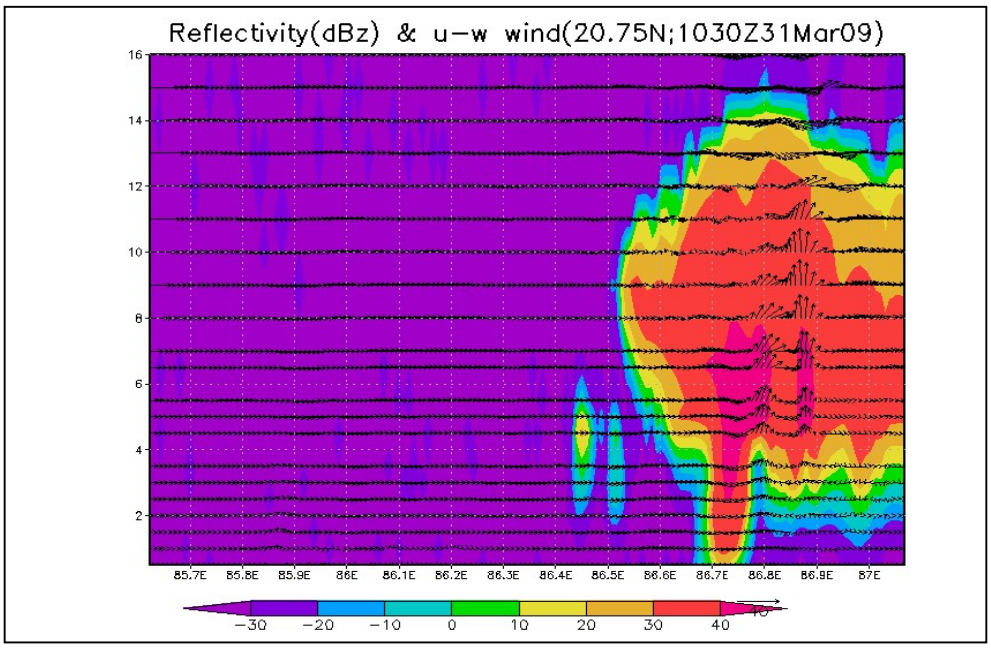


Fig. 4.14: WRF simulated Reflectivity(dBz) and u-w wind(m/s) at 20.75N at1030Z 31Mar2009

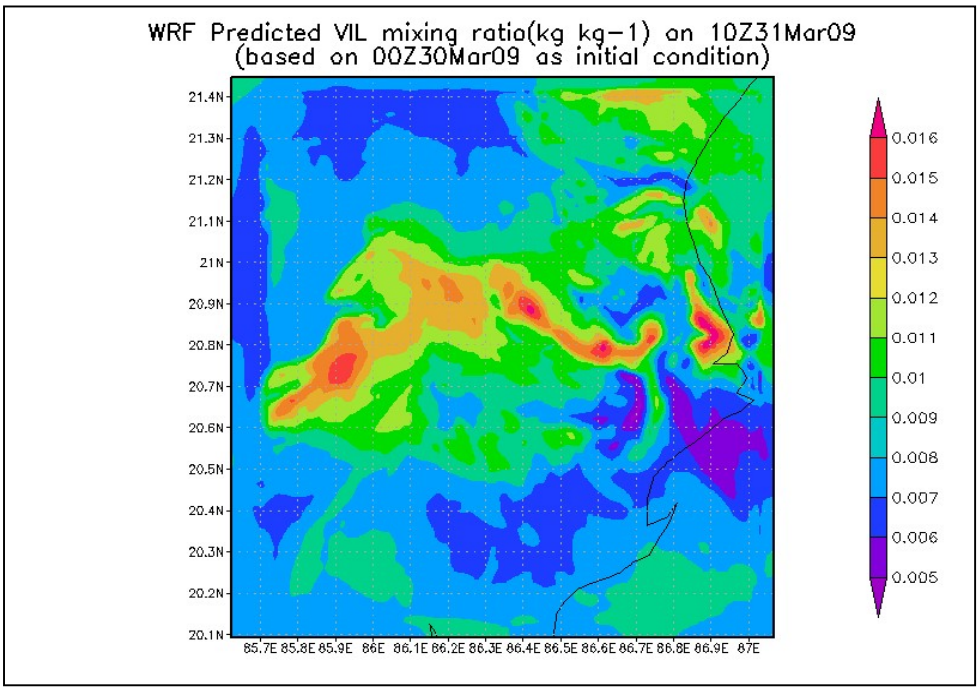


Fig. 4.15: WRF simulated Vertically Integrated liquid Water Mixing ratio (kg kg $^{-1}$) at 1000Z

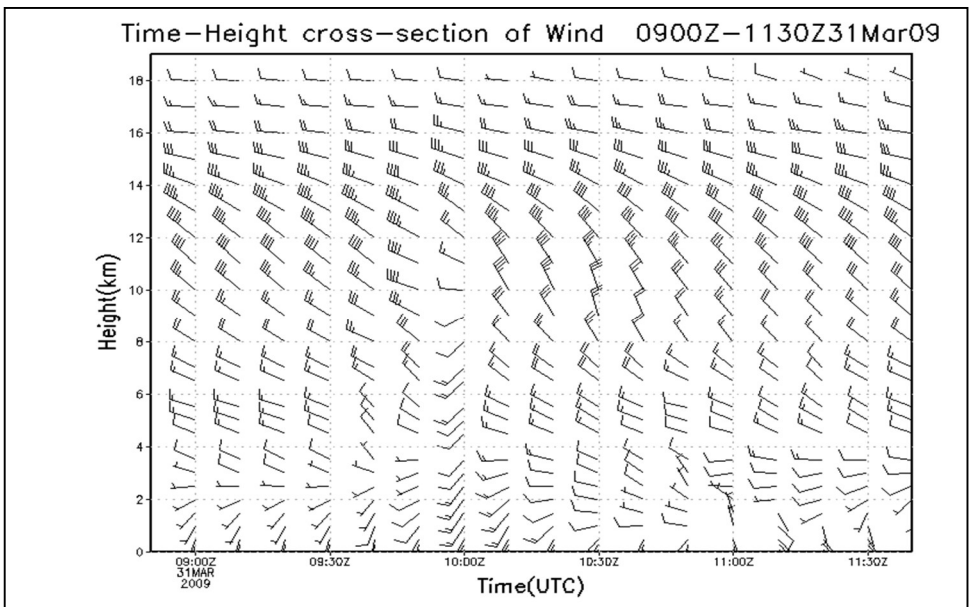


Fig. 4.16: WRF simulated time-height cross-section of wind at 0900Z-1130Z 31Mar2009

WRF simulated 24 hour accumulated rainfall is plotted in fig.3.17 and a rainfall of 35mm is produced over the tornado site. The nearby rainfall observation available is of Balasore which recorded 41 mm.

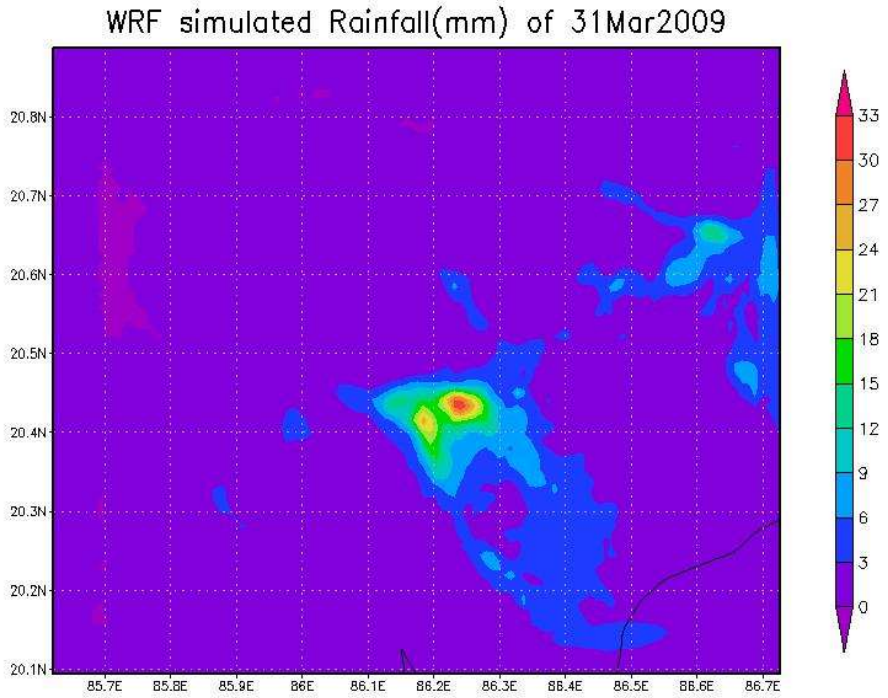


Fig.4.17: WRF simulated rainfall of 31 March 2009

## 4.6. Conclusion

The severe tornadic thunderstorm event occurred over Orissa on 31 March 2009 is simulated using the Weather Research Forecast (WRF-ARW) model. The dynamical changes occurring in the atmosphere especially troposphere prior and during the event is well simulated with a horizontal resolution of 1 km and analysed for the better understanding of the phenomena.

The simulated output fields such as reflectivity, vertical velocity, vorticity etc plotted for every 10 minutes clearly depict the spatial distribution and temporal evolution of clouds. The output parameters are studied in order to understand the following aspects of the convective system:

a) genesis and growth of convective cells
b) spatial distribution and vertical structure
c) characteristics of updrafts and downdrafts
d) wind speed and direction of the convective system
e) life time of the convective system

The longitude-wise and latitude wise vertical cross-section of reflectivity reveals the horizontal and vertical extent of the convective system. The reflectivity profile at different vertical levels gives the spatial distribution of cloud cover in each vertical level thereby providing an overall distribution of convective system in the troposphere.

The vertical vorticity plotted during the different stages of the storm brought out the two positive vorticity centres exceeding a vertical vorticity of 0.01 s-1 which indicates the presence of mesocyclone which is a unique characteristic of a supercell thunderstorm.

The updraft, downdraft as well as temporal evolution of vertical velocity are studied. The presence of a strong updraft with a vertical velocity

of 30 m/s and a strong vorticity of 0.01 $s^{-1}$ in the mid-upper troposphere shows the existence of a meso-cyclone which characteristics the supercell formation. These dynamical changes happening in the mid and upper troposphere during the event reveals that the event was a supercell thunderstorm.

Numerical simulation of the supercell thunderstorm exhibits interesting features such as huge single updraft (of the order of 30 m/s), double vortex circulation, mesocyclone formation, cell splitting and secondary cell formation. The analysis of the tornadic thunderstorm reveals that the mid troposphere and upper troposphere is showing significant dynamical changes especially changes in humidity, vertical vorticity, liquid water content etc a few hours ahead of the event.

Hence a close monitoring of the upper and mid tropospheric dynamics can provide valuable information for the nowcasting of severe convective weather events. This study indicates that the simulation of a severe thunderstorm with a horizontal resolution of 1 km can be utilised to understand the genesis, structure and evolution of severe weather events over Indian region. However numerical simulation of more events over Indian region with very high horizontal resolution are required to generalize the structure and evolution of supercell storms.

# Chapter 5
# Study of two unusual heavy rainfall episodes over southern Indian peninsula using WRF model

## 5.1 Introduction

The southern Indian Peninsula consisting of Tamil Nadu, Kerala, Karnataka and Andhra Pradesh experienced unusually heavy rainfall during the two spells beginning on 12$^{th}$ and 19$^{th}$ March 2008. These heavy spells are record highs for the month of March since the year 1875 and the area weighted average rainfall was 915 % of its long period average (CDBI ,2008). Hence an attempt is made to simulate the heavy rainfall episodes on 12-14 March 2008 and 19-22 March 2008 employing Kain-Fritsch cumulus scheme and WSM3 simple ice microphysics scheme with a horizontal spatial resolution of 5 km.

## 5.2 Experimental setup

The simulation domain set up by the WPS for the simulation of heavy rainfall events over Southern peninsula is shown in Fig 5.1. Two domains D1 and D2 with two way nesting technique have been used for the model runs. The model domain D1 extended from 69.19$^0$E -88.81$^0$E and 2.31$^0$N -18.09$^0$N and D2 covered 75.5 $^0$E- 77.5$^0$E and 7.5$^0$N -13$^0$N. The model was integrated for a period of 54 hours (Case1) and 96 hours (Case 2) with a horizontal spatial resolution of 5 kms and a temporal resolution of 10 s for the inner domain.

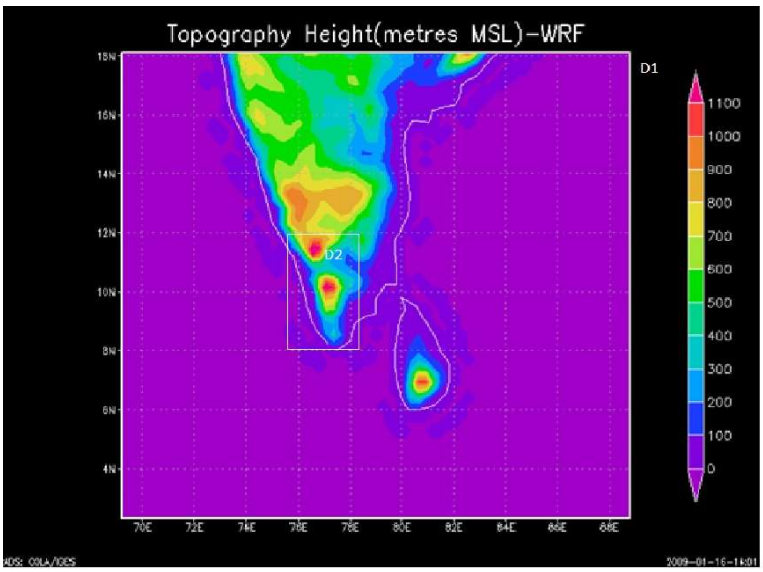


Fig.5.1.: Domain configured for the simulation of a heavy rainfall event occurred over Southern peninsula on 12-14 March 2008 and 22-24 March 2008 along with topographic height.

The model is run using the Kain-Fritsch (new Eta) scheme for cumulus parameterization (Kain and Fritsch,1993), Yonsei University (YSU) scheme for the boundary layer parameterization (Hong et. al, 2006, Hong, 2010), WSM 3 class simple ice scheme for microphysics (Hong. et. al, 2004) and Rapid Radiative Transfer Model (RRTM) for long wave radiation (Mlawer et. al, 1997) and Dudhia scheme for short wave radiation (Dudhia, 1989). The grid staggering is the Arakawa C-grid. The model uses the Runge-Kutta 2$^{nd}$ and 3$^{rd}$ order time integration schemes and 2$^{nd}$ to 6$^{th}$ order advection schemes in both the horizontal and vertical. It uses a time-split small step for acoustic and gravity-wave modes.

## 5.3 Data used

The initial and lateral boundary conditions for the model run is taken from the Final (FNL) Operational Global Tropospheric Analyses of National Centre for Environmental Prediction (NCEP) on $1^0$ x $1^0$ grids prepared operationally every six hours. This FNL dataset is developed from the Global Data Assimilation System (GDAS), which continuously collects observational data from the Global Telecommunications System (GTS) and other sources. The United States Geological Survey (USGS) global datasets with 30 sec horizontal resolution were used to create terrain/topography and landuse/vegetation fields. The WRF model simulated rainfall is validated using TRMM 3B42 ($0.25^0$ x$0.25^0$) daily precipitation data and Satellite based Automatic Weather Stations (AWSs) data.

**Case 1: Heavy rainfall episode during 12-14 March 2008 over Indian peninsular region.**

**Synoptic situation**

Kerala and Tamil Nadu experienced widespread rainfall activity on 13th and 14th March 2008 in association with a large amplitude easterly trough and a mid-latitude westerly trough. The southern peninsula experienced unusually heavy rainfall due to the interaction of lower and upper level troughs and the formation of a well-marked low off Karnataka-Kerala coast. The widespread rainfall activity commenced over Puducherry and Tamil Nadu from 13th March onwards and moved towards Kerala on 14th March. The satellite imageries (Fig.5.2-5.3) clearly show the presence of deep convective clouds over peninsular Indian region during 13th and 14th March 2008.

On 11th March 2008, a trough is seen at sea level over the southwest Bay of Bengal off the Tamil Nadu - Sri Lanka coast. Another trough was observed at 0.9 km above sea level which extended from Lakshadweep area

to Konkan and Goa. A westerly trough with its axis along $65^0$E to the north of $15^0$N were seen in the mid and upper tropospheric levels.

The analysis of wind pattern by IMD during 12-14 March 2008 (Fig 5.4) has shown that a trough extending from Lakshadweep-Comorin to South Konkan and Goa was present in the low level easterlies (at 850 mb) with an embedded cyclonic circulation over Comorin and neighbourhood. The easterly trough was seen extended upto 700 mb. A mid-tropospheric westerly trough was seen on 12th March. Then it moved eastwards on 13th March and it moved further eastwards on 14th March.

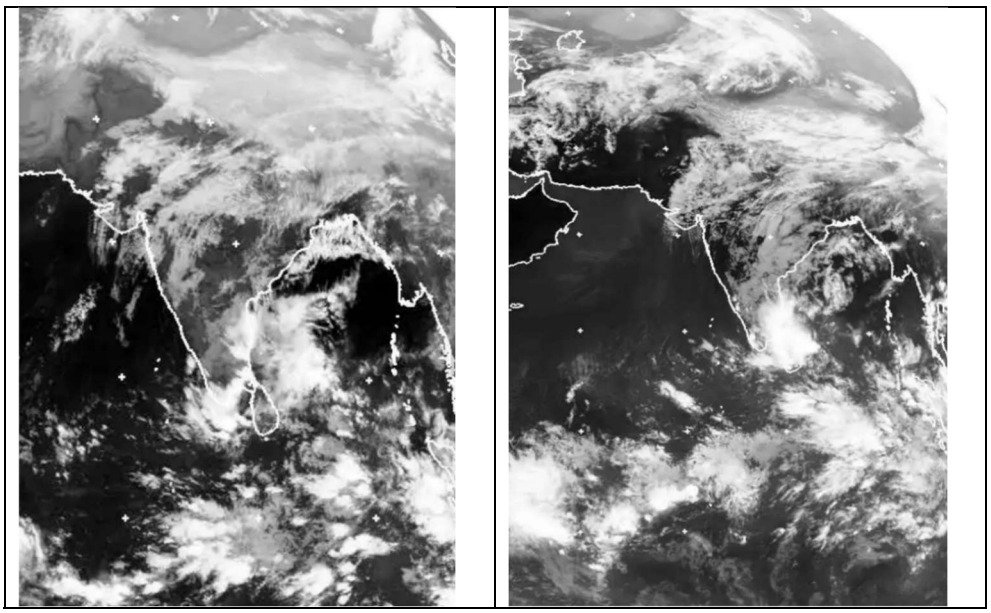

Fig 5.2: Meteosat satellite imagery a) at 0000 UTC of 12th March 2008
b) 1200 UTC of 12th March 2008

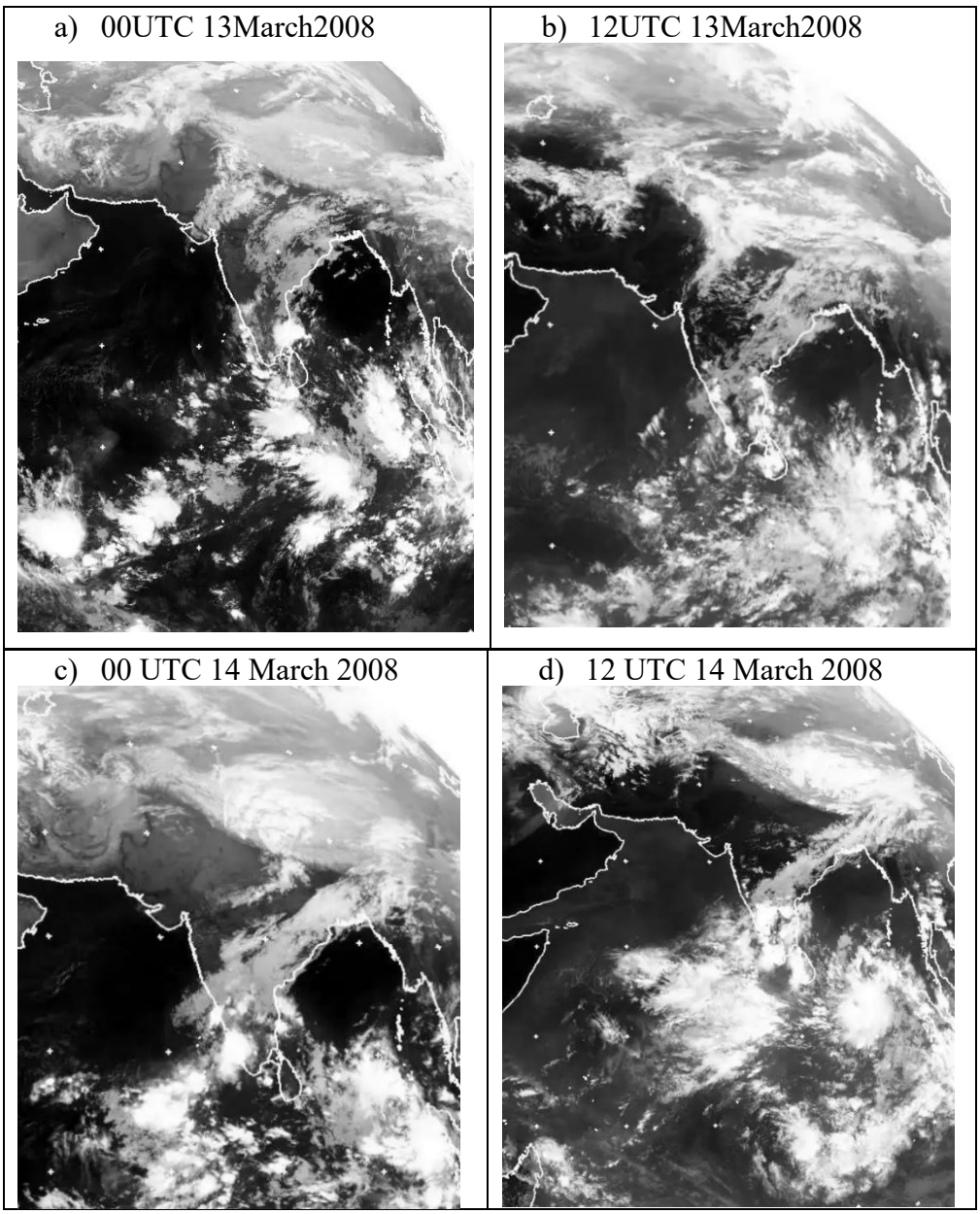


Fig. 5.3: Meteosat satellite imagery a) at 0000 UTC of 13th March 2008 b) 1200 UTC of 13th March 2008 c) at 0000 UTC of 14th March 2008 d) 1200 UTC of 14th March 2008

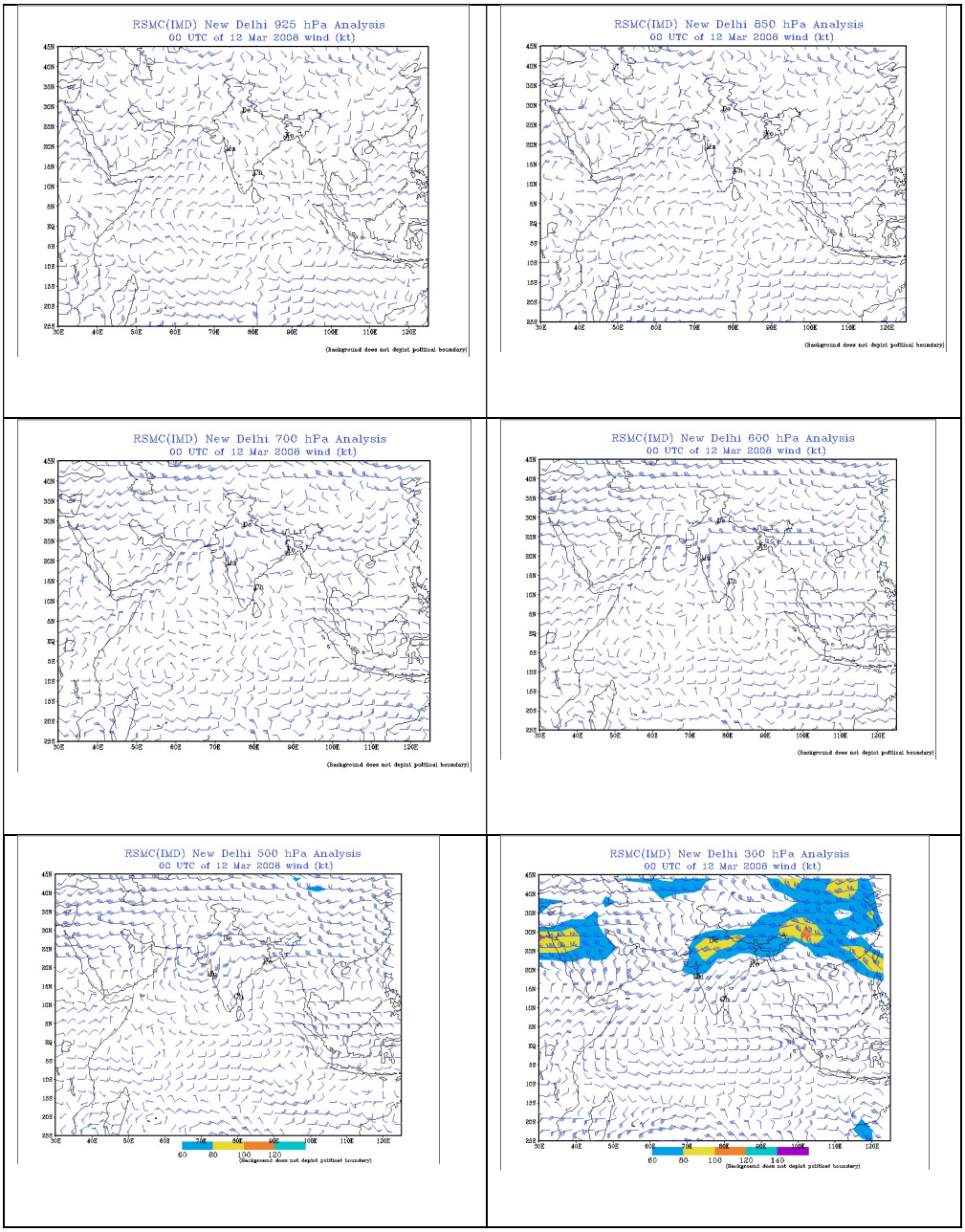


Fig. 5.4: IMD wind analysis at different at standard pressure levels for 00UTC of 12 March 2008

## Results & Discussion

The model could successfully simulate the heavy rainfall episode during 12-14 March 2008. Rainfall is plotted for every 3 hours starting from 00UTC 12 March 2008. The WRF model simulated three hourly accumulated rainfall (mm) is plotted in Fig.5.5a to Fig.5.5c. The model simulated rainfall is found in good agreement with the observations. The model simulated rainfall is compared with Satellite based AWSs data of 13$^{th}$ March 2008 and 14$^{th}$ March 2008 and has shown good agreement with the observations (Fig. 5.7 and Fig.5.8). The satellite based AWS at certain locations is placed along with IMD raingauges. The comparison between AWS and IMD observed data of such stations were compared and plotted in Fig.5.9

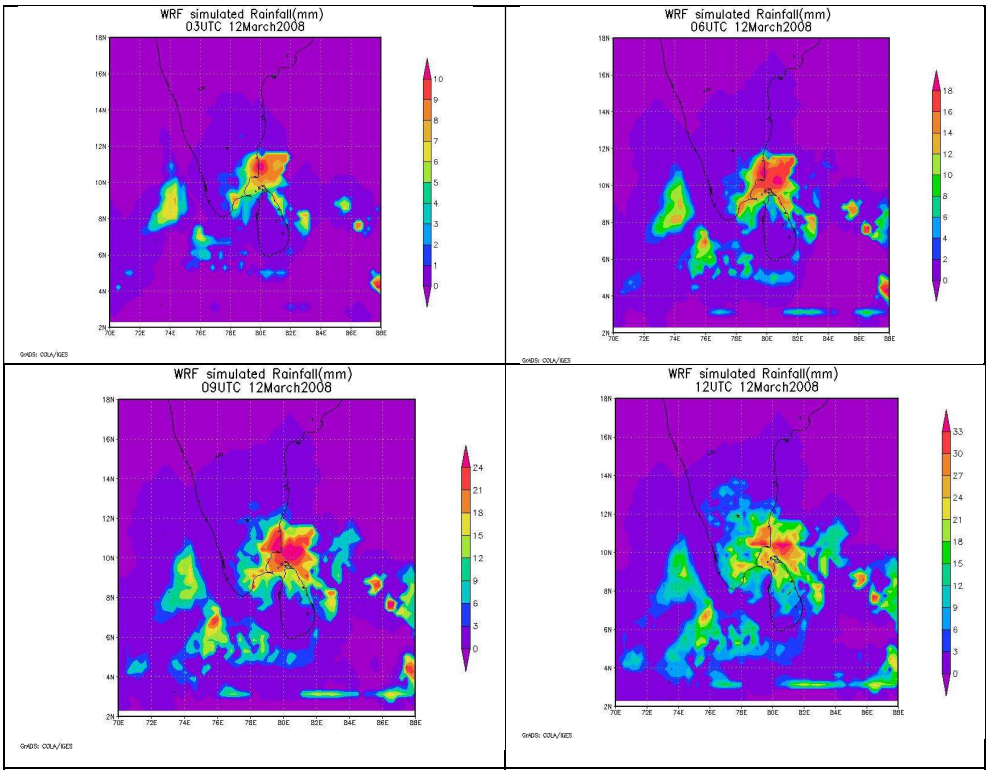


Fig.5.5a : WRF predicted accumulated rainfall(mm) from 0300UTC-1200 UTC of 12 March 2008

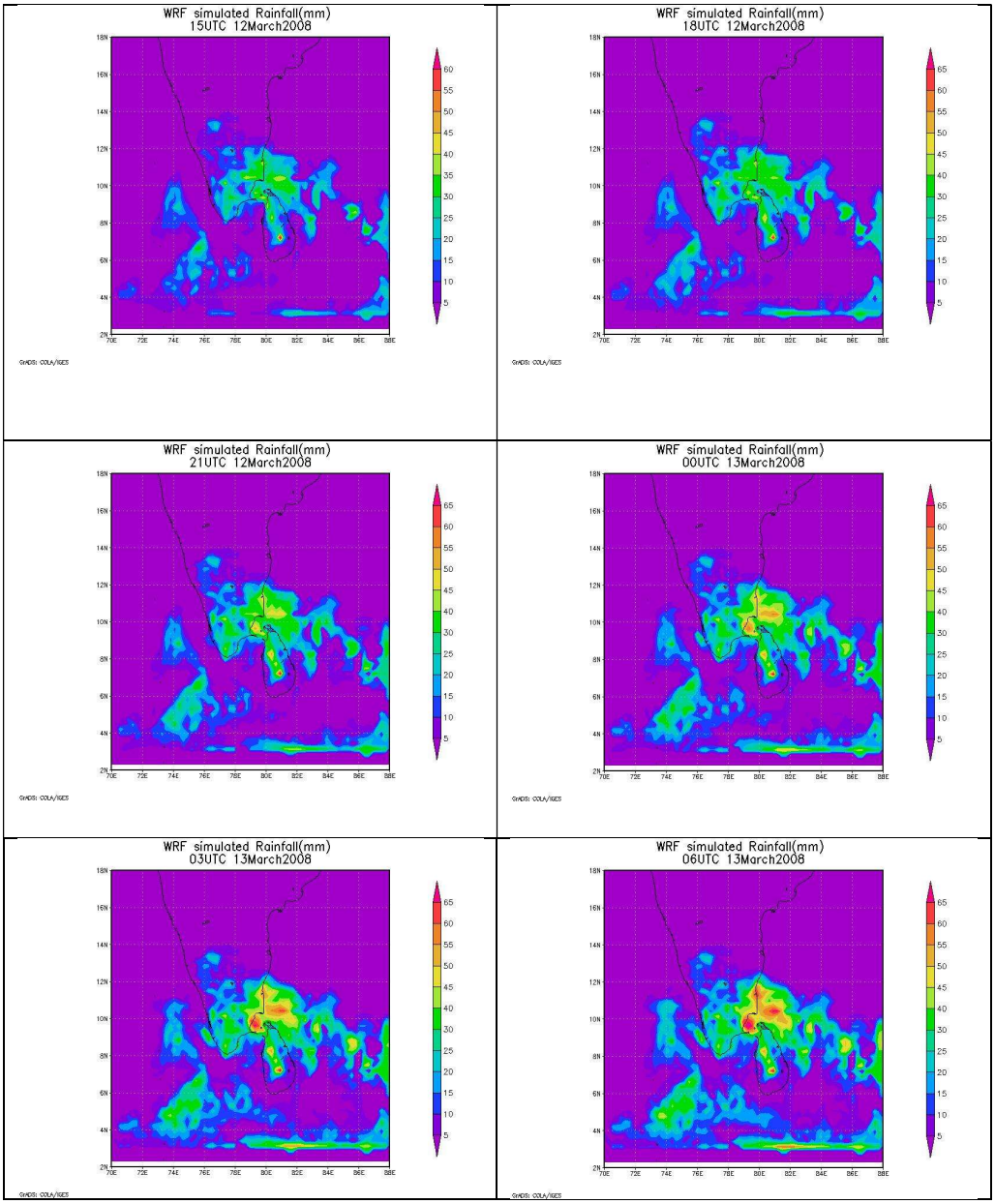


Fig.5.5b: WRF predicted accumulated rainfall(mm) from 1500UTC 12 March 2008 to 0600 UTC 13 March2008

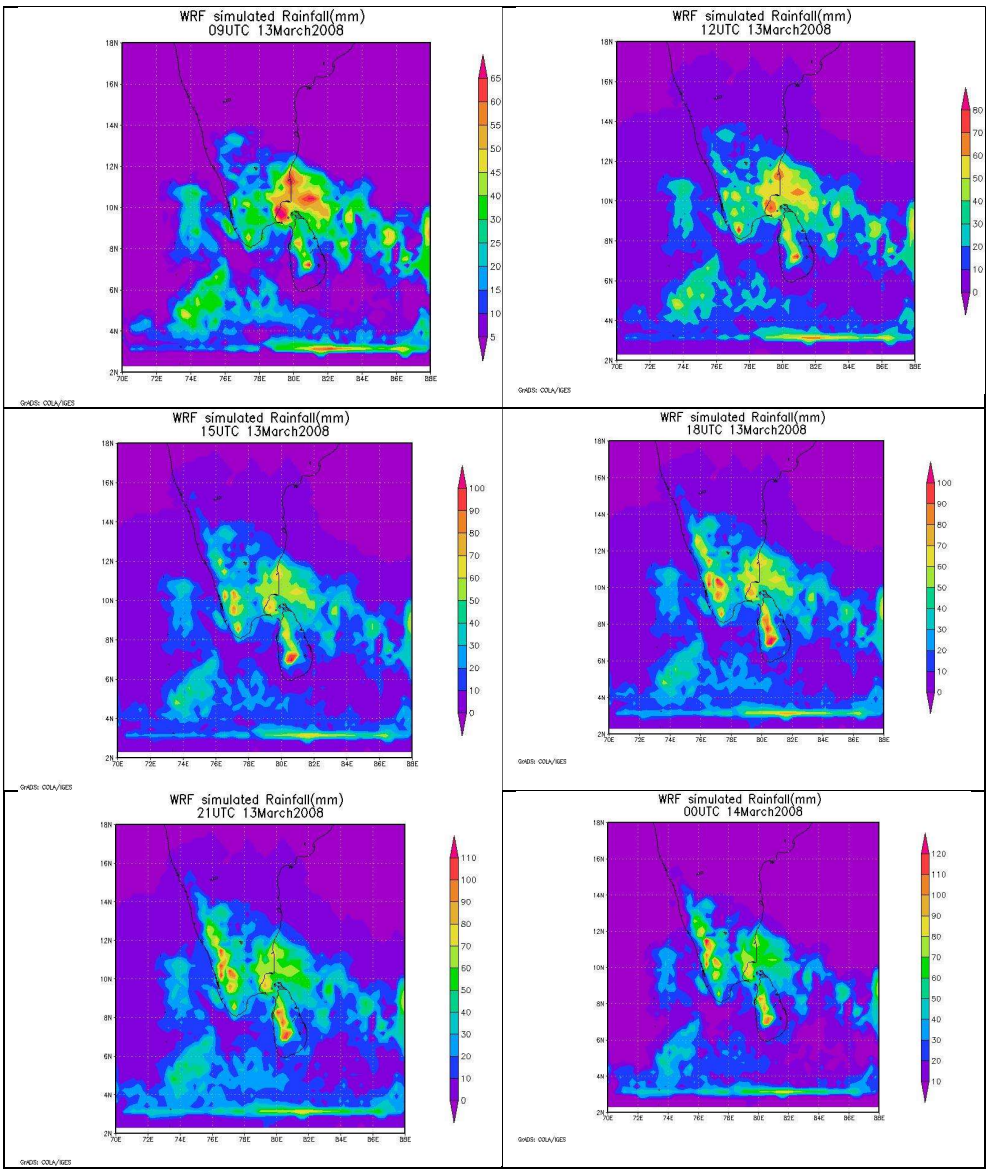


Fig.5.5c: WRF predicted accumulated rainfall(mm) from 0900UTC 13 March 2008 to 0000 UTC 14 March2008

The WRF simulated rainfall is compared with TRMM 3B42 daily precipitation data ($0.25^0$ x $0.25^0$) and is plotted in Fig.5.6. The simulation shows good agreement with TRMM data and reveals more finer spatial distribution of rainfall since the model is run with a higher horizontal resolution (5 km) than TRMM (~27.75 km).

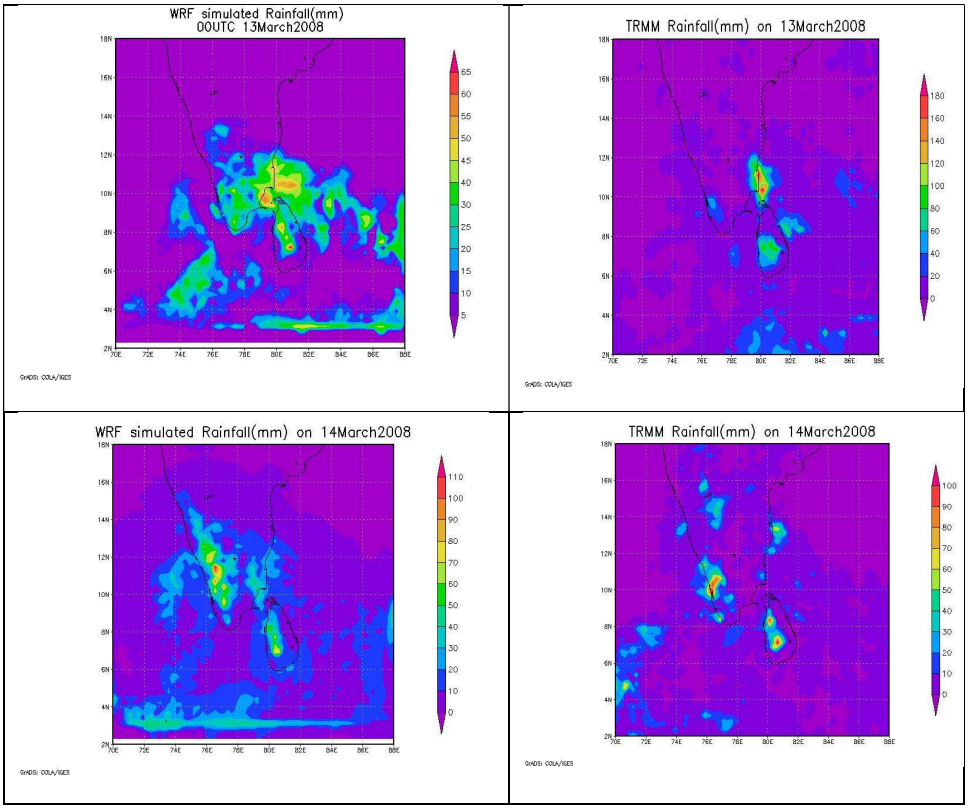


Fig.5.6: Comparison between WRF Model simulated Rainfall(mm) and TRMM Rainfall(mm)

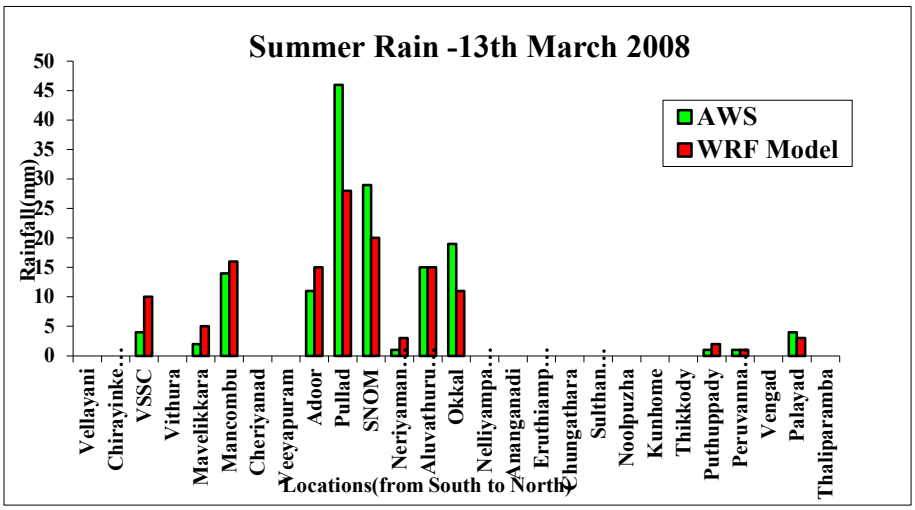


Fig.5.7: Comparison of WRF model simulated rainfall with AWS recorded rainfall on 13th March 2008

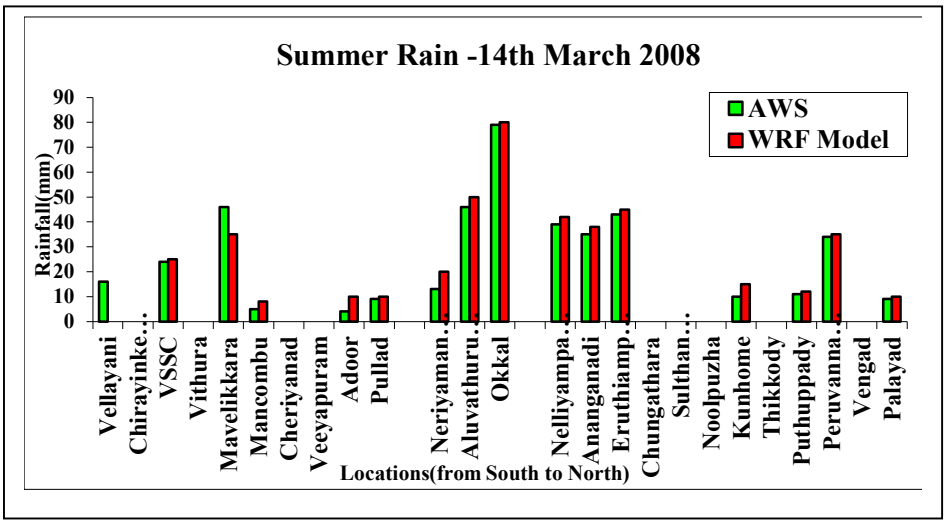


Fig.5.8: Comparison of WRF model simulated rainfall with AWS recorded rainfall on 14th March 2008

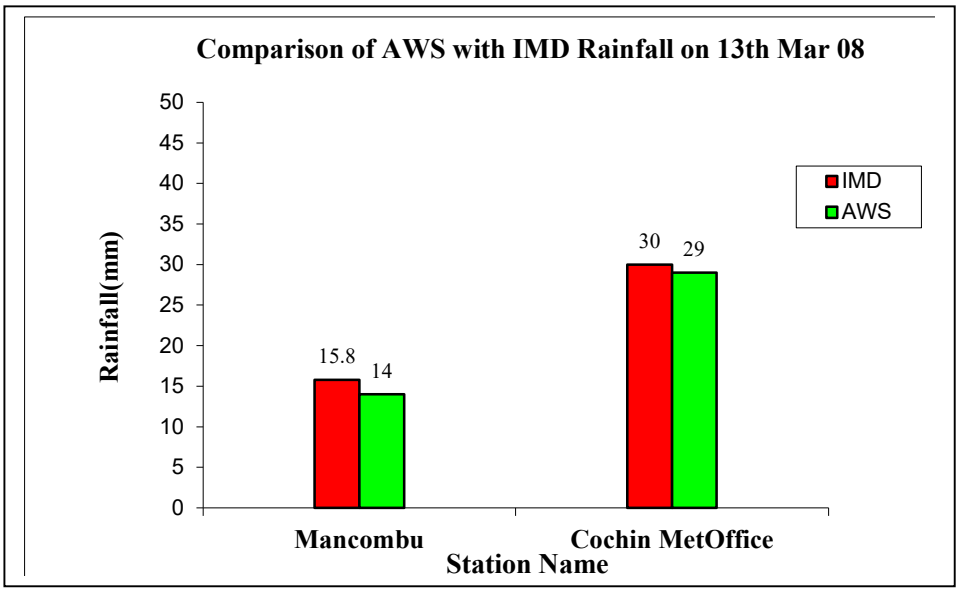


Fig.5.9: Comparison of IMD rainfall with AWS recorded rainfall on 13th March 2008

The model could bring out many mesoscale features of the synoptic system especially the wind circulation features. The model simulated wind at standard pressure levels of 00 UTC of 13th March is plotted in Fig.5.10 and is compared with the IMD wind analysis (Fig.5.13). The model simulated wind at 850 hPa has clearly shown the presence of two bands of strong easterlies with a speed of 12m/s. The one band of strong easterlies was seen over peninsular Indian region with its peak centered at $12.5^0$N and $77^0$E. This band of easterlies brought moisture laden winds from the Bay of Bengal. The other band of easterlies was observed in the latitude belt $16^0$N-$18^0$N with its peak centered at $78.5^0$E. The southerly winds were also seen at 850 hPa and helped in the moisture incursion from Indian Ocean. An embedded cyclonic circulation centered at $75^0$E and $9^0$N were also observed in the simulated wind pattern which matches with actual observations. A trough in the easterlies was also seen at 850 hPa. Eventhough the two bands of easterlies extended up to

700 hPa, the easterly band seen over the latitude belt $16^0$N-$18^0$N strengthened at 700 hPa. The intrusion of strong westerlies with a speed of 18m/s were seen at 500 hPa with its peak centered at $74^0$E;$17.8^0$N. A mid-tropospheric trough was observed in the simulated wind pattern at 500 hPa on 13th March. The model simulated wind at standard pressure levels on 14th March 2008 is plotted in Fig.5.11 and is compared with IMD wind analysis (Fig.5.12).

On 14th March the easterlies became more organised especially at 700 hPa along with the northward propagation of cyclonic circulation. The easterlies were observed in 600 hPa and also seen at 500 hPa along with westerlies. The strong westerlies with a speed of 24 m/s are observed in the simulated wind pattern at 300 hPa with its peak centered at $18^0$N and $80^0$E. The vertical velocity and vorticity from 450 mb - 200 mb is plotted (Fig.5.14).

The association of mid-level westerly trough with low-level easterly trough resulted in the development of embedded thunderstorm cells which manifested as widespread heavy rainfall activity. This simulation enabled us to study the dynamics of embedded convective systems formed due to the interaction between low level convergence due to easterlies and mid-level westerlies. It also enabled us to study the precipitation characteristics of thunderstorm cells embedded inside an easterly trough and an overlying westerly trough.

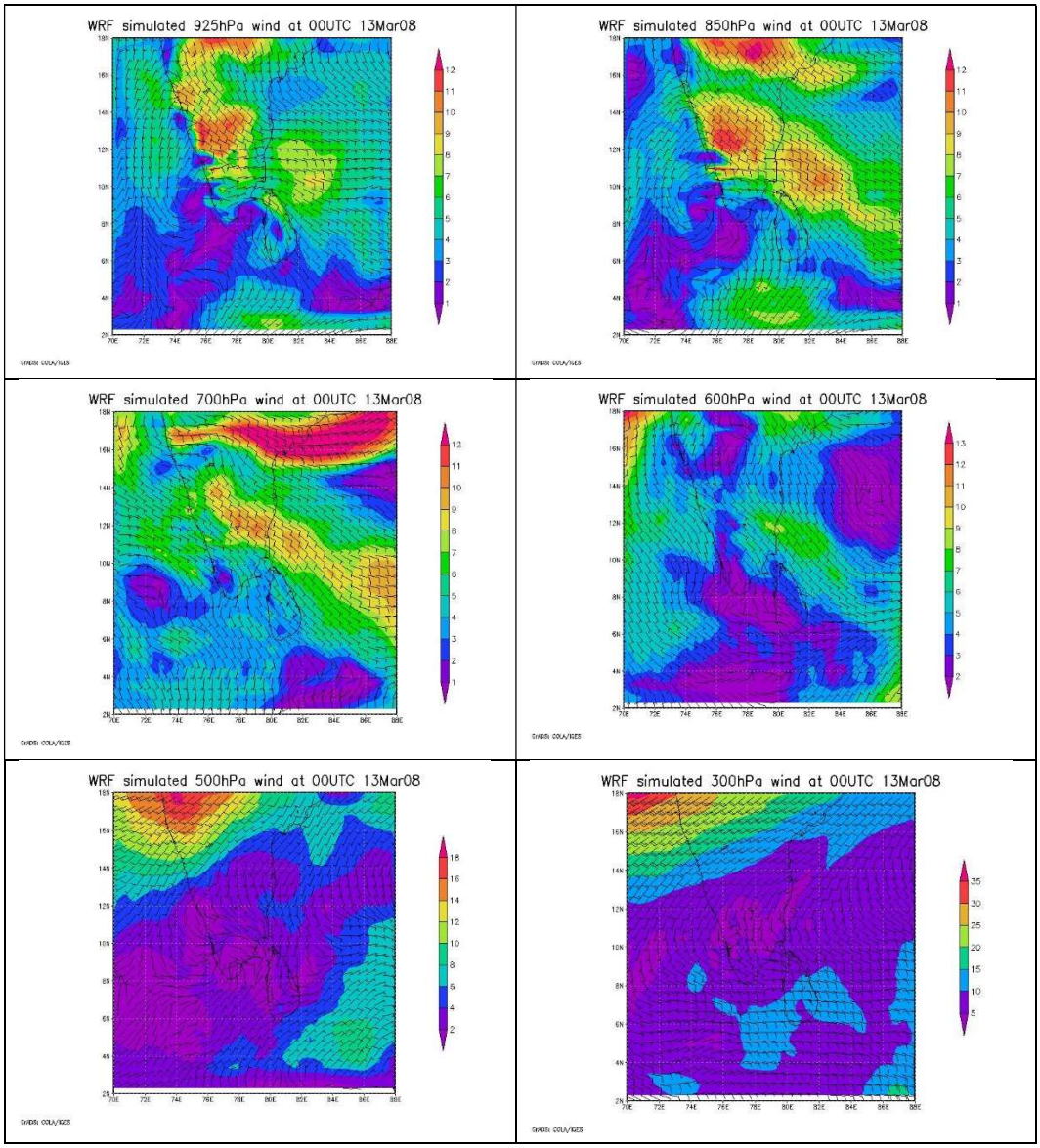


Fig.5.10: Model simulated wind at standard pressure levels at 00UTC of 13th March 2008

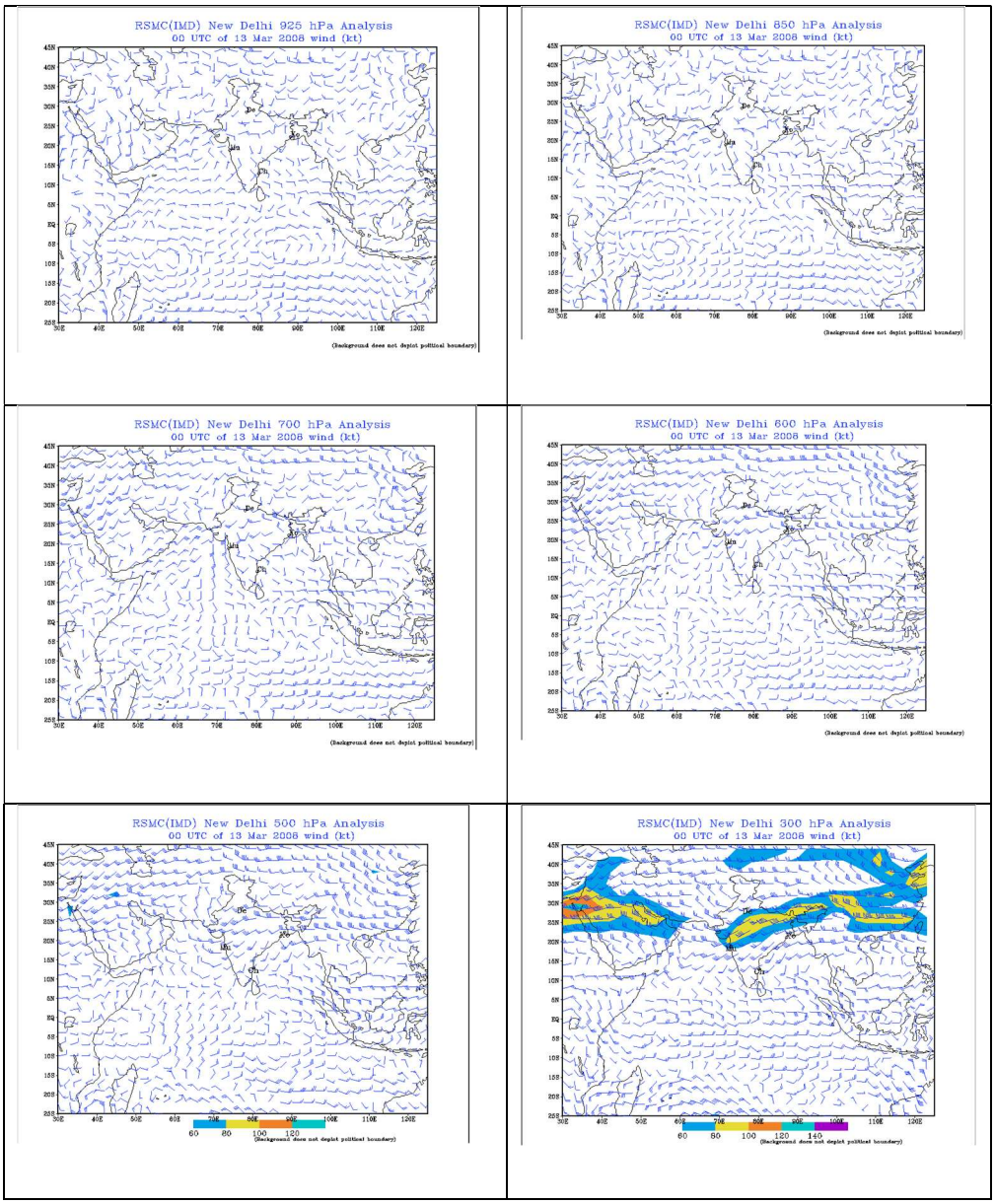


Fig.5.11: IMD wind analysis at standard pressure levels at 00UTC of 13th March 2008

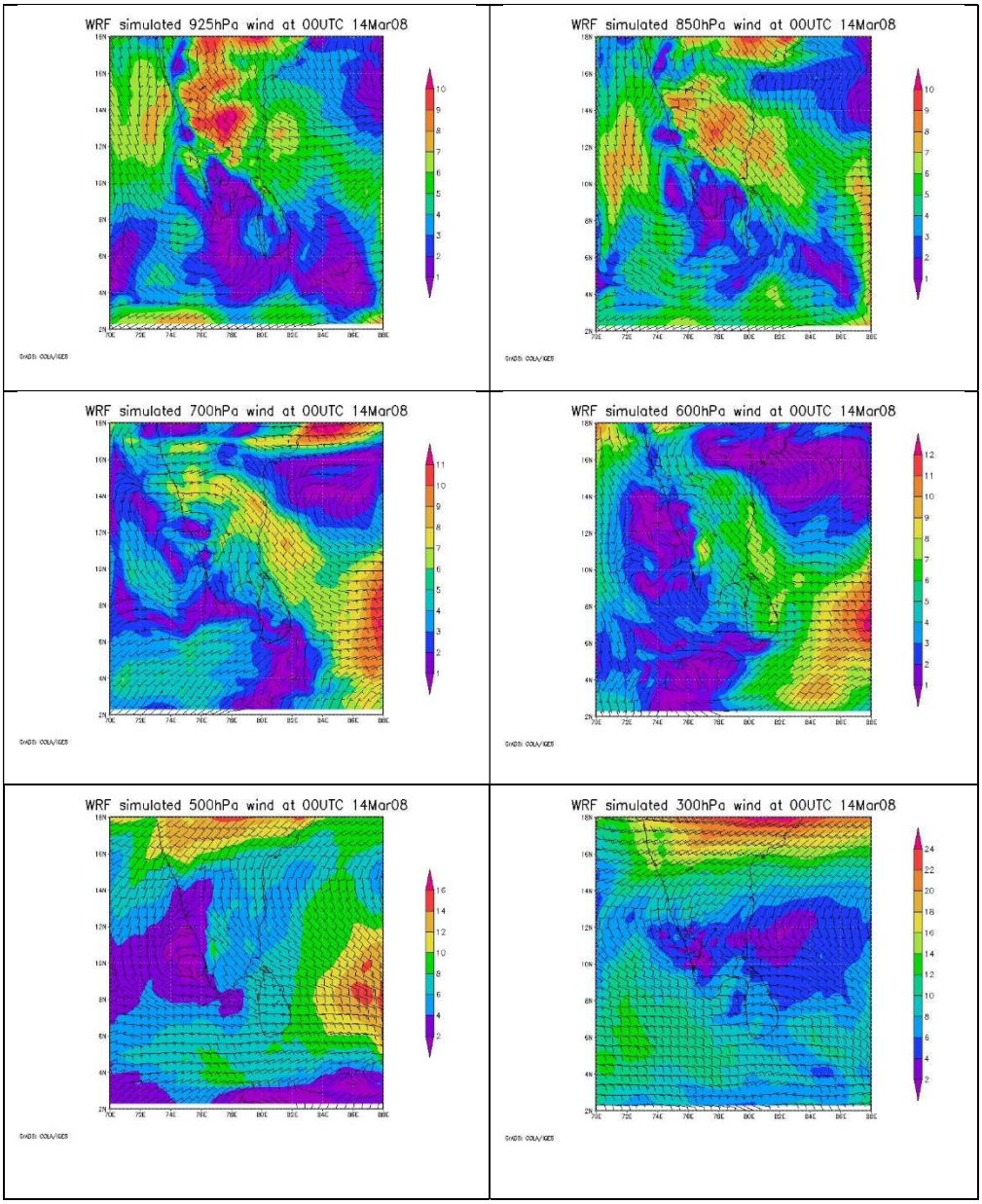


Fig.5.12: Model simulated wind at standard pressure levels at 00UTC of 14th March 2008

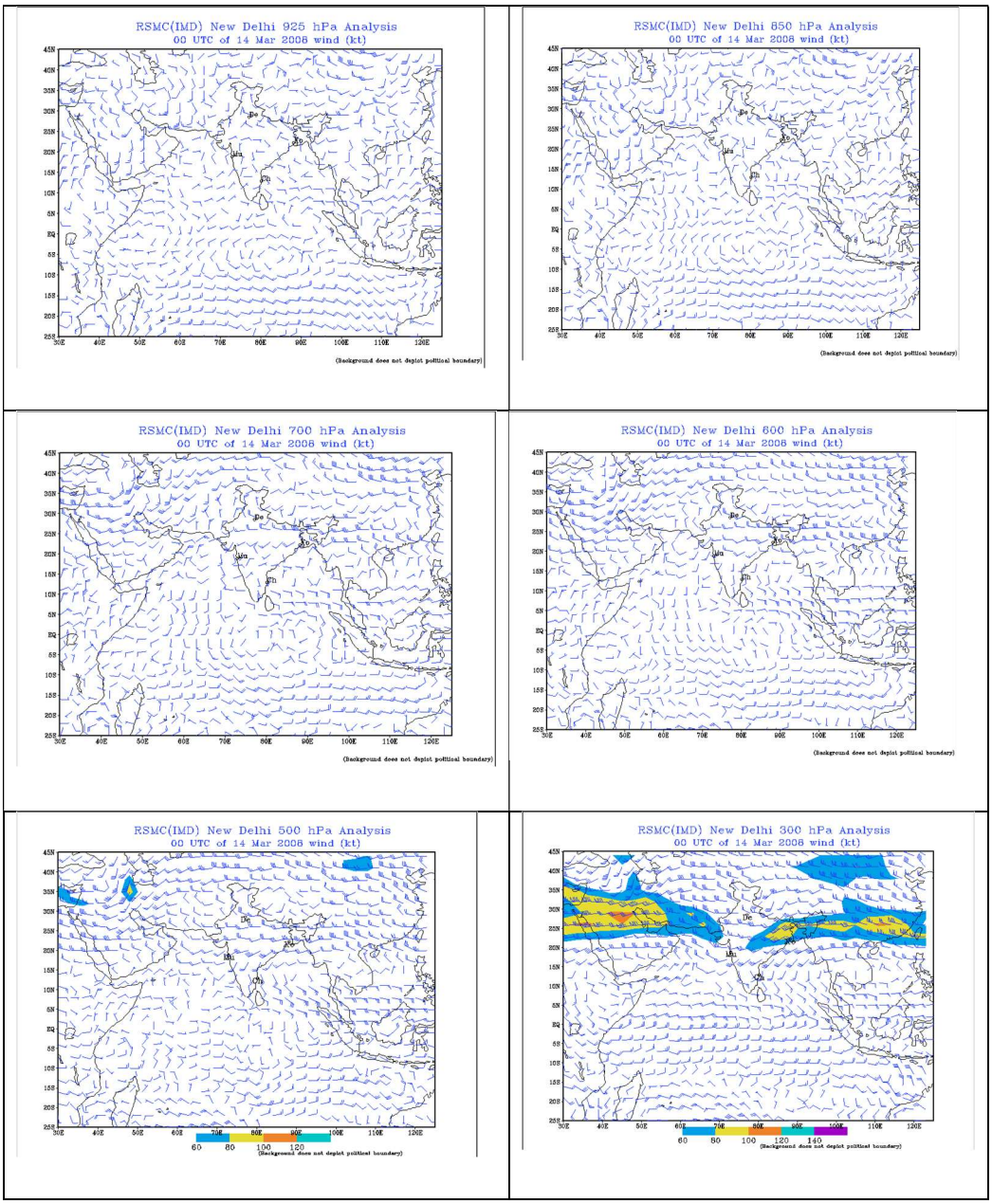


Fig.5.13: IMD wind analysis at standard pressure levels at 00UTC of 14th March 2008

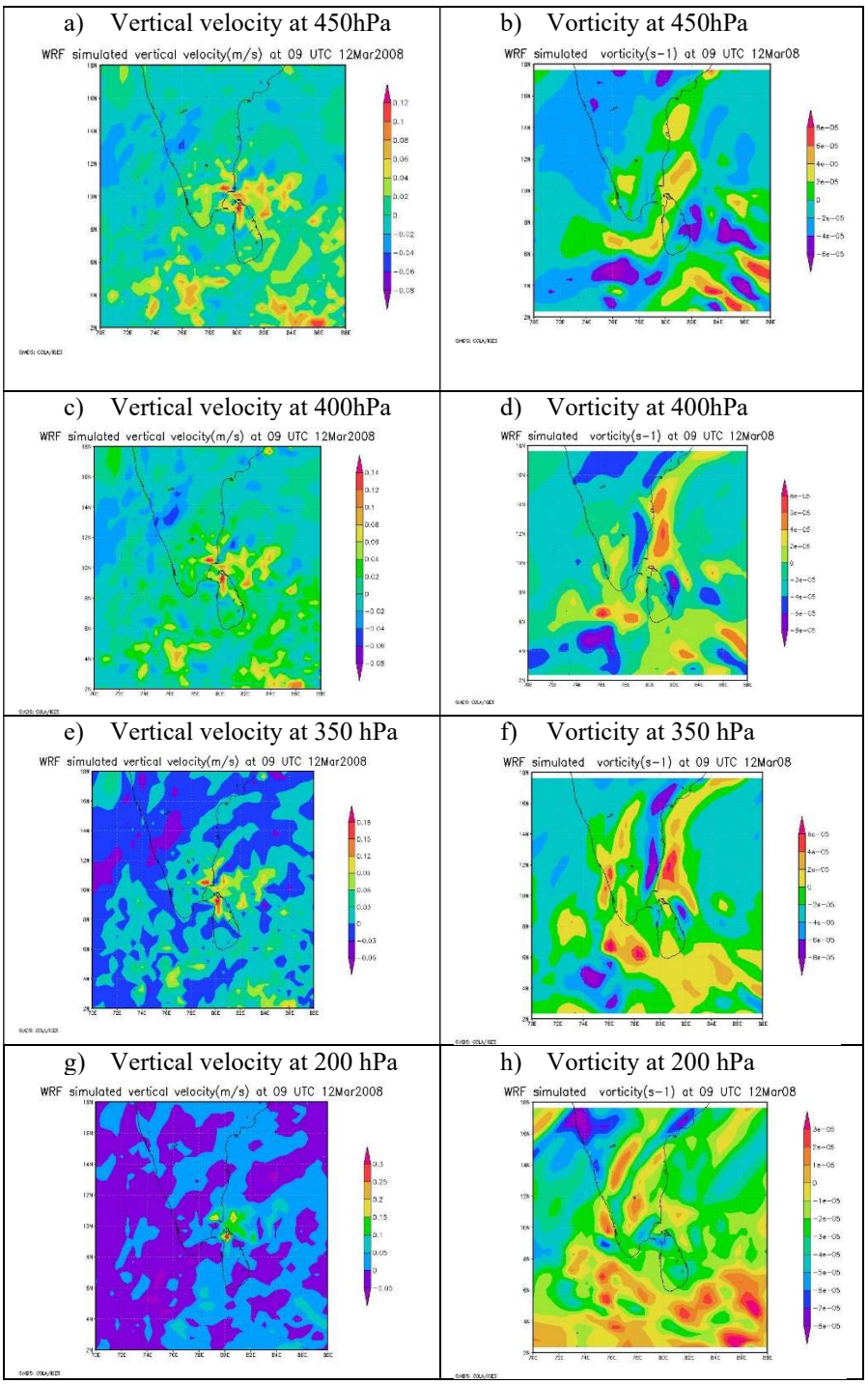


Fig.5.14: The spatial distribution of vertical velocity and vorticity from 450 mb - 200 mb

## Case 2: Heavy rainfall episode on 19-22 March 2008 over Indian peninsular region.

### Synoptic situation (IMD analysis)

Southern peninsular region experienced widespread rainfall activity during 19-22 March 2008. Analysis of synoptic features revealed the presence of two cyclonic circulations (cycir), one over Lakshadweep area lying between 1.5 and 3.1 km above m.s.l and the other over south Tamil Nadu and adjoining Sri Lanka extending upto 0.9 km above sea level on 18$^{th}$ March 2008. Two troughs were also observed, one at sea level over Lakshadweep and adjoining south east and east-central Arabian sea. Another trough was observed over the southeast Bay of Bengal and adjoining Andaman Sea. The cycir over Lakshadweep-Comorin area was seen over the Maldives on 19$^{th}$ March and a low formed over southeastern Arabian Sea on 20$^{th}$ March. The low persisted over southeastern Arabian sea and the adjoining Lakshadweep area off Kerala coast with associated cycir extending up to 4.5 km above m.s.l on 21$^{st}$ March. It became a well-marked low over the same region with an associated cycir extending upto 500 hPa on 22$^{nd}$ March. On 23$^{rd}$ March, it was a low with cycir extending upto 3.6 km above m.s.l. The low eventually became less marked by 24$^{th}$ March. The Meteosat satellite imagery from 19-22 March 2008 is given in Fig. 5.15 and Fig. 5.16

a) 00UTC 19March2008

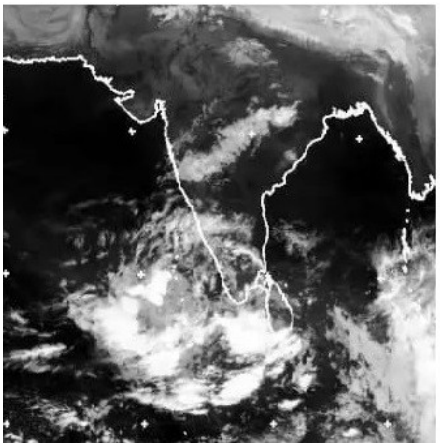

b) 12UTC 19March2008

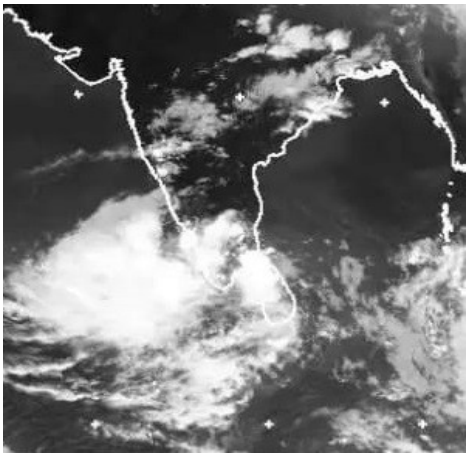

c) 00UTC 20March2008

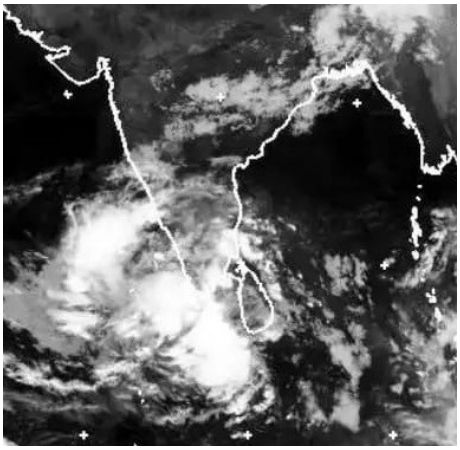

d) 12UTC 20March2008

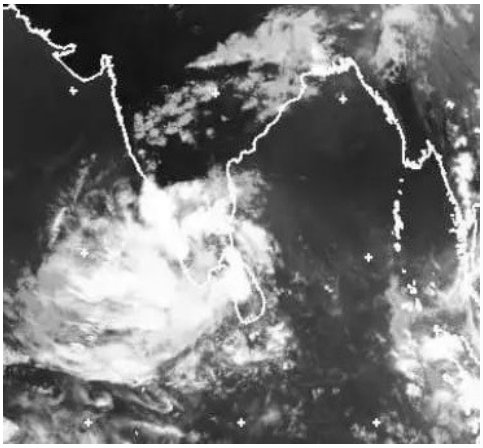

Fig 5.15: Meteosat satellite imagery at a)0000 UTC of 19th March 2008 b) 1200 UTC of 19th March 2008 c) 0000 UTC of 20th March 2008 d) 1200 UTC of 20th March 2008

a) 00UTC 21March2008

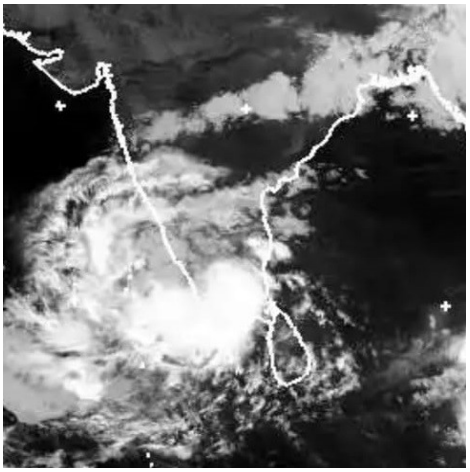

b) 12UTC 21March2008

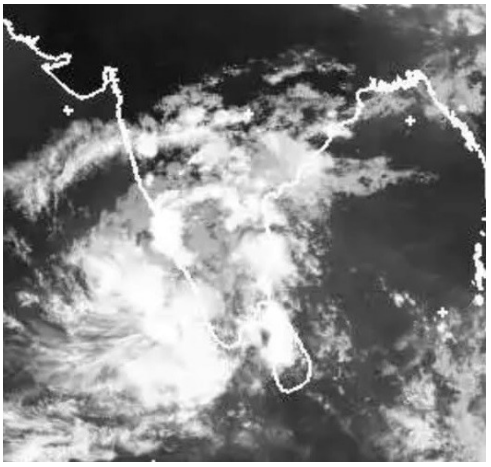

c) 00UTC 22March2008

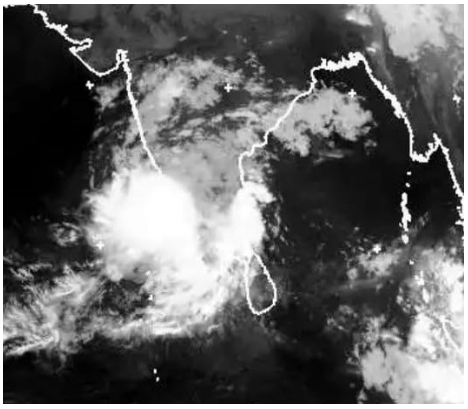

d) 12UTC 22March 2008

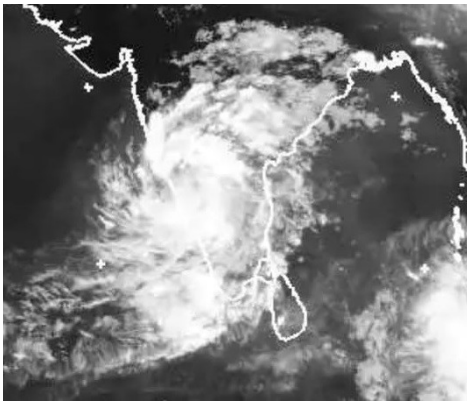

Fig 5.16: Meteosat satellite imageries at a) 0000 UTC of 21st March 2008 b) 1200 UTC of 21st March 2008 c) 0000 UTC of 22nd March 2008 d) 1200 UTC of 22nd March 2008

## Results and Discussion

The model could simulate the heavy rainfall episode during 19-22 March 2008 with good spatial and temporal accuracy.

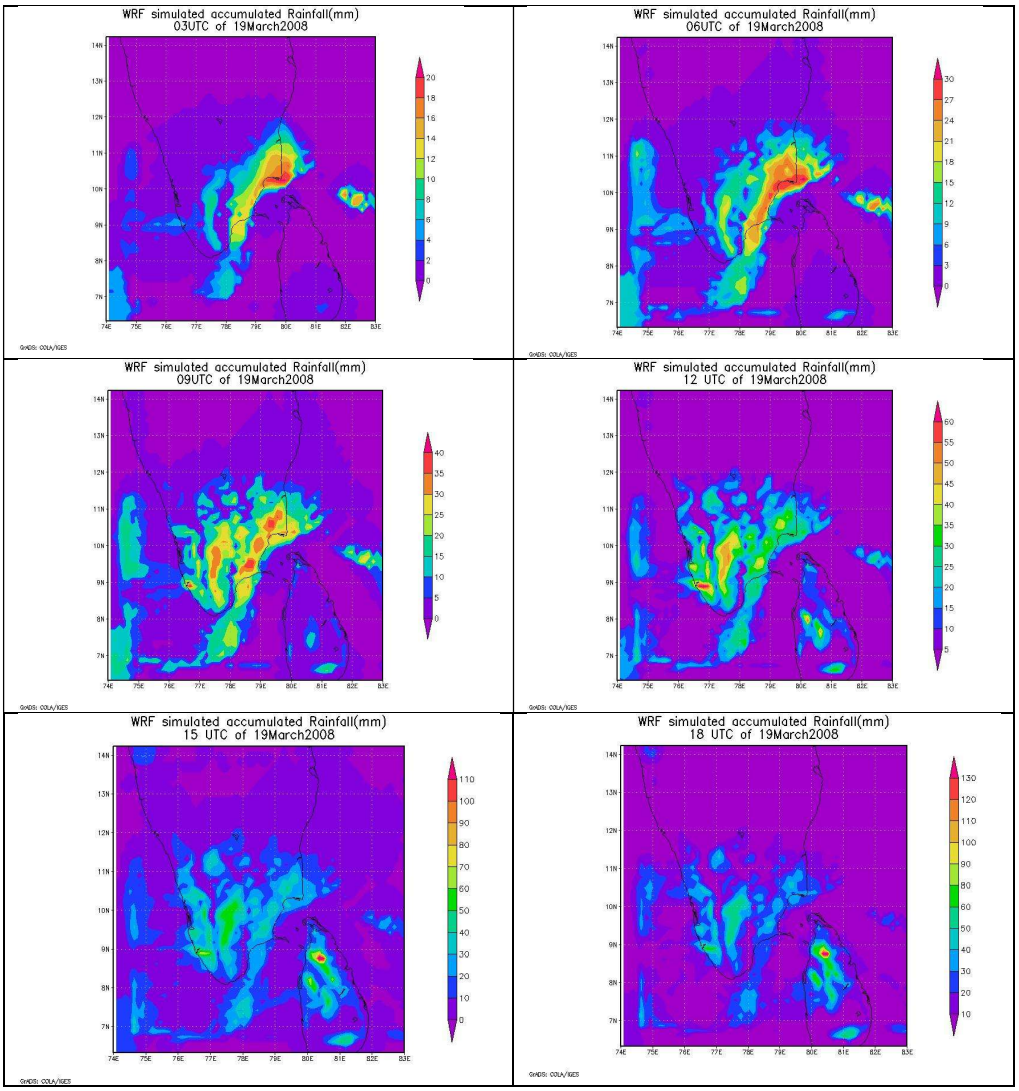


Fig.5.17a: WRF predicted accumulated rainfall(mm) from 0300UTC 19 March 2008 to 1800 UTC 19 March2008

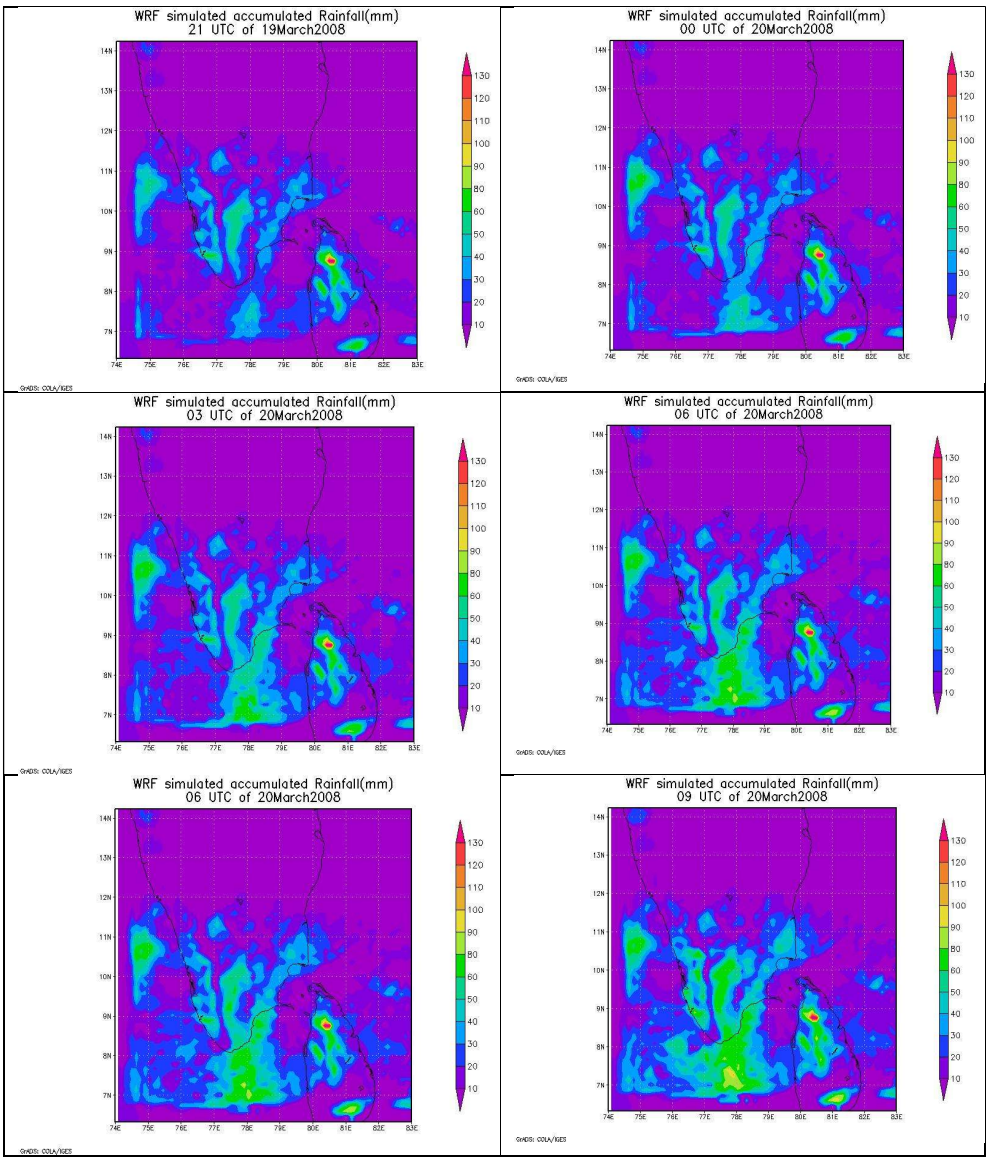


Fig.5.17b: WRF predicted accumulated rainfall(mm) from 2100UTC 19 March 2008 to 0900 UTC 20 March2008

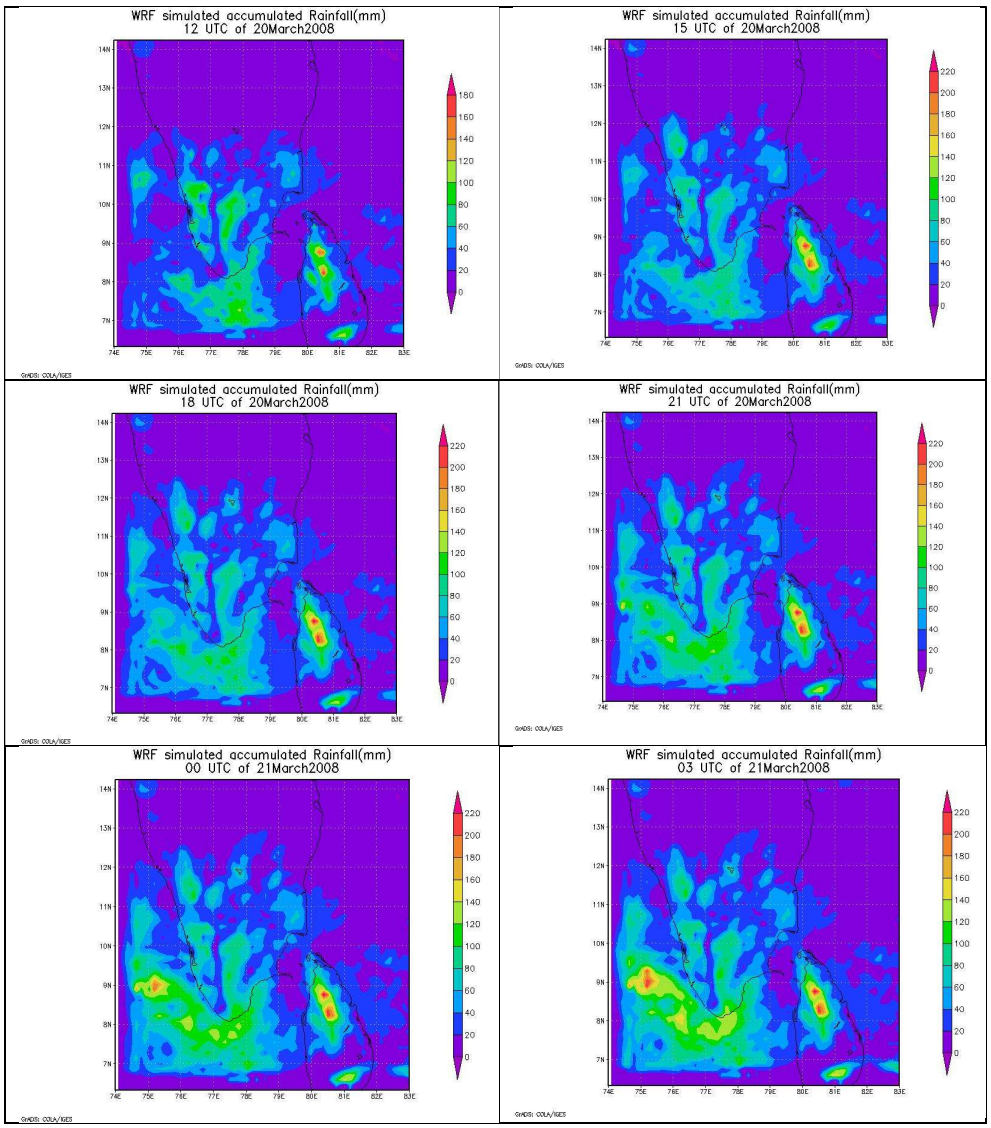


Fig.5.17c: WRF predicted accumulated rainfall(mm) from 1200UTC 20 March 2008 to 0300 UTC 21March 2008

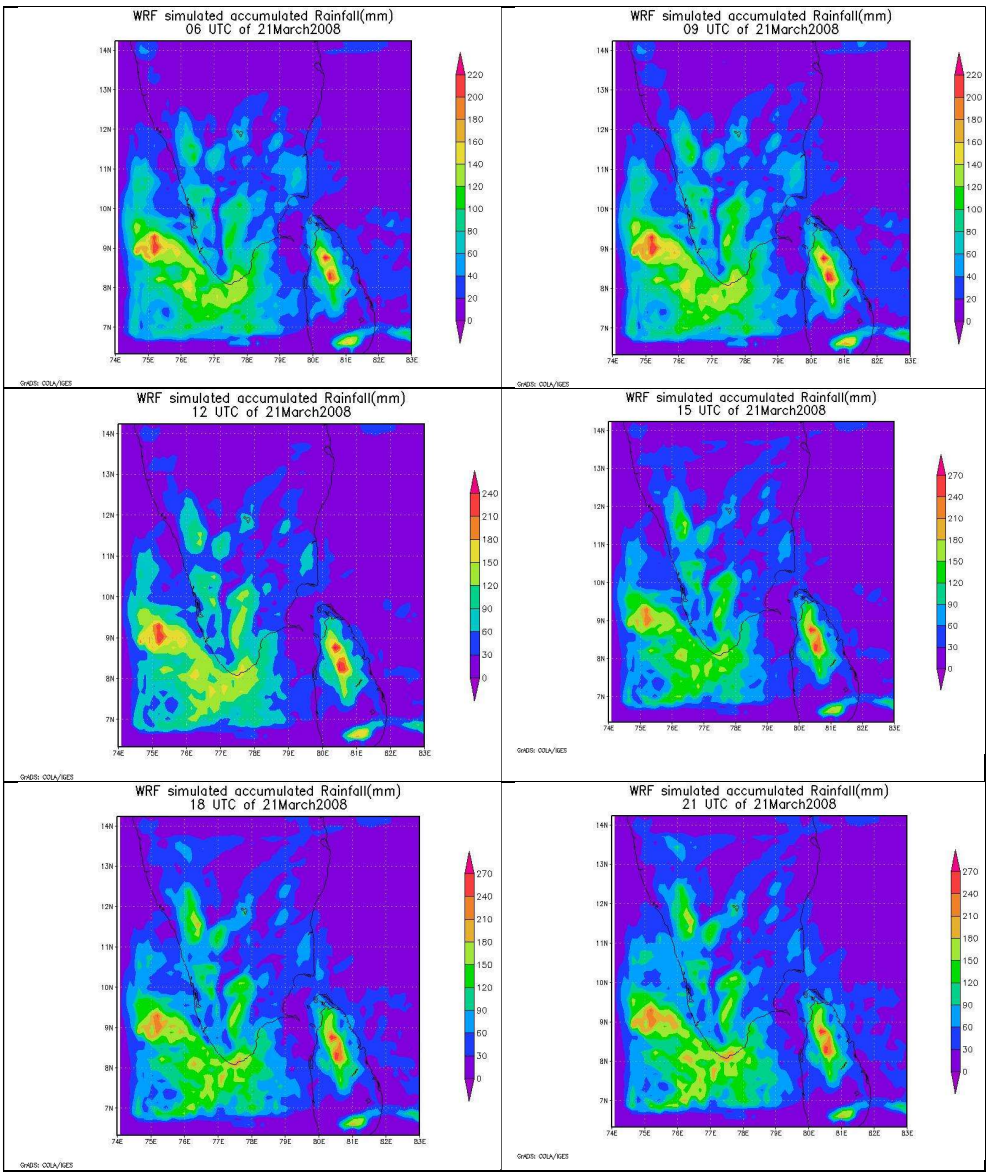


Fig.5.17d: WRF predicted accumulated rainfall(mm) from 0600UTC March 2008 to 2100 UTC 21March 2008

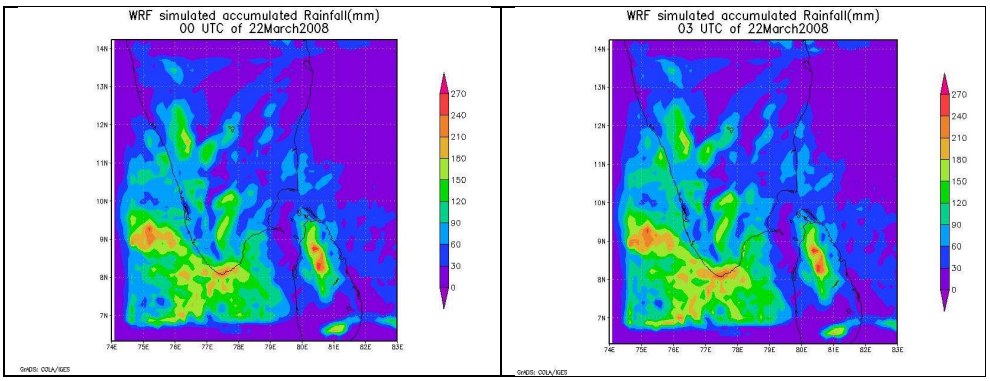


Fig.5.17e: WRF predicted accumulated rainfall(mm) from 0000UTC 22 March 2008 to 0300 UTC 22March 2008

The model simulated 3 hourly accumulated rainfall is plotted in Fig.5.17.a to Fig.5.17e. The 24 hourly accumulated rainfall of 20-22 March is plotted and compared with TRMM 3B42 daily precipitation data and comparison plot is given in Fig.5.18. The AWS observational data for Kerala and Tamil Nadu are given in Fig.5.19 and Fig.5.20 respectively. The model output shows good agreement with the observations. The three hourly variations in the 850 hPa wind of 19$^{th}$ March 2008 are plotted in Fig.5.21. The analysis of wind pattern at 850 hPa on 19$^{th}$ March has shown the interaction between the dry northerly component of wind from northwestern part of India and the southerly to southeasterly winds from the Indian ocean and Bay of Bengal. The model simulated wind at standard pressure levels at 00UTC of 20-22 March 2008 is plotted in Fig.5.22 a to Fig 5.22 c. The temporal evolution of model simulated wind at 850 hPa from 19-22 March 2008 is plotted in Fig.5.23 A cyclonic circulation was prevailing below 6$^0$N on 20$^{th}$ March. On 21$^{st}$ March the cyclonic circulation strengthened and showed northward propagation. The cyclonic circulation extended from 925 hPa to 500 hPa and was centered at 9$^0$N;75$^0$E. An anticyclonic rotation was seen at 300 hPa at 12.5$^0$N;82$^0$E. The strong southerly winds of max speed 14 m/s were observed upto 700 hPa. The

southerly component of wind extended upto 600 hPa along with the cyclonic circulation which further propagated north-westwards and was seen centred at $11.5^0$N;$74^0$E. The wind flow towards the peninsular region became southwesterly on 22nd March due to the north-westward propagation of cyclonic circulation: it showed further northward propagation at 500 hPa and was centred at $13.5^0$N;$74^0$E. An anticyclonic circulation centred at $12^0$N;$83^0$E was seen at 300 hPa on 22nd March.

The vertical cross-section of vorticity($s^{-1}$) and vertical velocity(m/s) centered at $10^0$N at 06Z19March 2008 is plotted in Fig.5.24. The vorticity and the vertical velocity at 06 UTC of 19th March have shown a very active region extending from 6 km -12 km before its manifestation as a heavy rainfall event with a lesser magnitude when compared with supercell storm.

| Actual pressure level | Model vertical level |
|---|---|
| **1013 hPa** | **1** |
| **1000 hPa** | **2** |
| **925 hPa** | **5** |
| **850 hPa** | **7** |
| **700 hPa** | **10** |
| **600 hPa** | **12** |
| **500 hPa** | **14** |
| **450 hPa** | **15** |
| **400 hPa** | **16** |
| **350 hPa** | **17** |
| **300 hPa** | **18** |
| **250 hPa** | **19** |
| **200 hPa** | **20** |
| **150 hPa** | **21** |
| **100 hPa** | **22** |
| **50 hPa** | **24** |
| **10 hPa** | **27** |

Table 5.1 Model level versus actual pressure levels

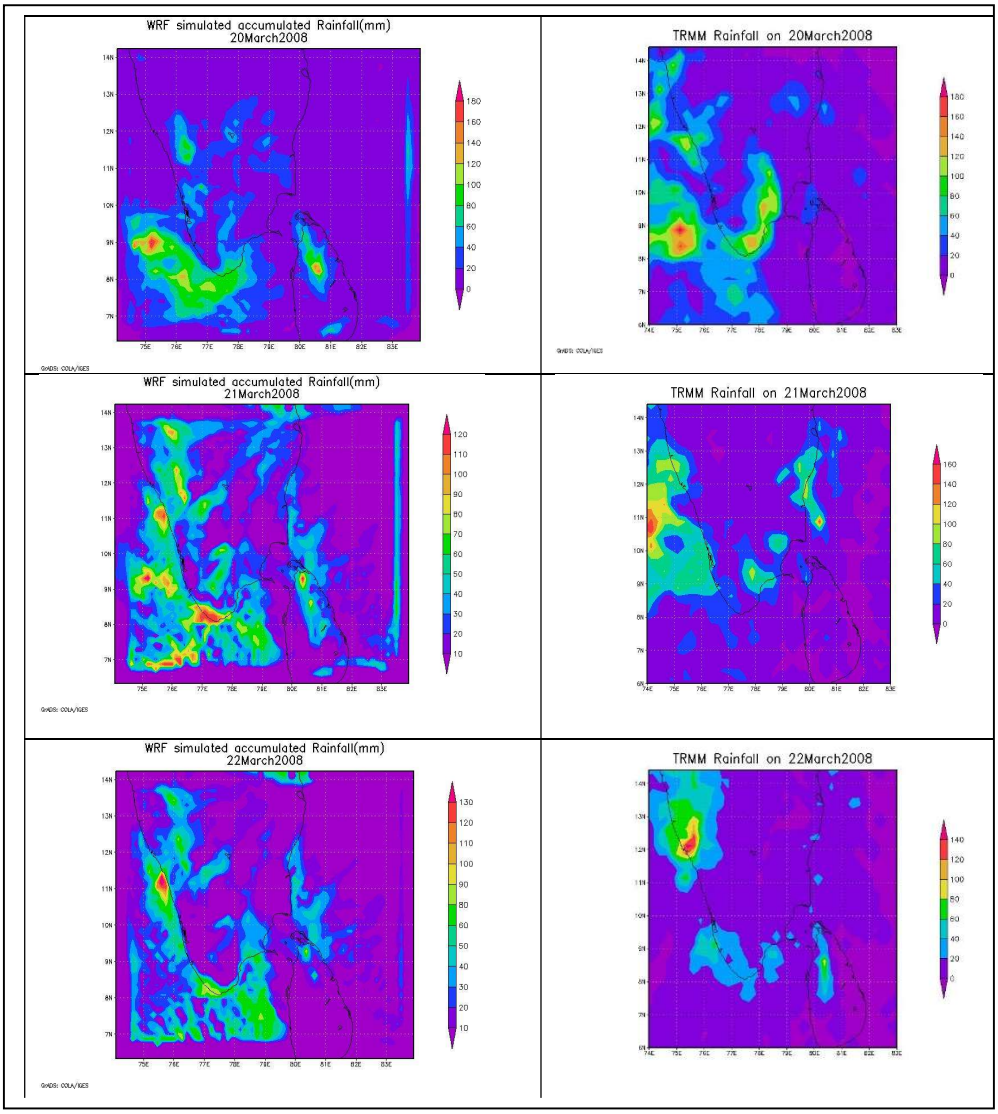


Fig.5.18: Comparison between WRF Model simulated Rainfall(mm) and TRMM Rainfall(mm)

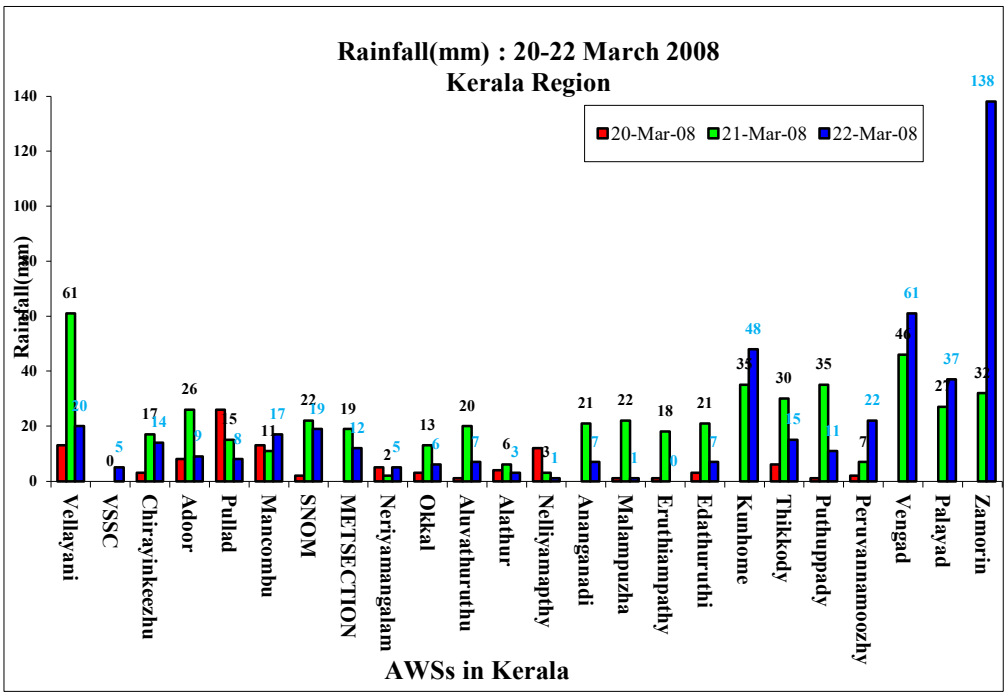


Fig.5.19: AWSs recorded rainfall during 20-22 March 2008 in Kerala from South to North

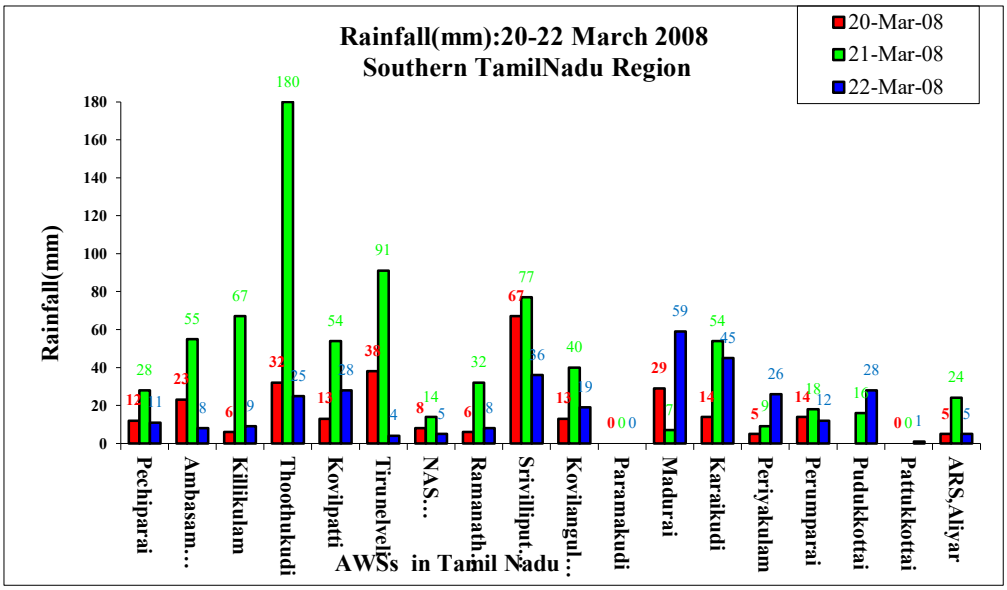


Fig.5.20: AWSs recorded rainfall during 20-22 March 2008 in Southern Tamil Nadu

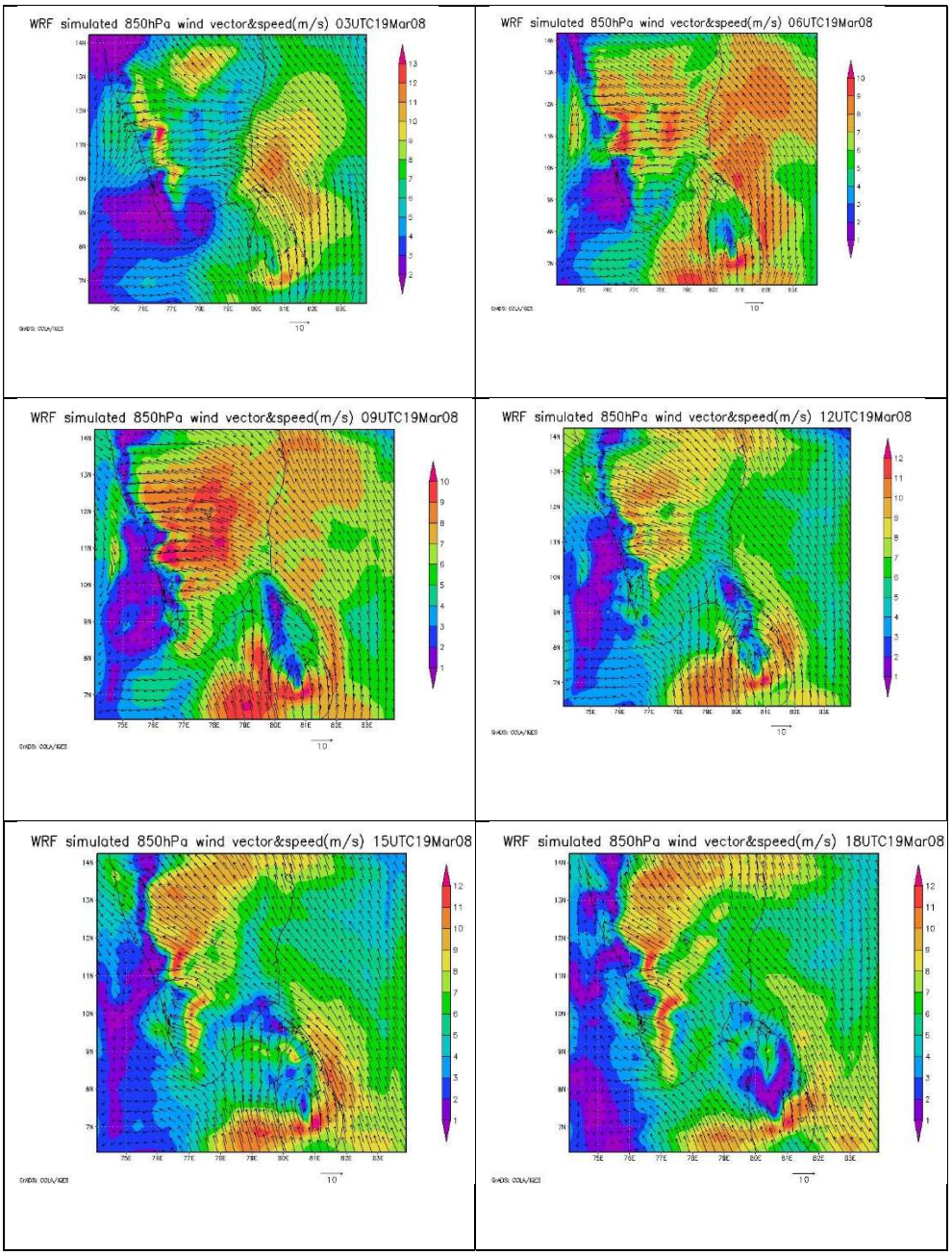


Fig.5.21: Temporal evolution of 850 hPa wind from 03UTC -18UTC of 19th March 2008

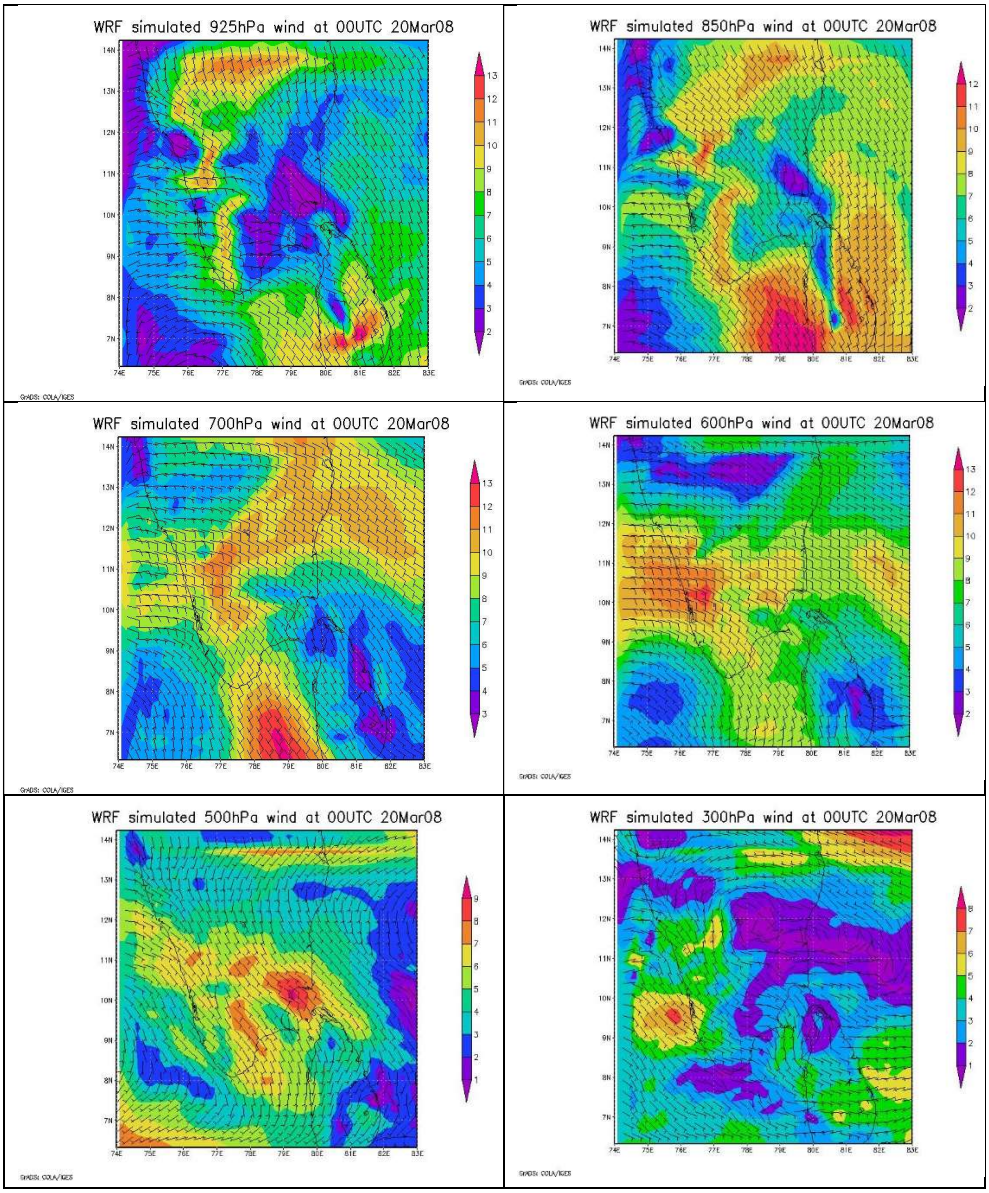


Fig.5.22a: Model simulated wind at standard pressure levels at 00UTC of 20th March 2008

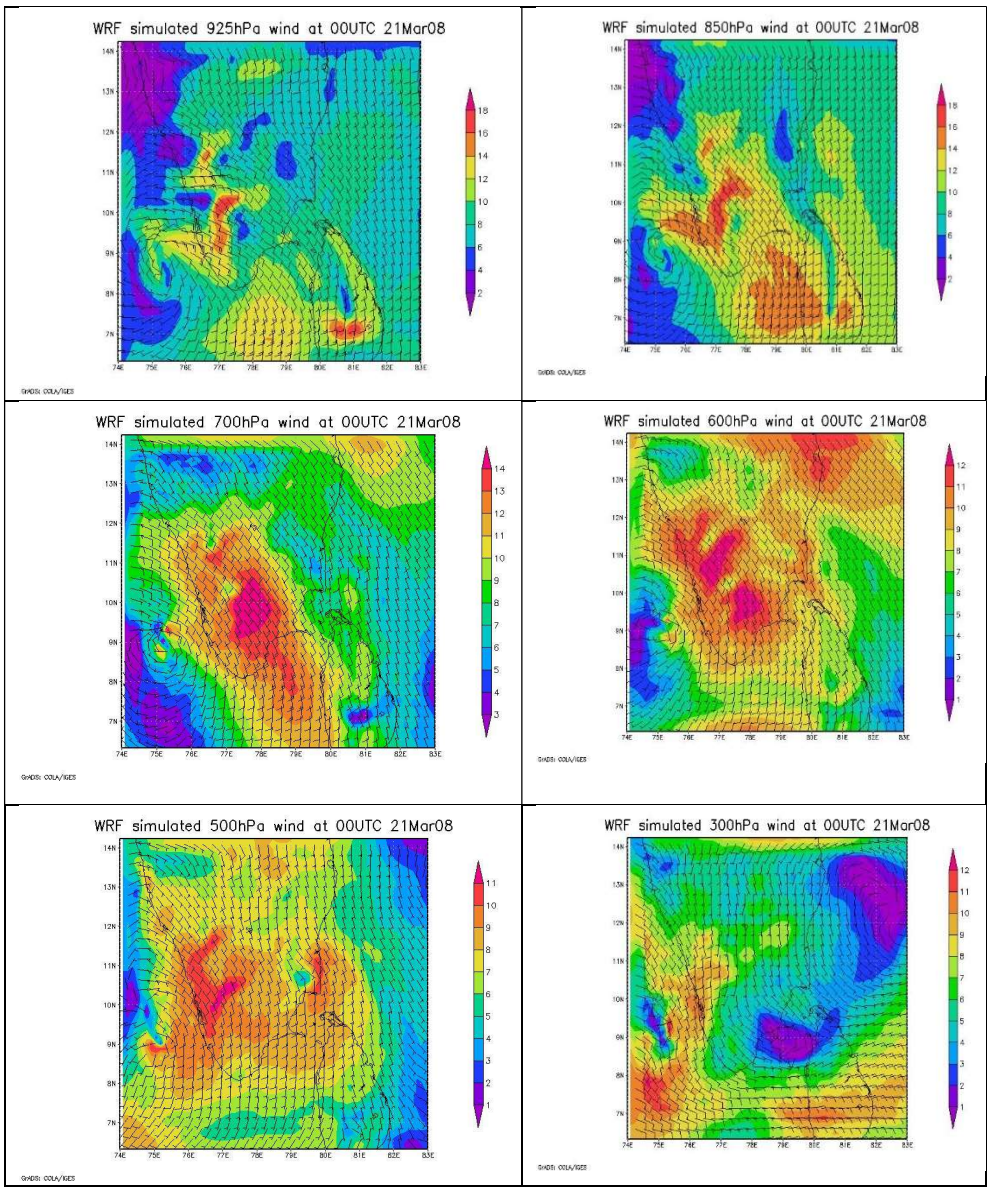


Fig.5.22b: Model simulated wind at standard pressure levels at 00UTC of 21st March 2008

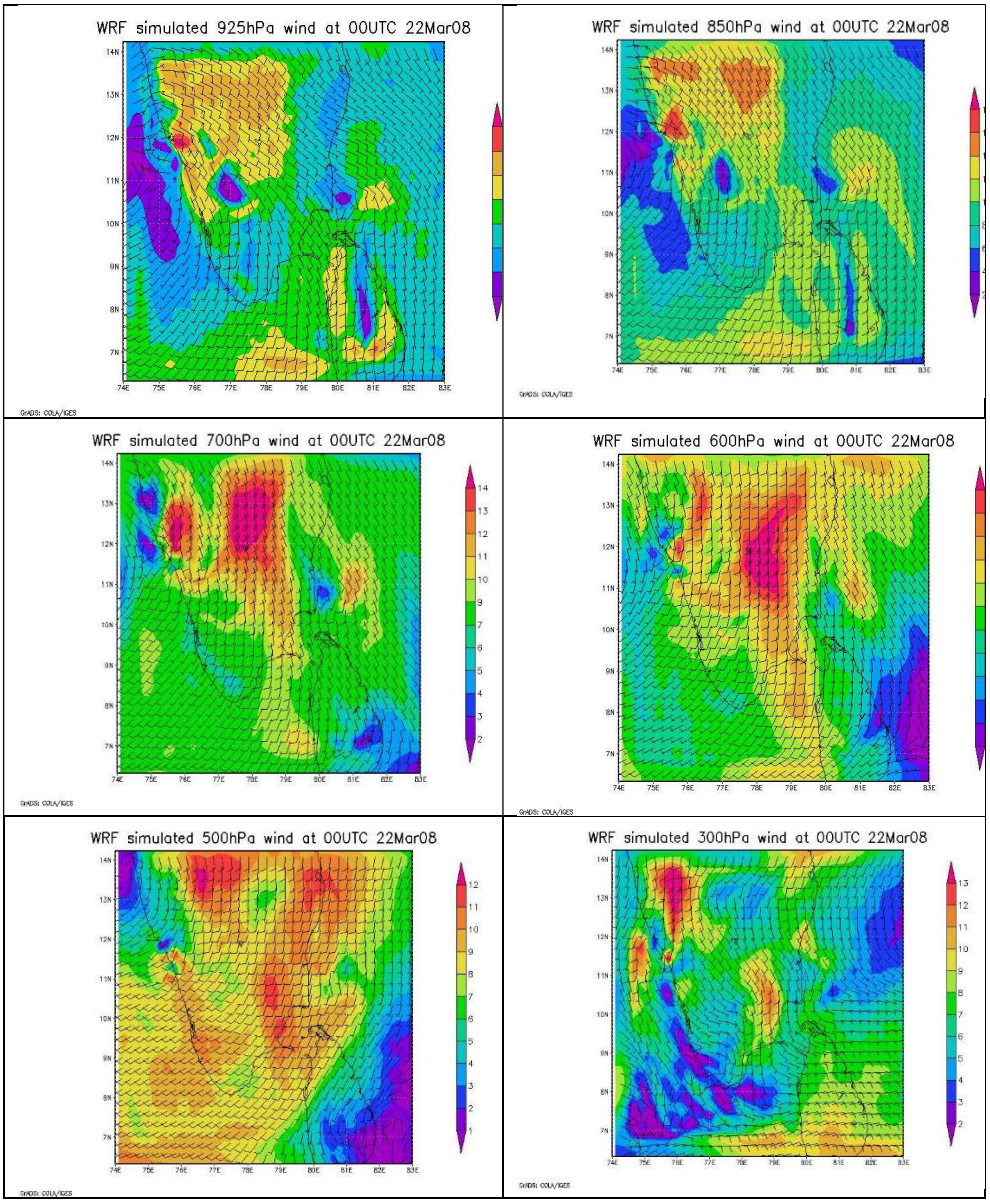


Fig.5.22c: Model simulated wind at standard pressure levels at 00UTC of 22nd March 2008

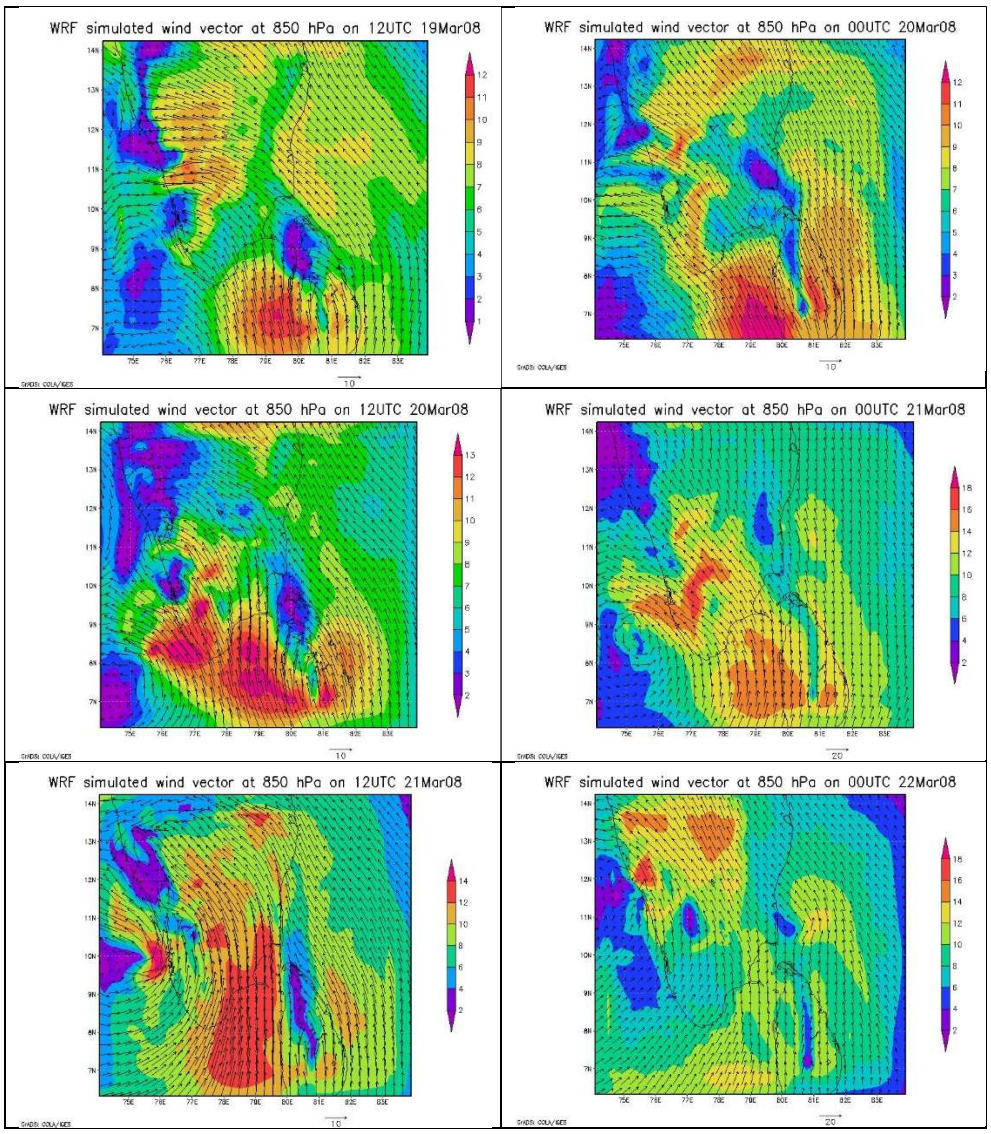


Fig.5.23: Temporal evolution of model simulated wind at 850 hPa from 19-22 March 2008

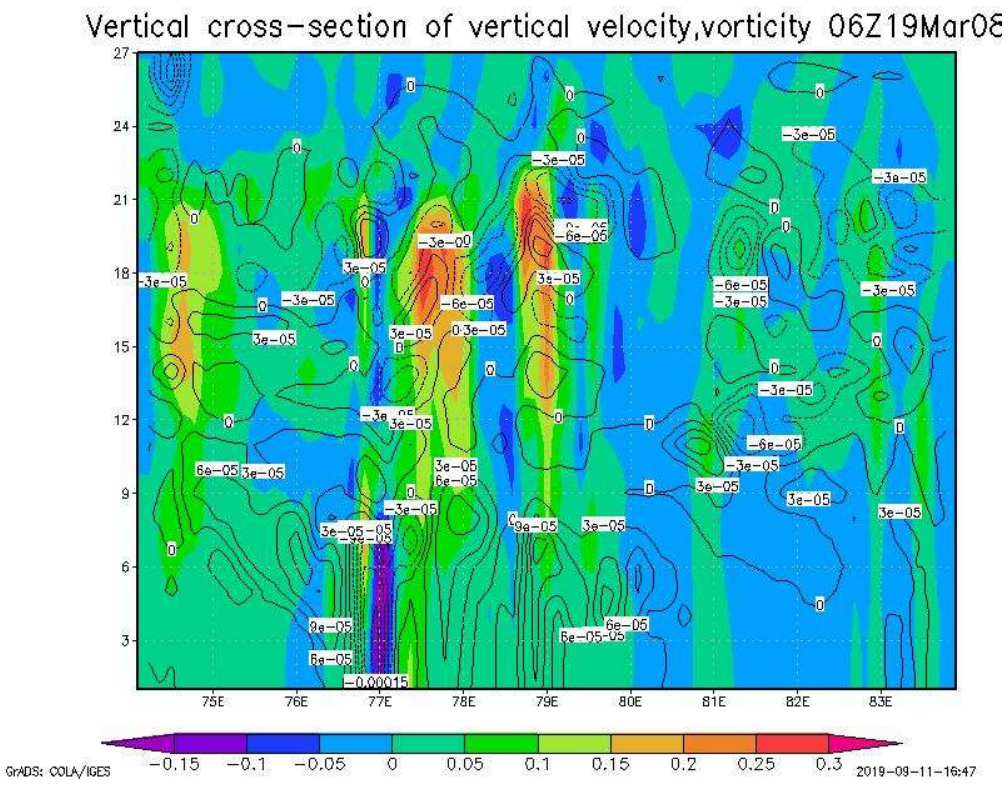


Fig.5.24 : Vertical cross-section of vorticity(s-1) and vertical velocity(m/s) centered at $10^0$N at 06Z19March 2008 (*Model levels plotted as y-axis*).

## 5.5 Conclusion/Summary

The model could simulate both the events with good spatial and temporal accuracy. The model predicted rainfall were compared with satellite based Automatic Weather Station (AWS) data and TRMM daily precipitation data.

In the first case study, the model simulated wind on $12^{th}$,$13^{th}$ and $14^{th}$ March 2008 showed the presence of strong easterlies which resulted in the low-level moisture convergence from the Bay of Bengal. A detailed analysis of the model predicted wind pattern at different vertical levels reveals mesoscale variations in circulation pattern and the presence of a coexisting low-level convergence and an upper level divergence. A large scale interacting vertical column of deep convection consisting of embedded cumulonimbus clouds at different stages was formed by deriving energy from these largescale systems. This resulted in embedded convective systems and unusual rainfall. This simulation enabled us to study the precipitation characteristics of thunderstorm cells embedded inside an easterly trough and an overlying westerly trough. It also helped us to study the nature of a convective system triggered and developed due to the presence of a large-scale phenomenon such as low level easterlies and middle and upper level westerlies.

The rainfall pattern has also shown that how a strong easterly wave could produce heavy rainfall at large no. of places with severe thunder activity. The rainfall activity which commenced over Tamil Nadu on $13^{th}$ March 2008 moved to Kerala on $14^{th}$ March 2008 due to the northward propagation of the trough in the low level easterlies and its interaction with mid level westerly trough.

In the second case study, the heavy rainfall episode during 19-22 March 2008 was simulated using WRF model with good spatial and temporal

accuracy. The model simulated rainfall was compared with TRMM 3B42 daily precipitation data and is in good agreement. This simulation enabled us to study many mesoscale circulation features associated with synoptic scale systems. The study has also shown how a deep persisting cyclonic circulation can influence the circulation pattern and weather. The low-pressure system formed over the Arabian Sea and an associated cyclonic circulation over Lakshadweep-Comorin area manifested as heavy rainfall over peninsular India especially Kerala and Tamil Nadu.

# Chapter 6
# A detailed study of an Extremely Severe Cyclonic Storm (ESCS) FANI (30 April 2019 – 03 May 2019) using WRF model

## 6.1 Introduction

A tropical cyclone is a large-scale convective system driven by a temperature difference between the hot tropical sea surface and the cold top of the troposphere and is characterised by a low-pressure centre surrounded by a spiral of strong converging winds towards the centre. The typical diameter varies from 200 to 2000 km with wind speed 20 - 85 m/s and the typical central pressure ranges from 990- 870hPa with a corresponding central pressure drop of 20-140 hPa. Tropical cyclones with maximum wind speeds larger than 33 m/s are called typhoons in the western North Pacific, hurricanes in the eastern North Pacific and western North Atlantic and severe tropical cyclones in other regions. [Bergeron (1954) and Emanuel (2003)].

An Extremely Severe Cyclonic Storm FANI occurred during 30$^{th}$ April 2019- 03$^{rd}$ May 2019 in Bay of Bengal and hit Odisha on 3$^{rd}$ May 2019. Numerical simulation of FANI was carried out using WRF with the most suitable combination of parameterization schemes and is presented in this chapter.

## 6.2 Case Description

IMD tracked a depression located west of Sumatra on 26 April 2019, classifying it as BOB 02 and was upgraded to a deep depression on 27 April 2019. Six hours later, the IMD upgraded the system to a cyclonic storm

FANI. The Joint Typhoon Warning Center (JTWC) upgraded Fani to a Category 1-equivalent cyclone late on 29 April and on 30 April, Fani was upgraded to a very severe cyclonic storm at 00 UTC by the IMD. The organization of the system continued to improve, with tight spiral banding wrapping into a formative eye feature resulting in Fani being upgraded to an extremely severe cyclonic storm around 12:00 UTC while the JTWC upgraded the storm to a Category 3-equivalent cyclone hours later. Further development proceeded more slowly over the following days : Fani was upgraded to a Category 4-equivalent cyclone by the JTWC at 0600 UTC of 2$^{nd}$ May. Shortly after, Fani started another period of rapid intensification. At 0800 hrs IST of 3$^{rd}$ May, Fani made landfall near Puri, Odisha as a severe cyclonic storm, with 3-minute sustained winds of 185 km/h (115 mph). This made Fani the most intense storm to make landfall in India's Odisha state since the 1999 Odisha cyclone. Fani's convective structure degraded and it weakened to a Category 1-equivalent tropical cyclone soon after landfall and continued to weaken to a cyclonic storm later that day, before passing just north of Kolkata. On 4 May, Fani weakened to a deep depression and moved into Bangladesh before degenerating into a well-marked low later on the same day. Fani's remnant low dissipated over Bhutan on 5$^{th}$ May.

### 6.3 Experimental setup and Model configuration

In this study, the Weather Research Forecast (WRF) model (version 3.8.1) is run with three nested domains with a horizontal resolution of 9 km in the outer domain, 3 km in the middle domain and 1 km in the innermost domain. The simulation domain set up by the WPS program for the cyclonic storm is shown in Fig 6.3. The first domain is referred as D1, the second domain as D2 and the third domain as D3. Two-way nesting technique with three domains are selected for simulating this event with a horizontal

resolution of 1 km for the innermost domain. The model is run using the Kain-Fritsch (new Eta) scheme for cumulus parameterization (Kain and Fritsch 1993), Yonsei University (YSU) scheme for the boundary layer parameterization (Hong et al. 2006; Hong 2010), WSM 3 class simple ice scheme for microphysics (Hong et al. 2004) and Rapid Radiative Transfer Model (RRTM) for long wave radiation (Mlawer et al. 1997) and Dudhia scheme for short wave radiation (Dudhia 1989). The grid staggering is the Arakawa C-grid. The model uses the Runge-Kutta 2$^{nd}$ and 3$^{rd}$ order time integration schemes, and 2$^{nd}$ to 6$^{th}$ order advection schemes in both the horizontal and vertical. It uses a time-split small step for acoustic and gravity-wave modes.

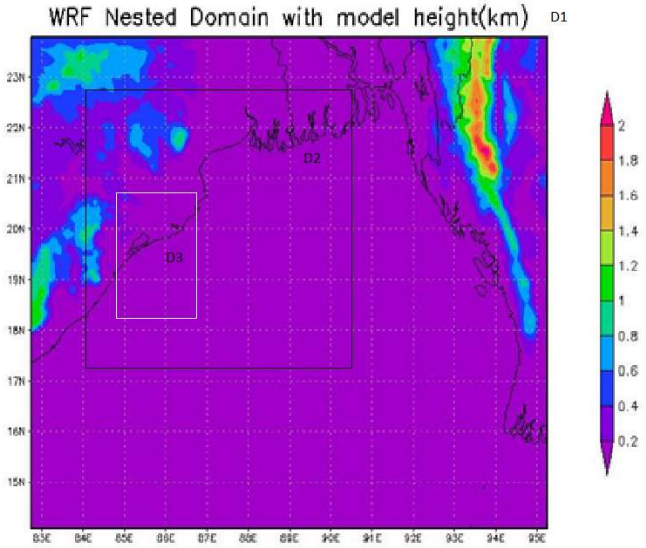


Fig.6.1: Two-way nested domains configured for the simulation of Extremely Severe Cyclonic Storm FANI during 30$^{th}$ April 2019 -03$^{rd}$ May2019. D1, D2, D3 refers to the first, second and third domain.

## 6.4 Data used

The initial and lateral boundary conditions for the model run is taken from the Final (FNL) Operational Global Tropospheric Analyses of National Centre for Environmental Prediction (NCEP) on $1^0$ x $1^0$ grids prepared operationally every six hours. This FNL dataset is developed from the Global Data Assimilation System (GDAS), which continuously collects observational data from the Global Telecommunications System (GTS) and other sources. The United States Geological Survey (USGS) Global dataset with 30 sec horizontal resolution were used to create terrain/topography and landuse/vegetation fields. Half hourly INSAT IR imageries (KALPANA-1) embedded with cloud top temperature ($^0$C) contours over east and northeast India as well as the composite reflectivity imageries from Doppler Weather Data, Kolkata of India Meteorological Department (IMD) is also utilised in this study to observe the occurrence and evolution of this event.

Fig.6.2 Sat Image showing the ESCS FANI at peak intensity on 06 UTC 2May 2019

## 6.5 Results and Discussion

The structure and evolution of FANI is studied using the model simulated reflectivity, sea level pressure, wind speed and direction etc. Fig. 6.3 – Fig. 6.6 shows the WRF simulated reflectivity of the cyclonic storm from 1200UTC 01May2019 to 0900UTC 03 May2019. The composite reflectivity is plotted for every 3 hour and it shows the spiral band structure of the cyclone, eyewall as well as the eye of the system. Reflectivity analysis have shown the advancement and intensity (maximum reflectivity exceeded 50dBz) of the system as well as structural details. The advancement of the convective system is compared with observed path and the model simulated track matches very well with the observed track and the comparison is given in Table 6.1.

The structure as well as the spatial and temporal evolution of the cyclone is simulated with good accuracy. FANI made landfall in Puri, Odisha at 0300 UTC of 3$^{rd}$ May 2019. The reflectivity plotted for the 0300UTC of 3$^{rd}$ May 2019 has clearly shown the landfall in Puri and the advancement of the cloud bands over land.

Fig. 6.7 - Fig. 6.10 show the model simulated sea level pressure (SLP) from 1200UTC 01May2019 – 0900 UTC 03May2019. The sea level pressure is plotted for every three hour and is compared with the observations it is in good agreement with the observations with minimum pressure of 940 hPa against the observed value of 932 hPa.

The observed wind speed and estimated central pressure are given in Fig.6.12 and the model simulated wind speed and central pressure were in good agreement with the observations. The sharp pressure drop during the advancement of FANI towards the coast of Odisha at 00 UTC of 03 May 2019

was observed and is plotted in Fig.6.10. Fig 6.12 -Fig.6.14 show the WRF simulated accumulated rainfall(cm).

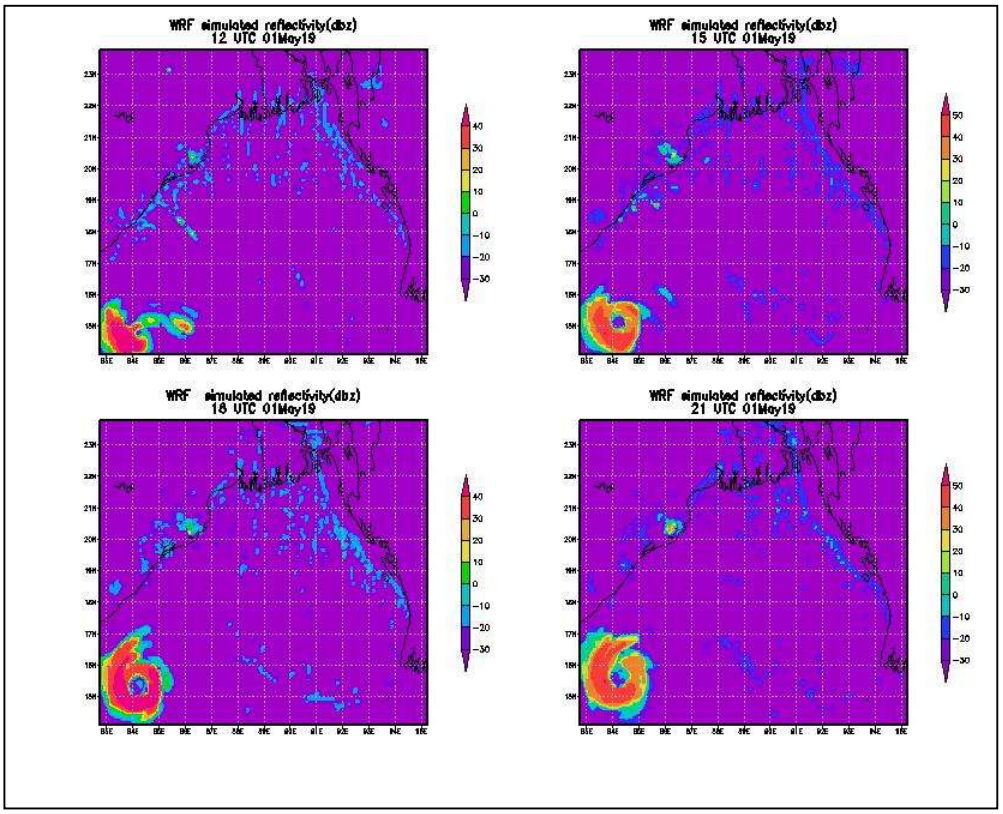


Fig.6.3 : WRF simulated Reflectivity(dBz) of cyclone FANI from 12UTC 01May19 to 21UTC 01May19

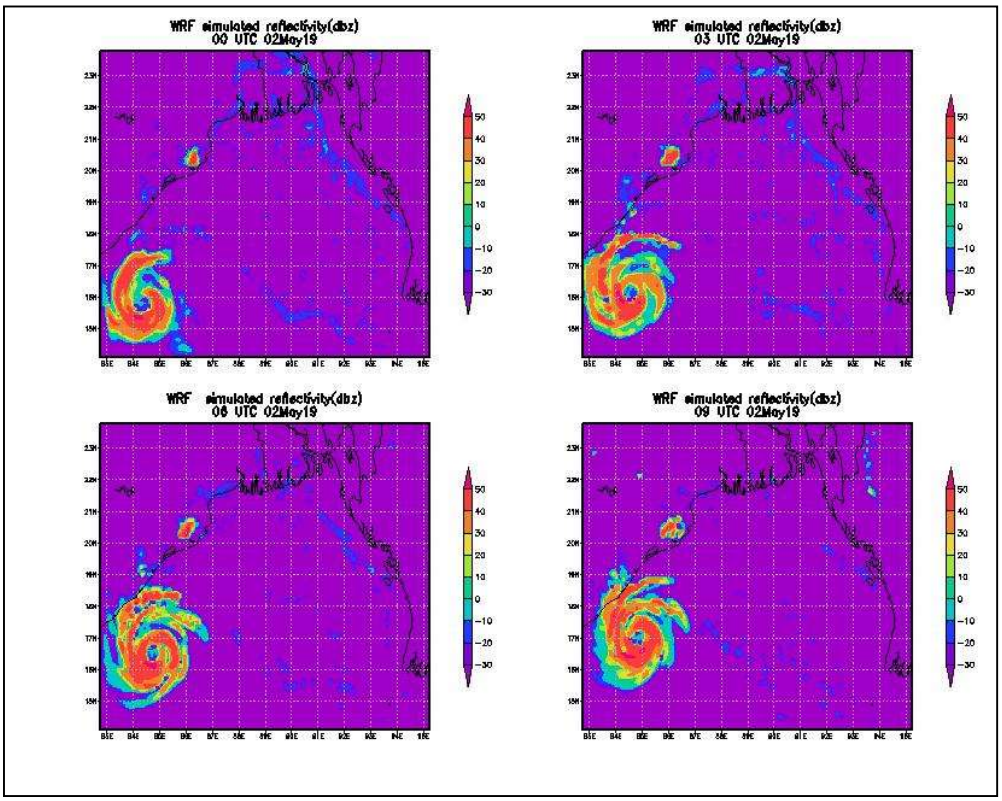


Fig.6.4 : WRF simulated Reflectivity(dBz) of cyclone FANI from 00UTC 02May19 to 0900Z 02May19

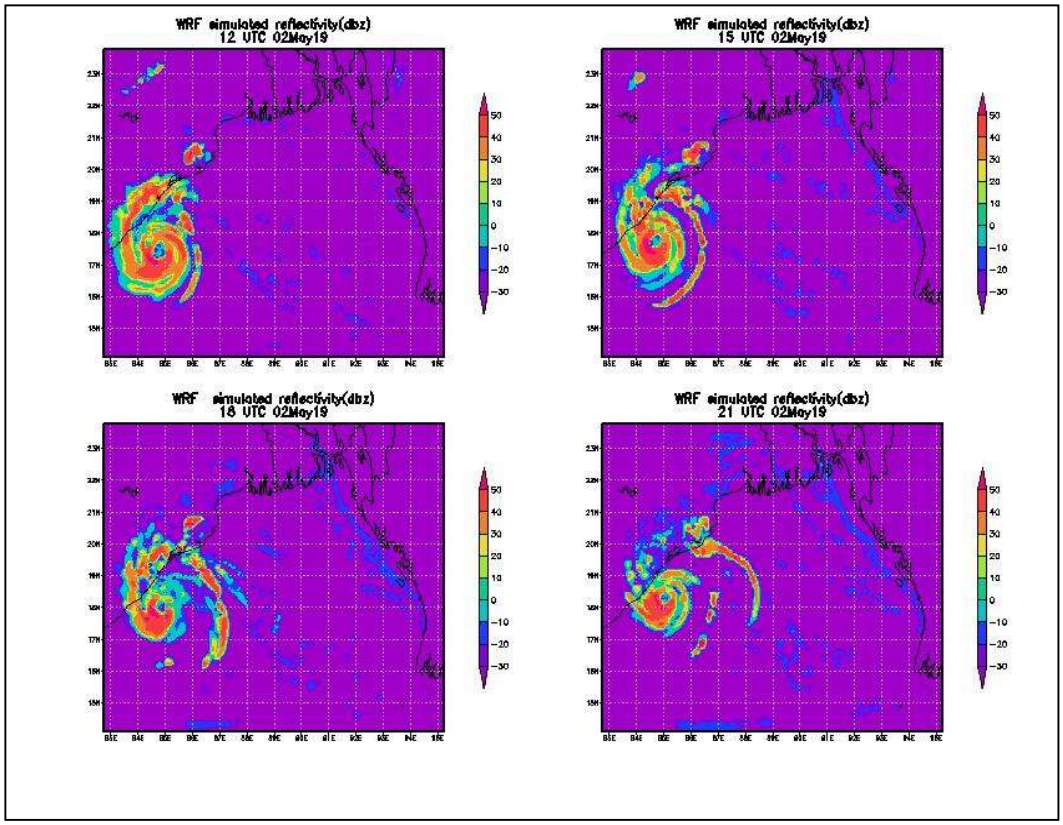


Fig.6.5 : WRF simulated Reflectivity(dBz) of cyclone FANI from 12UTC 02May19 to 21UTC 02May19

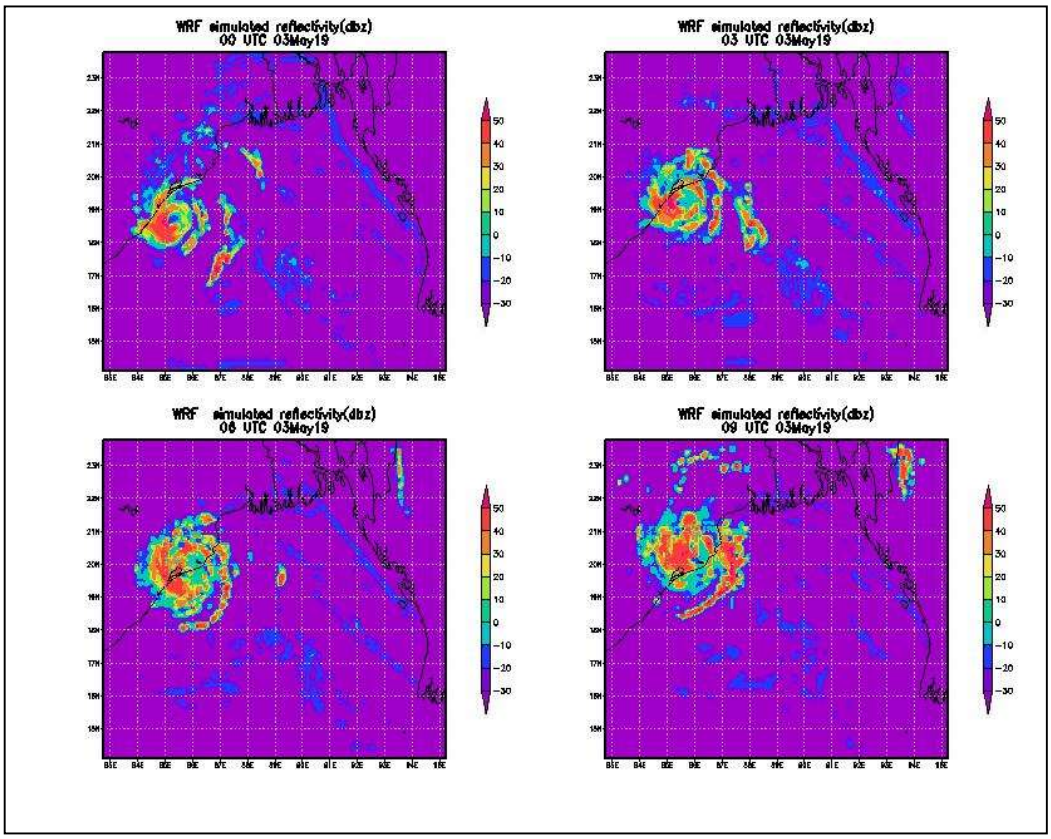


Fig.6.6 : WRF simulated Reflectivity(dBz) of cyclone FANI from 00UTC 03May19 to 0900Z 03May19

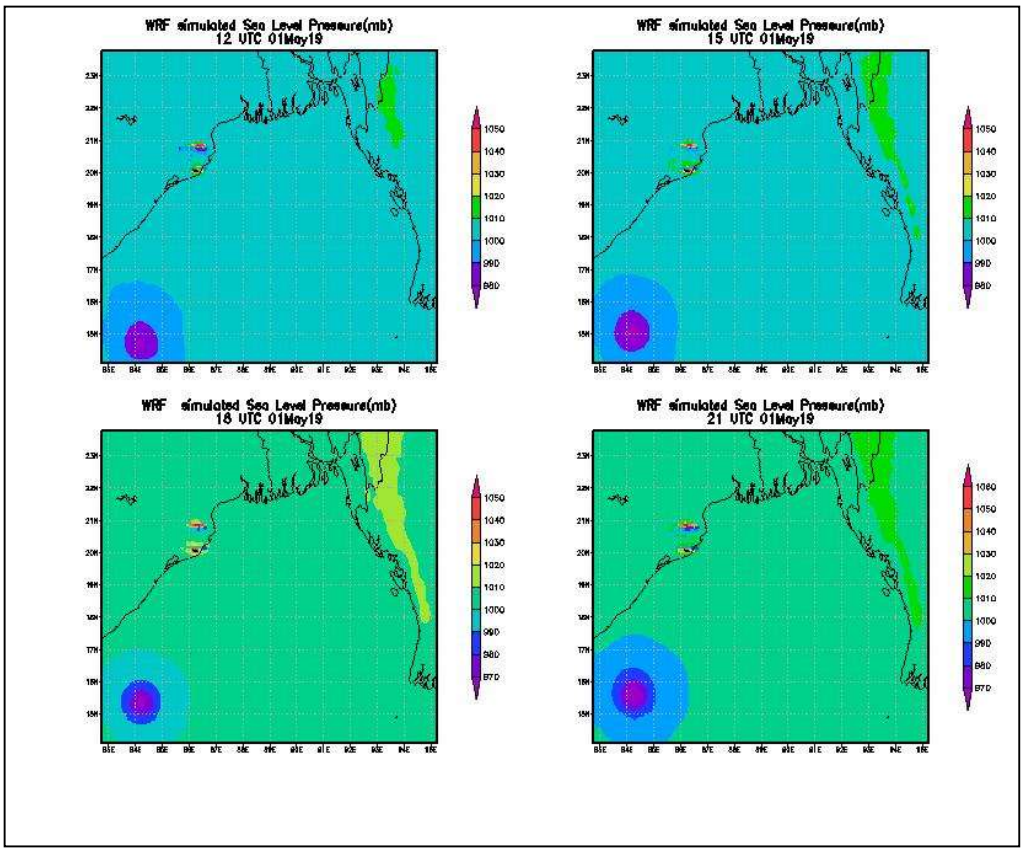


Fig.6.7 : WRF simulated Sea level Pressure from 12UTC 01May19 to 21UTC 01May19

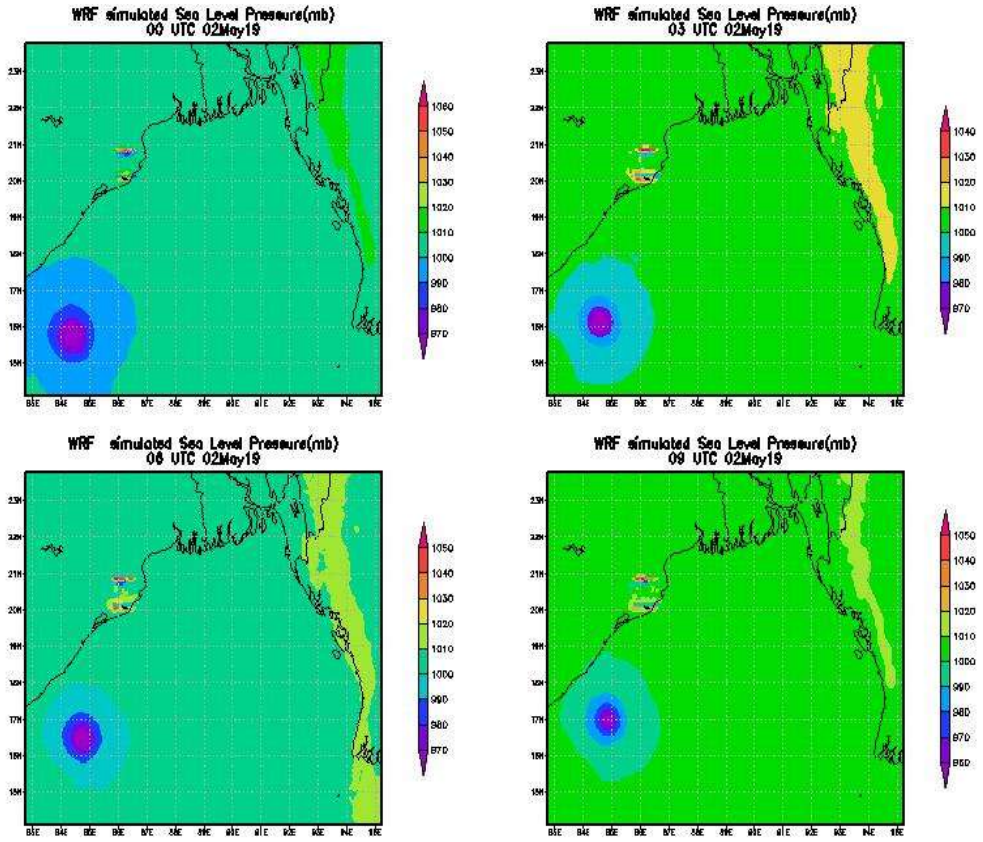


Fig.6.8 : WRF simulated Sea level Pressure from 00UTC 02May19 to 09UTC 02May19

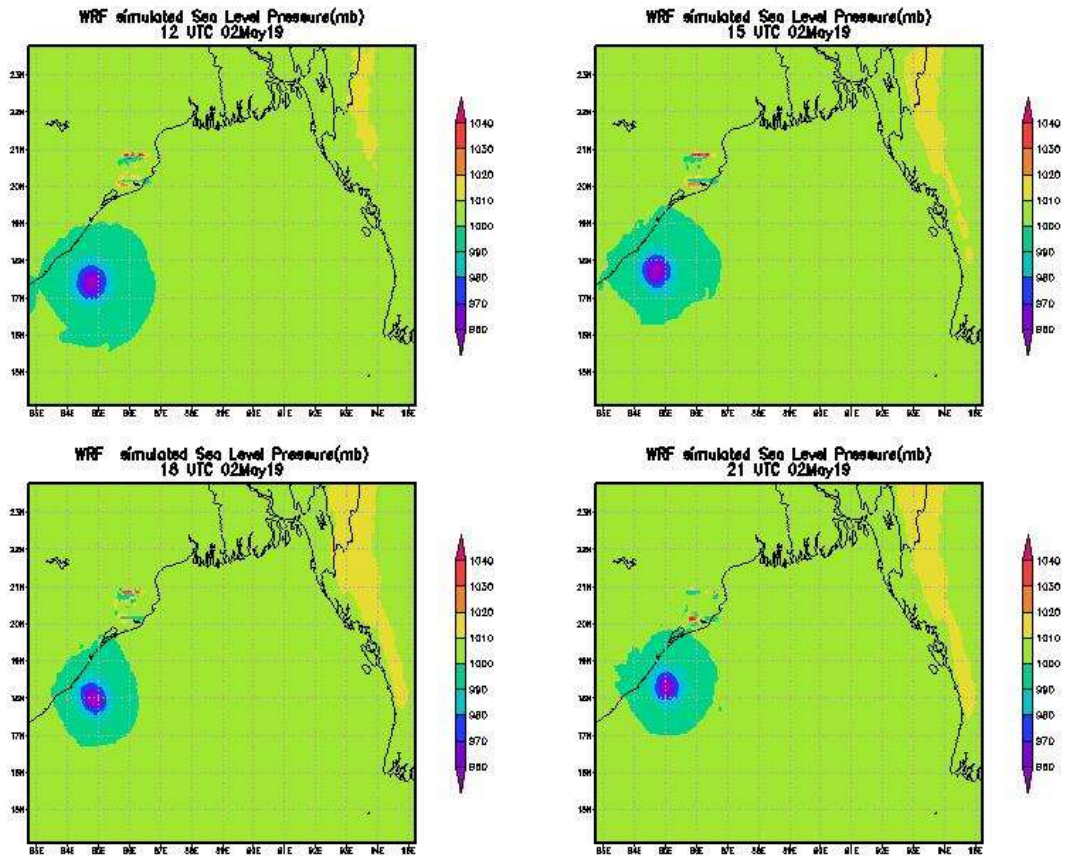


Fig.6.9 : WRF simulated Sea level Pressure from 12UTC 02May19 to 21UTC 02May19

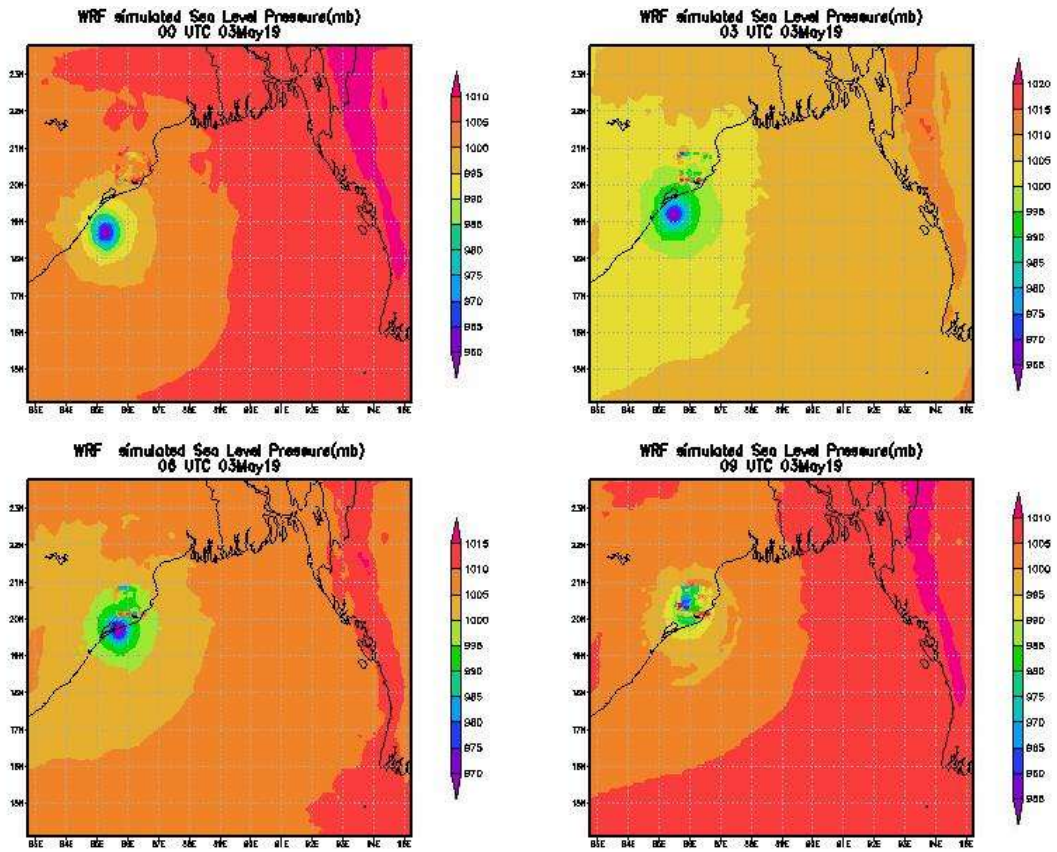


Fig.6.10 : WRF simulated Sea level Pressure from 00UTC 03May19 to 0900Z 03May19

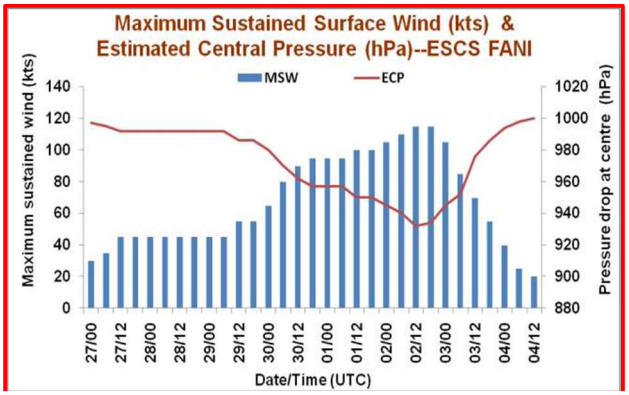


Fig.6.12 Observed Max. Sustained Surface Wind and estimated central Pressure(hPa) of ESCS FANI (Source : IMD REPORT)

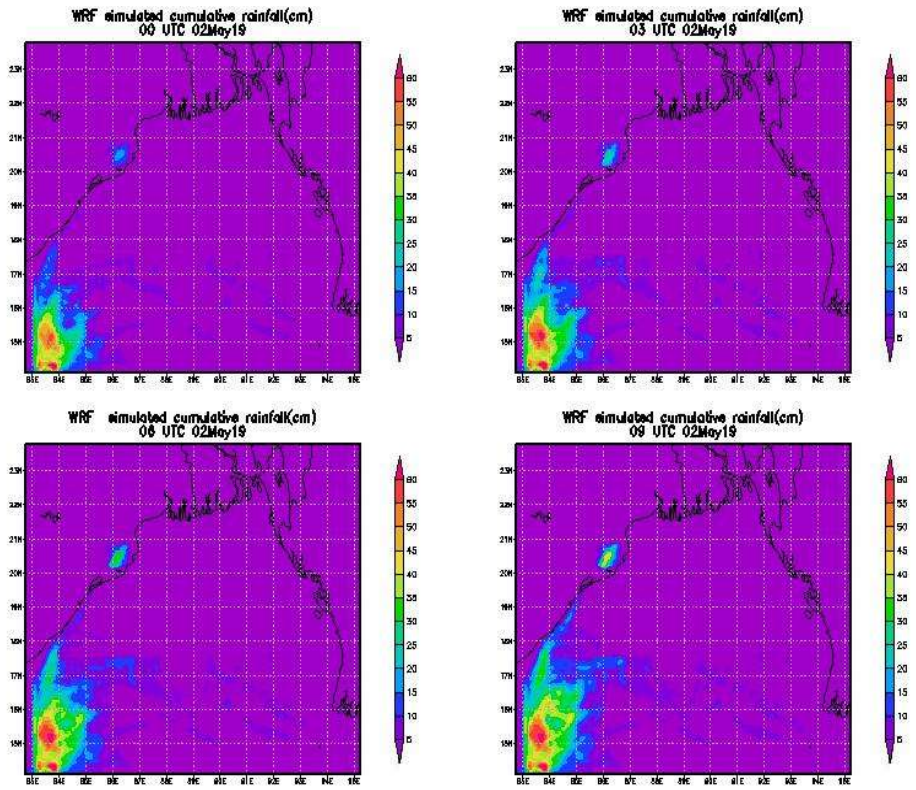


Fig.6.11: WRF simulated accumulated cumulative rainfall (cm) from 12UTC 01May19 to 21UTC 01May19

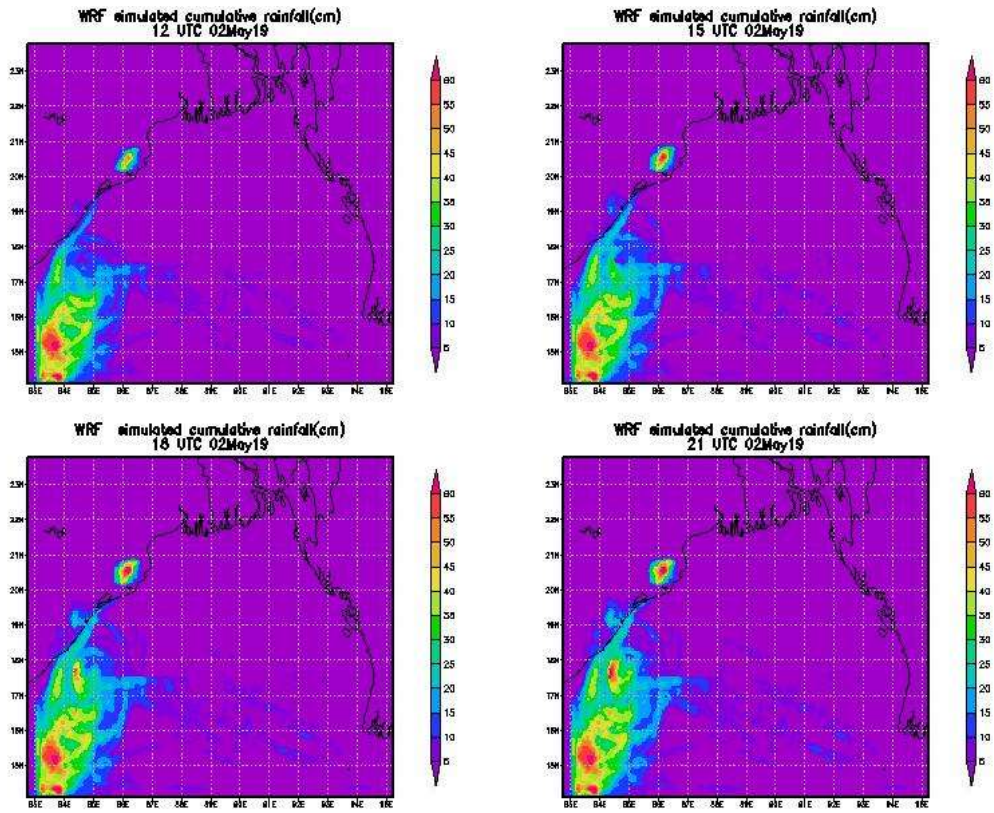


Fig.6.13: WRF simulated accumulated cumulative rainfall(cm) from 12UTC 02May19 to 21UTC 02 May19

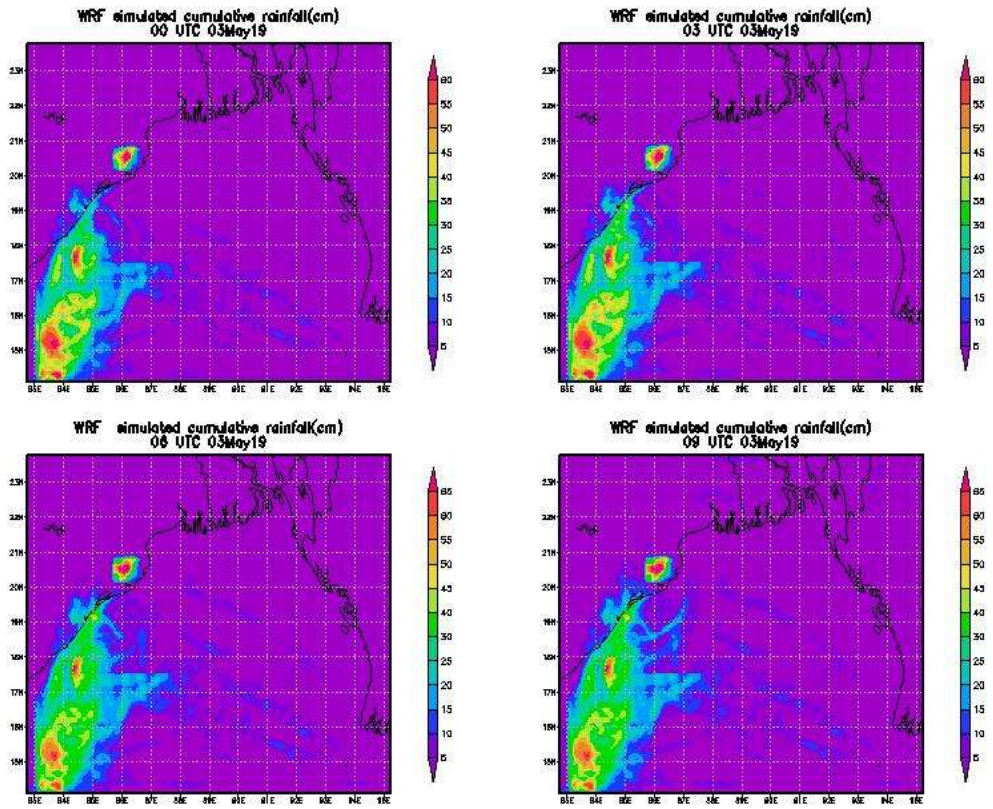


Fig.6.14: WRF simulated accumulated cumulative rainfall(cm) from 00UTC 03May19 to 09UTC 03 May19

Fig. 6.15 – Fig. 6.18 show the model simulated wind speed characteristics during the evolution of the system. As per IMD report, the system crossed Odisha coast close to Puri with maximum sustained wind speed of 175-185 kmph (48.6 – 51.3 m/s) on 3rd May 2019 between 0800 to 1000 hrs IST. Fig.7.18 shows the wind speed of FANI on 3rd May. The simulated max wind speed was 45m/s and is in good agreement with the observation.

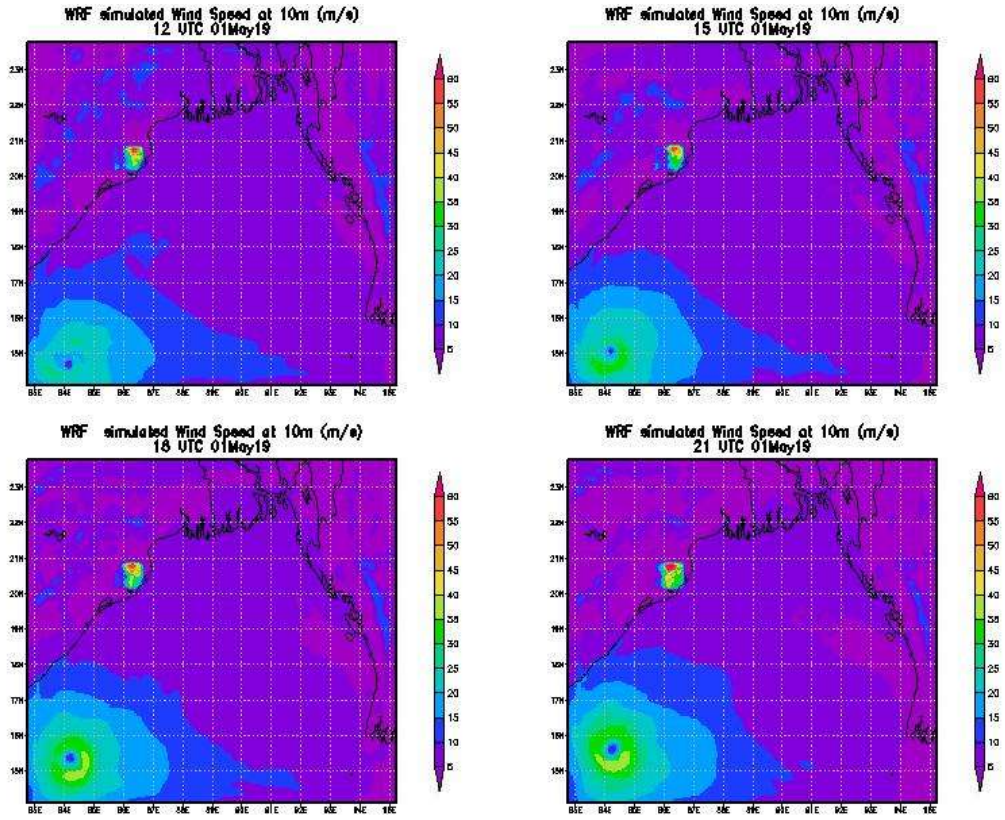


Fig.6.15: WRF simulated wind speed (m/s) ) from 12UTC 01May19 to 21UTC 01May19

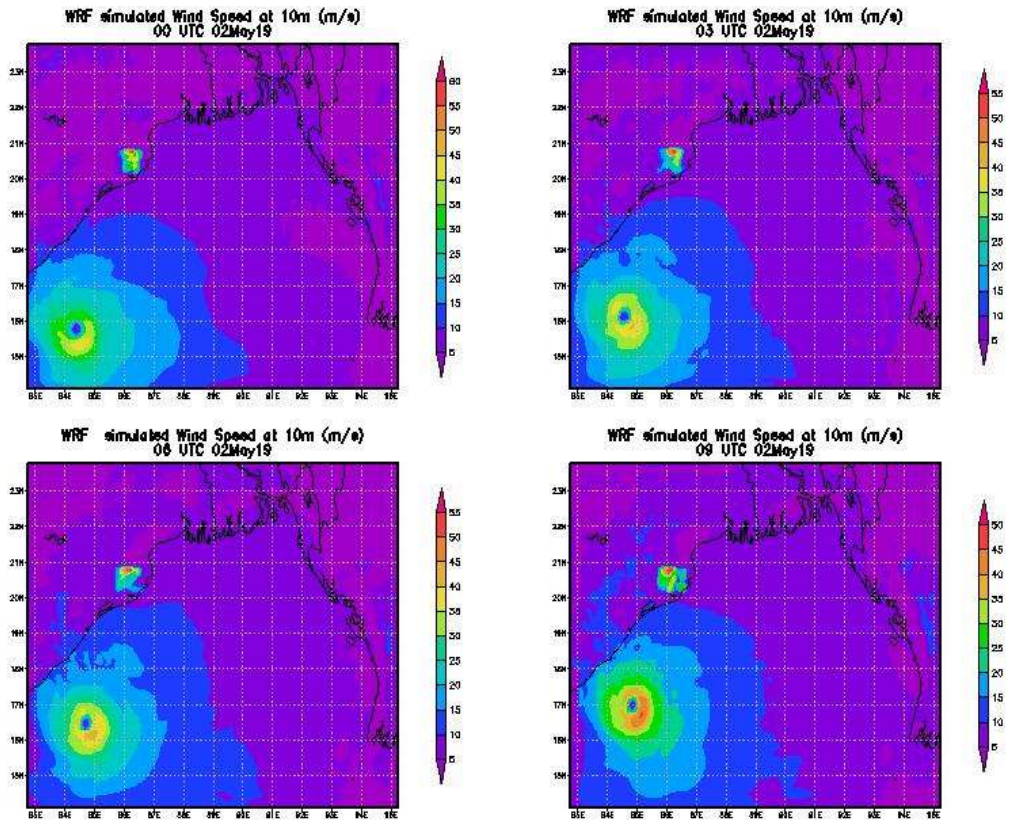


Fig.6.16: WRF simulated wind speed (m/s) ) from 00UTC 02May19 to 09UTC 02May19

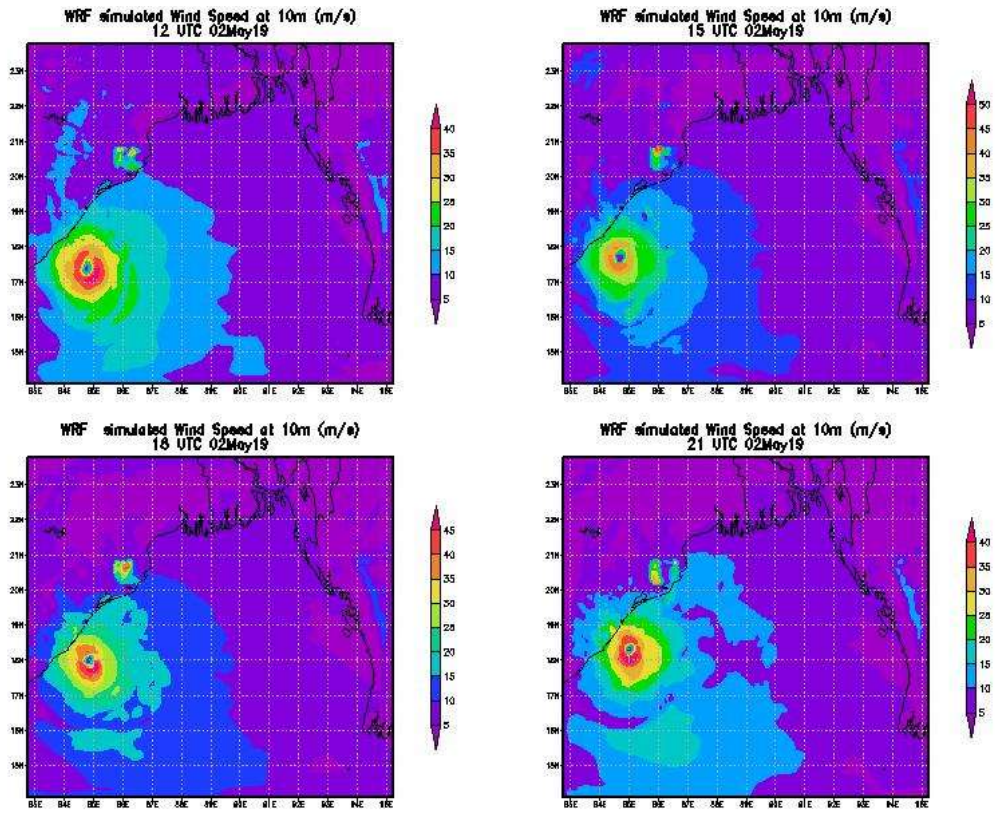


Fig.6.17: WRF simulated wind speed (m/s) ) from 12UTC 02May19 to 21UTC 02May19

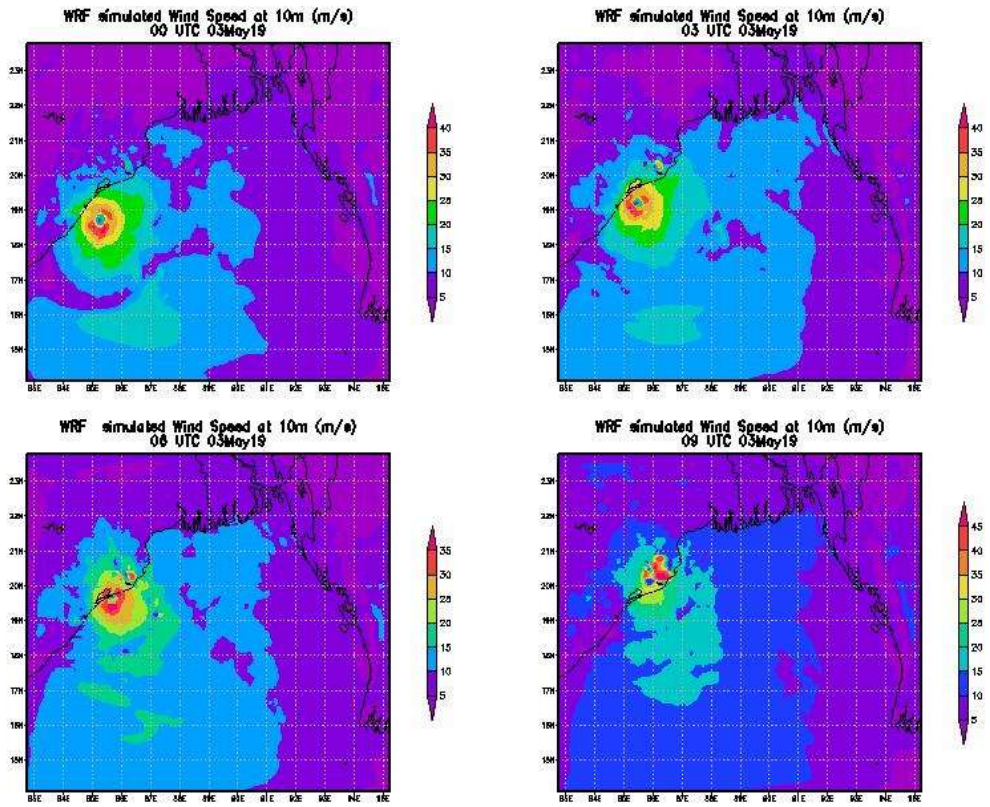


Fig.6.18: WRF simulated wind speed (m/s) ) from 00UTC 03May19 to 09UTC 03May19

| **01 May 2019** | **Observed location** | | **Model location** | |
|---|---|---|---|---|
| | **Lat($^0$N)** | **Lon($^0$E)** | **Lat($^0$N)** | **Lon($^0$E)** |
| 12UTC | 14.9 | 84.1 | 14.9 | 84.1 |
| 15 UTC | 15.1 | 84.1 | 15.1 | 84.1 |
| 18 UTC | 15.2 | 84.1 | 15.2 | 84.1 |
| 21 UTC | 15.5 | 84.2 | 15.5 | 84.1 |
| **02 May 2019** | | | | |
| 00UTC | 15.9 | 84.5 | 15.9 | 84.5 |
| 03 UTC | 16.2 | 84.6 | 16.2 | 84.6 |
| 06 UTC | 16.7 | 84.8 | 16.7 | 84.8 |
| 09 UTC | 17.1 | 84.8 | 17.1 | 84.8 |
| 12UTC | 17.5 | 84.8 | 17.5 | 84.8 |
| 15 UTC | 17.8 | 84.9 | 17.8 | 84.9 |
| 18 UTC | 18.2 | 85 | 18 | 84.9 |
| 21 UTC | 18.6 | 85.2 | 18.5 | 85 |
| **03 May 2019** | | | | |
| 00UTC | 19.1 | 85.5 | 19 | 85.4 |
| 03UTC | 19.6 | 85.7 | 19.4 | 85.5 |

Table 6.1: Comparison of observed and simulated location of ESCS FANI

The model simulated location of FANI is compared in Table 6.1. It reached its peak intensity at 06 UTC of 2$^{nd}$ May 2019 and hit Odisha coast on 03 May 2019. Here, an attempt is made to understand the characteristics of the cyclone during its peak intensity as well as during landfall. The characteristics of FANI in its peak intensity is studied and the results are plotted in Fig. 6.19 – Fig.6.23. The landfall characteristics are also studied and the results plotted in Fig.6.24- Fig.6.27. Fig.6.20 shows the vertical cross section of rotational wind component at 06UTC of 02$^{nd}$ May when it is in its peak intensity. Fig.6.24 shows the vertical cross section of rotational wind component at 03UTC of 03$^{rd}$ May when it hit Puri ,Odisha.

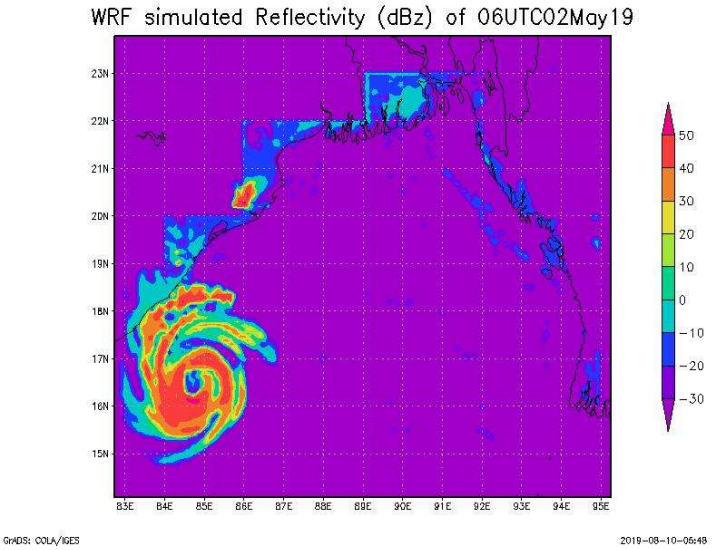


Fig.6.19: WRF simulated reflectivity when the cyclone is in its peak intensity (06UTC 02May19)

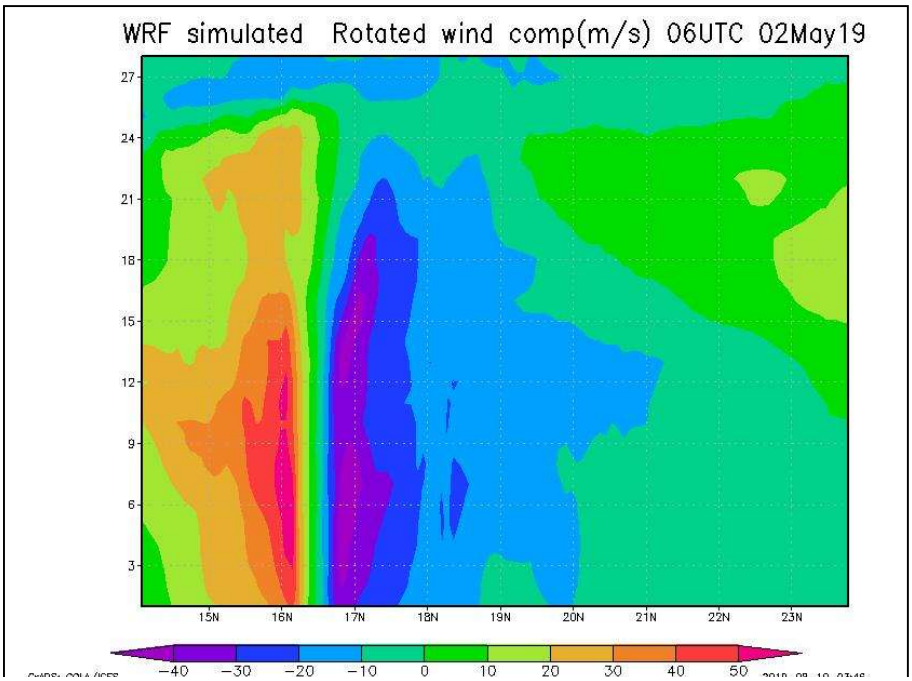


Fig.6.20:WRF simulated vertical cross section of rotational wind component at 06UTC of 02nd May when it is in its peak intensity

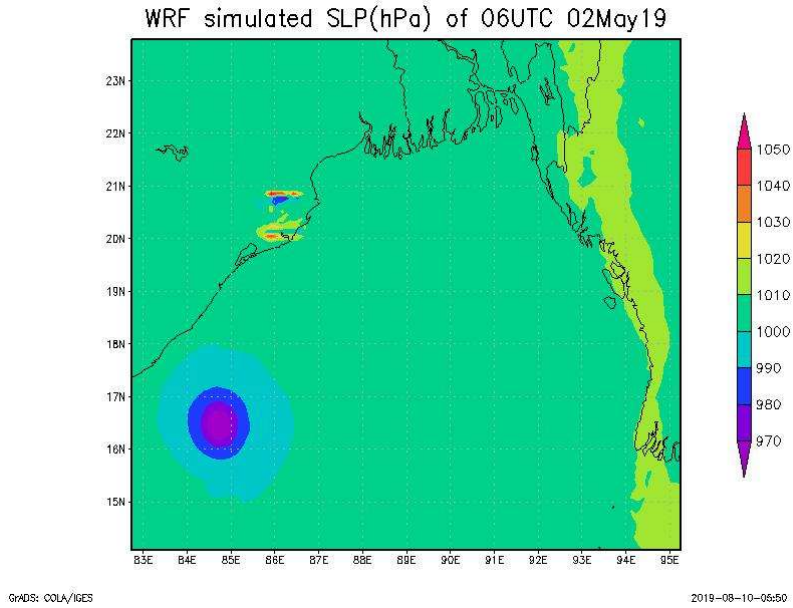


Fig.6.21: WRF simulated MSLP (hPa) when the cyclone is in its peak intensity (06UTC 02May19)

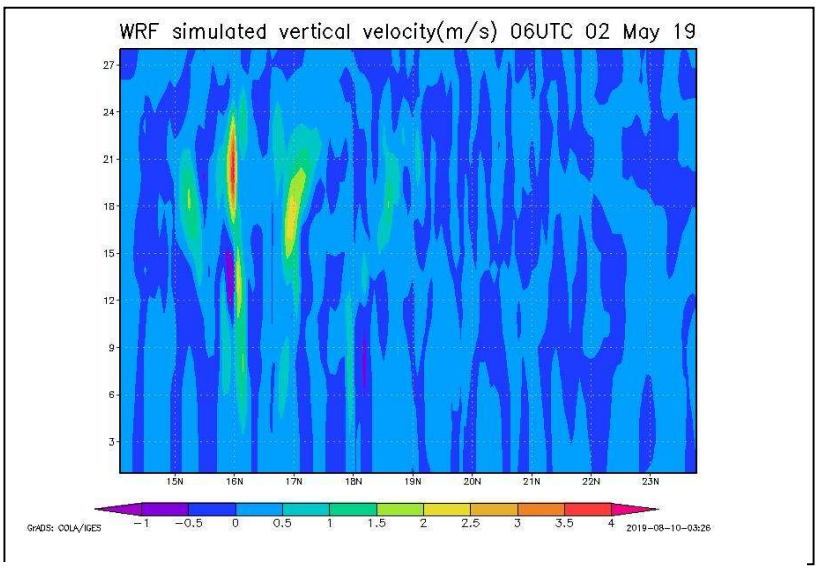


Fig.6.22: WRF simulated vertical cross section of vertical velocity (m/s) when the cyclone is in its peak intensity (06UTC 02May19)

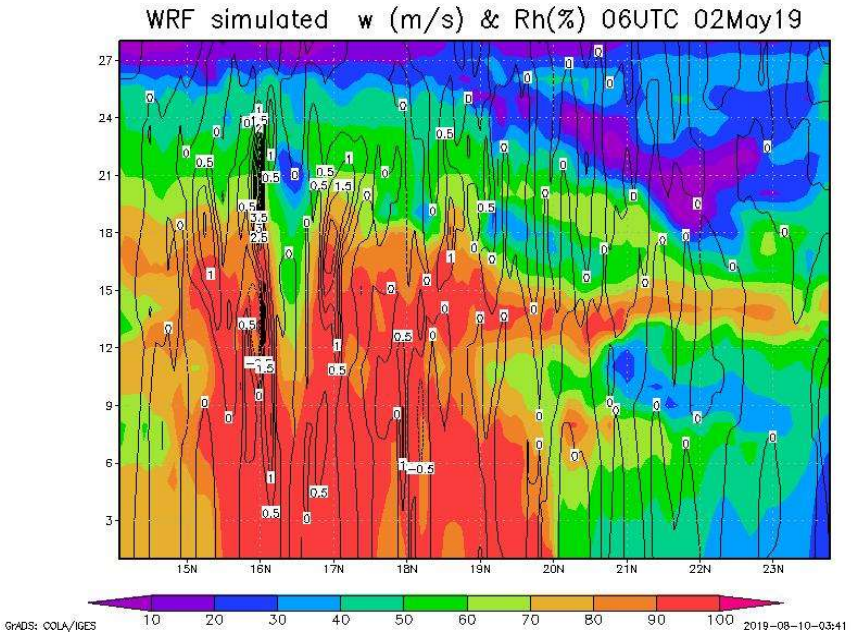


Fig.6.23: WRF simulated vertical cross section of vertical velocity (m/s) at 06UTC 02May19)

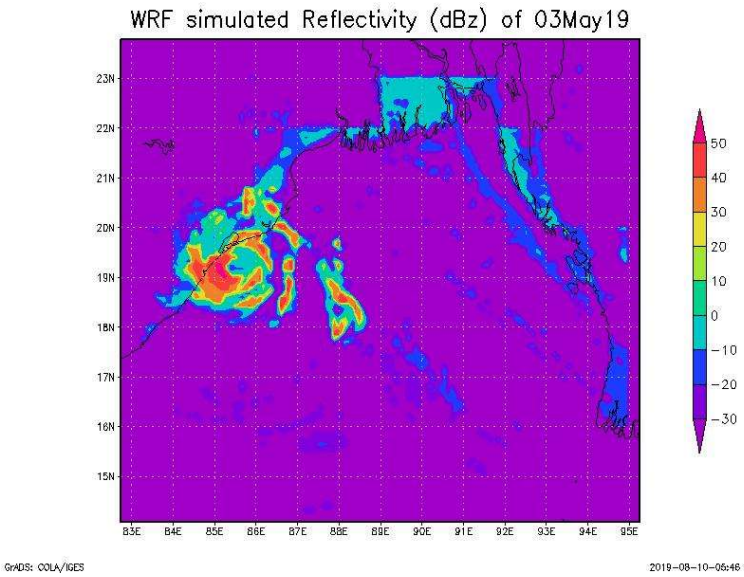


Fig.6.24: WRF simulated reflectivity when the cyclone is at 03UTC 03May19

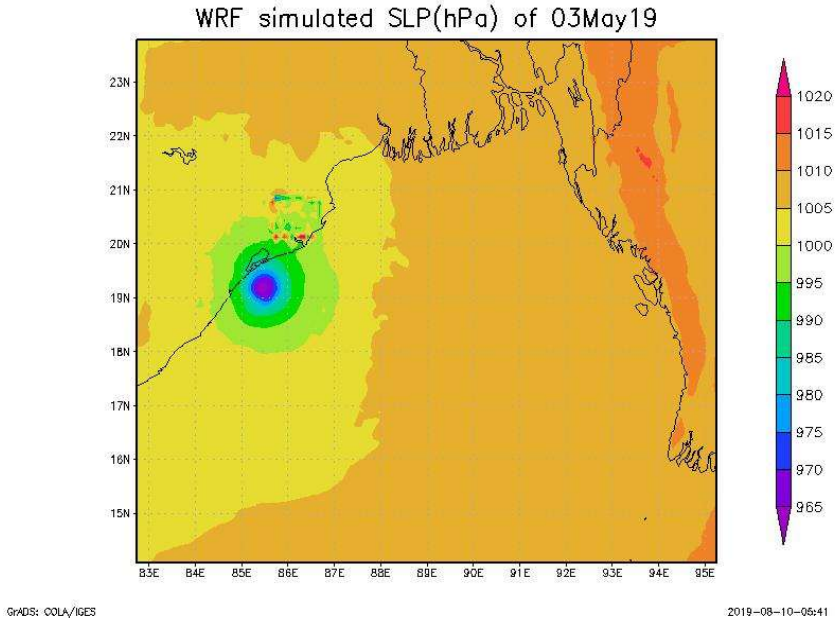


Fig.6.25: WRF simulated MSLP when the cyclone is at 03UTC 03May19

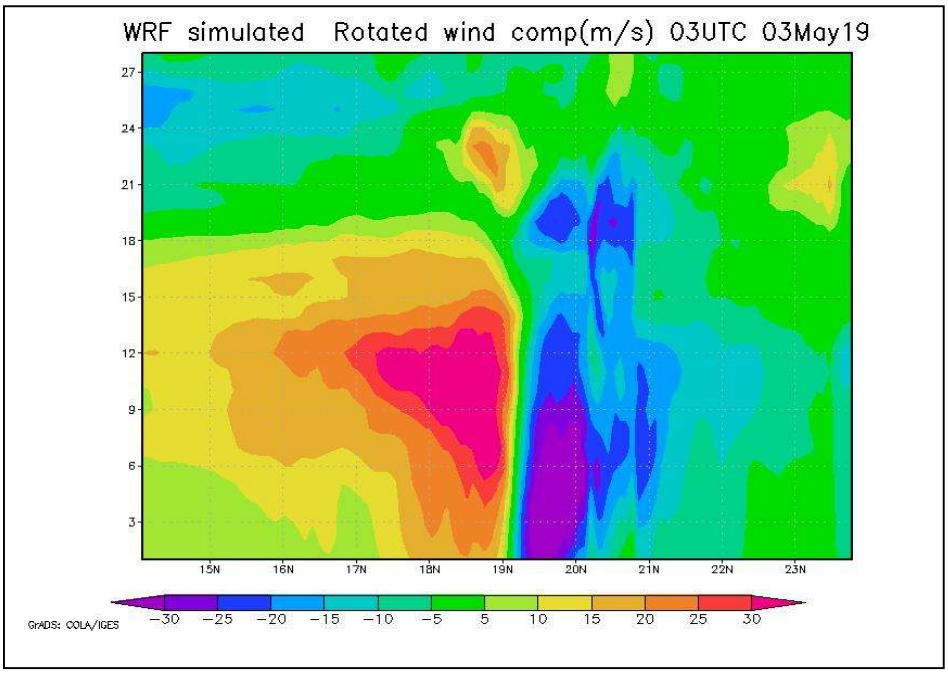


Fig.6.26 : The vertical cross section of rotational wind component at 03UTC of 03rd May when it hit Puri,Odisha.

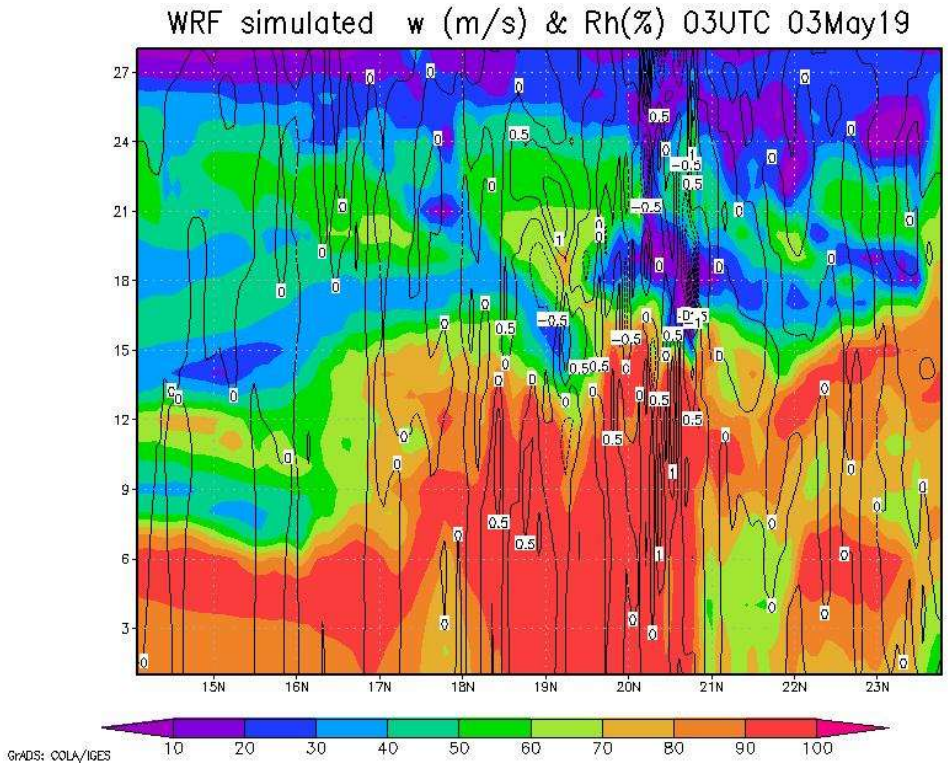


Fig.6.27: WRF simulated vertical cross section of vertical velocity (m/s) at 03 UTC 03May19

## 6.6 Summary and Conclusions

The numerical simulation of FANI has been carried out using WRF Model. The intensity, propagation and structure of FANI is studied using the model output parameters such as reflectivity, sea level pressure, wind speed and direction, rainfall etc. The model simulated output shows good agreement with the observations. The simulated output clearly shows the eyewall and spiral band structure as well as eye of the storm. The characteristics of FANI when it is at maximum intensity ie,,at 06 UTC of 02 May2019 are also studied. The landfall characteristics of FANI has been studied with a horizontal resolution of 1 km and a temporal resolution of 5 seconds. The study also discussed the characteristics of the atmosphere above the cyclone during its movement over the sea and towards the coast. The simulation could identify a highly active region in the troposphere vertically extending from 6 km – 12 km.

# Chapter 7
# Summary and Conclusions

The inherent nonlinearity in the dynamics and physics of convective systems as well as the smaller spatial and temporal scales of occurrence make their understanding and prediction a challenging task to atmospheric scientists even now. Hence, a better understanding of their underlying physics and dynamics are of utmost importance for the prediction of the phenomena. Numerical modelling is one of the most sophisticated techniques for a comprehensive study of most atmospheric phenomena.

The present investigation has been focused on the observational and high-resolution modelling studies of deep convective systems over the Indian region with the following objectives.

1. To understand the dynamics of deep convective systems over Indian region using the Weather Research and Forecast (WRF) Model.
2. To identify the most suitable combination of cumulus and microphysics parameterization schemes for the Indian region.
3. To identify the signatures/precursors in the atmosphere of severe weather events.
4. To study the structure and evolution of deep convective systems using the WRF Model

A comprehensive review of the scientific literature on deep convective systems is included in Chapter 1. The main objectives of the study and the structure of the thesis are discussed in this Chapter.

An overview of the WRF model is presented in Chapter 2. The governing equations, theoretical formulations of different parameterization schemes etc are discussed here. This chapter also discusses the details of all the observational data and the datasets used as the initial and lateral boundary conditions of the model.

Several experiments were designed with different combinations of cumulus and microphysics parameterization schemes with the objective of identifying the best suitable combination among them for the Indian region. The performance evaluation and sensitivity of the model for these simulation experiments are carried out to enable identification of the best suitable combination of parameterization schemes for the study region. The details of the experiments designed and the results are discussed in Chapter 3.

The study could identify the combination of Kain-Fritsch cumulus parameterization scheme and WSM 3-class simple ice microphysics scheme as the best suitable combination of schemes for the prediction of weather systems over the Indian region. After identifying the best combination of parameterization schemes, the model was run for different events over the Indian region: the results were validated with TRMM 3B42 daily precipitation data and AWS data. The model results are in good agreement with the observations. Again the model was run with a higher horizontal resolution of 5 km in order to check the predictability of the identified combination of parameterization schemes. Cyclone AILA which hit West Bengal on 06 UTC of 25$^{th}$ May 09 was selected for the model run. The model was initialized with 00UTC 22 May 2009 NCEP Global Forecast (GFS) data and integrated for 72 hours. The model-predicted wind and mean sea level pressure are in good agreement with the observations. The model could

predict the occurrence of Cyclone AILA three days ahead with very good accuracy

Numerical modelling studies of different convective systems were then carried out using the best suitable combination of cumulus and microphysics parameterization schemes. In order to understand the dynamics, structure and evolution of convective systems, a few events have been selected: most of these are different types of thunderstorms formed under different environmental conditions. They include

- A few thunderstorm events that occurred over Kerala which manifested as heavy rainfall.
- Supercell tornadic thunderstorm over Odisha embedded in a squall line
- Thunderstorms formed over peninsular Indian region in association with the northward propagation of trough in the low-level easterlies and its interaction with mid-level westerly trough which manifested as widespread unusual rainfall.
- An unusual heavy rainfall episode over peninsular Indian region triggered by a low pressure system over Arabian Sea and an associated cyclonic circulation over Lakshadweep-Comorin area.
- Cyclone AILA
- Extremely Severe Cyclonic Storm (ESCS) FANI

The observational and modelling study of the genesis, structure and evolution of a supercell thunderstorm over Odisha is presented in Chapter 4. The dynamical changes occurring in the atmosphere especially the troposphere prior and during the event is well simulated with a horizontal resolution of 1 km. The simulated output fields such as reflectivity, vertical

velocity, vorticity etc has been plotted for every 10 minutes interval: they clearly depict the spatial distribution and temporal evolution of clouds. The output parameters have been studied in order to understand the following aspects of the convective systems which include

i) The genesis and growth of convective cells

ii) The spatial distribution and vertical structure

iii) The characteristics of updrafts and downdrafts

iv) The direction of motion and speed of the movement of convective system

v) The life time of the convective system

The longitude-wise and latitude-wise vertical cross-section of reflectivity reveals the horizontal and vertical extent of the convective system. The reflectivity profile at different vertical levels gives the spatial distribution of cloud cover in each vertical level thereby providing an overall picture of the convective system.

The vertical vorticity plotted during the different stages of the storm brought out the two positive vorticity centres exceeding a vertical vorticity of 0.01 $s^{-1}$ which indicates the presence of a mesocyclone which is a unique characteristic of supercell thunderstorms. A double vortex is formed from 6.5 km to 12.5 km with its convective core at 11 km.

Numerical simulation of a supercell thunderstorm with high horizontal resolution exhibits the following interesting features such as huge single updraft (of the order of 30 m/s), double vortex circulation, mesocyclone formation, cell splitting and secondary cell formation. The study could identify a highly active layer of the troposphere extending from 6 – 12 km before the occurrence of the severe weather event. The study could reveal the co-existence of a very high positive vertical vorticity of 0.01 $s^{-1}$ and a negative vertical vorticity of the same magnitude in this layer one hour ahead

of the occurrence of the severe weather event. The study could also identify the presence of a very high vertical velocity of the order of 20-30 m/s in this vertical layer: high vertical velocity prevails in this layer for a longer period when compared with vorticity. Hence, a proper monitoring of the upper and mid tropospheric dynamics, especially vertical velocity and vorticity in this highly active layer of the troposphere (6–12 km) can contribute positively to the successful nowcasting of severe weather events.

The vertical as well as horizontal distribution of different parameters such as vorticity, vertical velocity and reflectivity clearly reveals the dynamical changes happening in the troposphere prior and during the event. This study clearly indicates that the simulation of a severe thunderstorm using WRF model with a horizontal resolution of 1 km can be utilised to understand the genesis, structure and evolution of severe weather events over the Indian region. However, modelling studies of more events over the region with very high horizontal resolution are required to generalize the structure and evolution of supercell storms.

Chapter 5 includes the simulation of two unusual heavy rainfall episodes over Peninsular Indian region in March 2008. The two heavy rainfall episodes during 12-14 March 2008 and 19-22 March 2008 have been simulated using WRF Model. The model could simulate both the events with good spatial and temporal accuracy. The model-predicted rainfall was compared with satellite based Automatic Weather Station (AWS) data and TRMM daily precipitation data.

The model-simulated wind during 12 -14 March 2008 has shown the presence of strong easterlies which resulted in the low-level moisture convergence from the Bay of Bengal. A detailed analysis of the model-predicted wind pattern at different vertical levels reveals many mesoscale features of the synoptic system. The association of mid-level westerly trough

with low-level easterly trough resulted in the development of embedded thunderstorm cells which manifested as widespread heavy rainfall activity. This simulation enabled us to study the dynamics and precipitation characteristics of embedded convective systems formed due to the interaction between low level convergence due to easterlies and mid-level westerlies. It also helped us to study the nature of the convective system triggered and developed due to the presence of a large-scale phenomenon such as low-level easterlies and middle and upper level westerlies.

The rainfall pattern has also shown that how a strong easterly wave could produce heavy rainfall at a large number of places with severe thunder activity. The rainfall activity which commenced over Tamil Nadu on 13$^{th}$ March 2008 moved to Kerala on 14$^{th}$ March 2008 due to the northward propagation of the trough in the low level easterlies and its interaction with mid level westerly trough.

The heavy rainfall episode during 19-22 March 2008 was also simulated using WRF model with good spatial and temporal accuracy. The model simulated plot was compared with TRMM 3B42 daily precipitation data and is in good agreement. This simulation enabled us to study many mesoscale circulation features associated with synoptic scale systems. The study has also shown how a deep persisting cyclonic circulation can influence the circulation pattern and weather. The low-pressure system formed over the Arabian Sea and an associated cyclonic circulation over Lakshadweep-Comorin area manifested as heavy rainfall over peninsular India. Both these events showed a very active region extending from 6 -12 km before their manifestation as heavy rainfall events.

The numerical simulation of FANI has been carried out and the details and results are presented in Chapter 6. The intensity, propagation and

structure of FANI has been studied using the model output parameters such as reflectivity, sea level pressure, wind speed and direction, rainfall etc. The model simulated output shows good agreement with the observations. The simulated output clearly shows the eyewall and spiral band structure as well as the eye of the storm.

The characteristics of FANI when it was at its maximum intensity at 06 UTC of 02 May 2019 have been also studied. The landfall characteristics of FANI has been studied with a horizontal resolution of 1 km and a temporal resolution of 5 seconds. The study also investigated the characteristics of the atmosphere above the cyclone during its movement over the sea and towards the coast. The simulation could identify the highly active region in the troposphere vertically extending from 6 – 12 km. However, simulations of more events are required to generalize the observations.

The major conclusions of the present study are:

- The combination of Kain-Fritsch cumulus scheme and WSM3 simple ice microphysics scheme is identified as the most suitable combination of parameterization schemes for different types of convective systems over Indian region

- The structural and dynamical changes occurring in the troposphere prior to and during the occurrence of convective systems are well studied with very high spatial and temporal resolution. The identification of a highly active region of the troposphere vertically extending from 6 – 12 km about one hour before the manifestation of the event could be used as a precursor of severe convective systems. The vorticity and vertical velocity of this layer shows very significant changes before the occurrence of the event and their magnitude

increases with severity. The vorticity and vertical velocity of this active region can be conceived as significant signatures of severe weather events. Hence, a proper monitoring of the upper and mid tropospheric dynamics could contribute to the successful nowcasting of severe weather events.

The outcomes of this study would be useful for a better understanding of deep convective systems over the Indian region for further research studies especially in the field of cloud microphysics. The results of this investigation could help the development of new parameterization schemes which could improve nowcasting of severe weather events.

# REFERENCES

Ali, H. and Mishra, V., 2018: Contributions of dynamic and thermodynamic scaling in subdaily precipitation extremes in India. *Geophysical Research Letters*, ***45***(5), 2352-2361.

Alvi, S.M.A. and Punjabi, K.G., 1966.: Diurnal and seasonal variations of squalls in India. *Indian J. Meteor. Geophys*, *17*, pp.207-216.

Beljaars, A.C.M., 1994: The parameterization of surface fluxes in large-scale models under free convection, *Quart. J. Roy. Meteor. Soc.*, **121**, 255–270.

Betts, A. K., 1986: A new convective adjustment scheme. Part I: Observational and theoretical basis. *Quart. J. Roy. Meteor. Soc.*, **112**, 677–691.

Betts, A. K., and M. J. Miller, 1986: A new convective adjustment scheme. Part II: Single column tests using GATE wave, BOMEX, and arctic air-mass data sets. *Quart. J. Roy. Meteor. Soc.*, **112**, 693–709.

Chen, S.-H., and W.-Y. Sun, 2002: A one-dimensional time dependent cloud model. *J. Meteor.Soc. Japan*, **80**, 99–118.

Chou M.-D., and M. J. Suarez, 1994: An efficient thermal infrared radiation parameterization for use in general circulation models. NASA Tech. Memo. 104606, 3, 85pp.

Collins, W.D. et al., 2004: Description of the NCAR Community Atmosphere Model (CAM 3.0), NCAR Technical Note, NCAR/TN-464+STR, 226pp.

Dudhia, J., 1989: Numerical study of convection observed during the winter monsoon experiment using a mesoscale two-dimensional model, *J. Atmos. Sci.*, **46**, 3077–3107.

Dudhia, J., S.-Y. Hong, and K.-S. Lim, 2008: A new method for representing mixed-phase particle fall speeds in bulk microphysics parameterizations. *J. Met. Soc. Japan*, *Ser. II*, ***86***, 33-44

Dyer, A. J., and B. B. Hicks, 1970: Flux-gradient relationships in the constant flux layer, *Quart. J. Roy. Meteor. Soc.*, **96**, 715–721.

Fels, S. B. and M. D. Schwarzkopf, 1975: The Simplified Exchange Approximation: A New Method for Radiative Transfer Calculations, *J. Atmos. Sci.*, **32**, 1475–1488.

Grell, G. A., and D. Devenyi, 2002: A generalized approach toparameterizing convection combining ensemble and data assimilation techniques. *Geophys. Res. Lett.*, **29(14)**, Article 1693.

Guhathakurta, P., Sreejith, O.P. and Menon, P.A., 2011. Impact of climate change on extreme rainfall events and flood risk in India. *Journal of earth system science*, *120*(3), p.359.

Gunwani, P. and Mohan, M., 2017. Sensitivity of WRF model estimates to various PBL parameterizations in different climatic zones over India. *Atmospheric research*, *194*, pp.43-65.

Gupta, H.N. and Chorghade, S.L., 1961. A statistical study of thunderstorm activity over Agartala airfield. *Indian J. Met. Geophys*, ***12***(1), 109-114

Haltiner, G. J., and R. T. Williams, 1980: *Numerical prediction and dynamic meteorology.* John Wiley & Sons, Inc., 477pp.

Hobbs.P.V.,1991: Research on clouds and precipitation :past,present and future,Part II. Bull.Amer.Meteor.Soc 72(2):184-191

Holtslag, A. A. M. and B. A. Boville, 1993: Local versus non-local boundary layer diffusion in a global climate model, *J. Climate*, **6**, 1825–1842.

Hong, S.-Y., 2007: Stable Boundary Layer Mixing in a Vertical Diffusion Scheme. The Korea Meteor. Soc., Fall conference, Seoul, Korea, Oct. 25-26.

Hong, S.-Y., and H.-L. Pan, 1996: Nonlocal boundary layer vertical diffusion in a medium-range forecast model, *Mon. Wea. Rev.*, **124**, 2322–2339.

Hong, S.-Y., and J.-O. J. Lim, 2006: The WRF Single-Moment 6-Class Microphysics Scheme (WSM6), *J. Korean Meteor. Soc.*, **42**, 129–151.

Hong, S.-Y., and Y. Noh, and J. Dudhia, 2006: A new vertical diffusion package with an explicit treatment of entrainment processes. *Mon. Wea. Rev.*, **134**, 2318–2341.

Hong, S.-Y., H.-M. H. Juang, and Q. Zhao, 1998: Implementation of prognostic cloud scheme for a regional spectral model, *Mon. Wea. Rev.*, **126**, 2621–2639.

Hong, S.-Y., J. Dudhia, and S.-H. Chen, 2004: A Revised Approach to Ice Microphysical Pro- cesses for the Bulk Parameterization of Clouds and Precipitation, *Mon. Wea. Rev.*, **132**, 103–120.

Hong, S.Y., Lim, K.S.S., Lee, Y.H., Ha, J.C., Kim, H.W., Ham, S.J. and Dudhia, J., 2010. Evaluation of the WRF double-moment 6-class microphysics scheme for precipitating convection. *Advances in Meteorology*, *2010*.

Huang, X.-Y. and P. Lynch, 1993: Diabatic Digital-Filtering Initialization: Application to the HIRLAM Model., *Mon. Wea. Rev.*, **121**, 589–603.

Janjic, Z. I., 1990: The step-mountain coordinate: physical package, *Mon. Wea. Rev.*, **118**, 1429–1443.

Janjic, Z. I., 1994: The step-mountain eta coordinate model: further developments of the con- vection, viscous sublayer and turbulence closure schemes, *Mon. Wea. Rev.*, **122**, 927–945.

Janjic, Z. I., 1996: The surface layer in the NCEP Eta Model, *Eleventh Conference on Numerical Weather Prediction*, Norfolk, VA, 19–23 August; Amer. Meteor. Soc., Boston, MA, 354–355.

Janjic, Z. I., 2000: Comments on "Development and Evaluation of a Convection Scheme for Use in Climate Models", *J. Atmos. Sci.*, **57**, p. 3686.

Janjic, Z. I., 2002: Nonsingular Implementation of the Mellor–Yamada Level 2.5 Scheme in the NCEP Meso model, *NCEP Office Note*, **No. 437**, 61 pp.

Kain, J. S., 2004: The Kain-Fritsch convective parameterization: An update. *J. Appl. Meteor.*,**43**, 170–181.

Kain, J. S., and J. M. Fritsch, 1990: A one-dimensional entraining/ detraining plume model and its application in convective parameterization, *J. Atmos. Sci.*, **47**, 2784–2802.

Kain, J. S., and J. M. Fritsch, 1993: Convective parameterization for mesoscale models: The Kain-Fritcsh scheme, *The representation of*

*cumulus convection in numerical models*, K. A. Emanuel and D.J. Raymond, Eds., Amer. Meteor. Soc., 246

Kar, I. and Bondhyopadhyay, R., 1998. A climatological study of pre-monsoon thunderstorm over Sriniketan, Alipore and Kalaikunda. *Mausam*, *49*, 262-263.

Kessler, E., 1969: On the distribution and continuity of water substance in atmospheric circu- lation, *Meteor. Monogr.*, **32**, Amer. Meteor. Soc., 84

Klemp, J. B., and R. Wilhelmson, 1978: The simulation of three-dimensional convective storm dynamics, *J. Atmos. Sci.*, **35**, 1070–1096.

Krishnamurthy, V., 1965. A statistical study of thunderstorms over Poona. *Indian J. Meteorol. Geophys*, *16*, 484.

Kumar, A., 1992. A climatological study of thunderstorms at Lucknow airport. *Mausam*, *43*(4), pp.441-444.

Lacis, A. A., and J. E. Hansen, 1974: A parameterization for the absorption of solar radiation in the earth's atmosphere. *J. Atmos. Sci.*, **31**, 118–133.

Laprise R., 1992: The Euler Equations of motion with hydrostatic pressure as as independent variable, *Mon. Wea. Rev.*, **120**, 197–207.

Lin, Y.-L., R. D. Farley, and H. D. Orville, 1983: Bulk parameterization of the snow field in a cloud model. *J. Climate Appl. Meteor.*, **22**, 1065–1092.

Lynch, P., and X.-Y. Huang, 1994: Diabatic initialization using recursive filters. *Tellus*, **46A**, 583–597.

Madala, S., Satyanarayana, A.N.V. and Rao, T.N., 2014: Performance evaluation of PBL and cumulus parameterization schemes of WRF ARW model in simulating severe thunderstorm events over Gadanki MST radar facility—case study. *Atmospheric research*, **139**, 1-17.

Martin,D. W.,and O Karst,1969: A census of cloud systems over the tropical Pacific.Studies in Atmospheric energetics based on Aerospace probings, Ann.Report 1968,Space Science and Engineering Center, University of Wisconsin

Martin. D and V.E Suomi,1972: A satellite study of cloud clusters over the tropical North Atlantic Ocean. Bull.Amer.Meteor.Soc. **53**, 135-156

McCumber, M., W.-K. Tao, J. Simpson, R. Penc, and S.-T. Soong, 1991: Comparison of ice- phase microphysical parameterization schemes using numerical simulations of tropical con- vection, *J. Appl. Meteor.*, **30**, 985–1004.

Mellor, G. L., and T. Yamada, 1982: Development of a turbulence closure model for geophysical fluid problems. *Rev. Geophys. Space Phys.*, **20**, 851–875.

Milly, P.C.D., Wetherald, R.T., Dunne, K.A. and Delworth, T.L., 2002. Increasing risk of great floods in a changing climate. *Nature*, *415*(6871), 514.

Mlawer, E. J., S. J. Taubman, P. D. Brown, M. J. Iacono, and S. A. Clough, 1997: Radiative transfer for inhomogeneous atmosphere: RRTM, a validated correlated-k model for the long- wave. *J. Geophys. Res.*, **102** (D14), 16663–16682.

Mohan, M. and Bhati, S., 2011: Analysis of WRF model performance over subtropical region of Delhi, India. *Advances in Meteorology*, ***2011***

Moid, S.A., 1996. A climatological study of thunderstorms at Mohanbari Airport. *Mausam*, **47**, pp.200-204.

Monin, A.S. and A.M. Obukhov, 1954: Basic laws of turbulent mixing in the surface layer of the atmosphere. *Contrib. Geophys. Inst. Acad. Sci.*, USSR, **(151)**, 163–187 (in Russian).

Morrison, H., and J. O. Pinto, 2006: Intercomparison of bulk microphysics schemes in mesoscale simulations of springtime Arctic mixed-phase stratiform clouds. *Mon. Wea. Rev.*, **134**, 1880– 1900.

Morrison, H., G. Thompson, and V. Tatarskii, 2008: Impact of cloud micrpohysics on the development of trailing stratiform precipitation in a simulated squall line: Comparison of one- and two-moment schemes. *Mon. Wea. Rev. 137(3),991-1007*.

Morrison, H., J. A. Curry, and V. I. Khvorostyanov, 2005: A new double-moment microphysics parameterization for application in cloud and climate models, Part I: Description. *J. Atmos. Sci.*, **62**, 1665–1677.

Mukherjee, A.K., Sen, P.N. and Chakrabarty, K.K., 1983. Dependence of diurnal variation of thunderstorm on physical features. *Vayu Mandal*, **13**, 105.

Mukhopadhyay, P., Sanjay, J. and Singh, S.S., 2003. Objective forecast of thundery/nonthundery days using conventional indices over three northeast Indian stations. *Mausam*, **54**(4), 867-880.

Noh, Y., W.G. Cheon, S.-Y. Hong, and S. Raasch, 2003: Improvement of the K-profile model for the planetary boundary layer based on large eddy simulation data. *Bound.-Layer Meteor.*, **107**, 401–427.

Noilhan, J., and S. Planton, 1989: A simple parameterization of land surface processes for meteorological models. *Mon. Wea. Rev.*, **117**, 536–549.

Ooyama K. V., 1990: A thermodynamic foundation for modeling the moist atmosphere, *J. Atmos. Sci.*, **47**, 2580–2593.

Orlanski.I.,1975 A rational subdivision of scales for atmospheric processes. Bull.Amer.Meteor.Soc 56: 527-530

Paulson, C. A., 1970: The mathematical representation of wind speed and temperature profiles in the unstable atmospheric surface layer. *J. Appl. Meteor.*, **9**, 857–861.

Pleim, J. E. and A. Xiu, 1995: Development and testing of a surface flux and planetary boundary layer model for application in mesoscale models. *J. Appl. Meteor.*, **34**, 16–32.

Pleim, J. E., 2006: A simple, efficient solution of flux-profile relationships in the atmospheric surface layer, *J. Appl. Meteor. and Clim.*, **45**, 341–347

Pleim, J. E., and A. Xiu, 2003: Development of a land surface model. Part II: Data Assimilation. *J. Appl. Meteor.*, **42**, 1811–1822.

Pleim, J.E. and R.C. Gilliam, 2008: An indirect data assimilation scheme for deep soil temper- ature in the Pleim-Xiu land surface model. Submitted to *J. Appl. Meteor. Climatol.* ***48***(7),1362-1376.

Rajeevan, M., Kesarkar, A., Thampi, S. B., Rao, T. N., Radhakrishna, B. and Rajasekhar, M., 2010: Sensitivity of WRF cloud microphysics to simulations of a severe thunderstorm event over Southeast India. *Annales Geophysicae* 28( 2), 603-619.

Raman, P. K. and Raghavan, K., 1961. Diurnal variation of thunderstorm in India during different seasons. Indian J. Met. & Geophys., **12**, 1, 115

Rao, K.N. and Raman, P.K., 1961. Frequency of days of thunder in India.

*Indian J. Meteorol. Geophys*, **12**, 103-108.

Riehl, H. and Malkus, J., 1961. Some aspects of hurricane Daisy, 1958. *Tellus*, ***13***(2), 181-213.

Roberts, R. E., J. E. A. Selby, and L. M. Biberman, 1976: Infrared continuum absorption by atmospheric water-vapor in 8–12 um window. *Applied Optics*, **15 (9)**, 2085–2090.

Rodgers, C. D., 1968: Some extensions and applications of the new random model for molecular band transmission. *Quart. J. Roy. Meteor. Soc.*, **94**, 99–102.

Rutledge, S. A., and P. V. Hobbs, 1984: The mesoscale and microscale structure and organization of clouds and precipitation in midlatitude cyclones. XII: A diagnostic modeling study of precipitation development in narrow cloud-frontal rainbands. *J. Atmos. Sci.*, **20**, 2949–2972.

Ryan, B. F., 1996: On the global variation of precipitating layer clouds. *Bull. Amer. Meteor.Soc.*, **77**, 53–70.

Santosh, K., Sarasakumari, R., Gangadharan, V. K. and Sashidharan, N. V., 2001: Some climatological features of thunderstorm at Thiruvananthapuram, Kochi and Kozhikode, Mausam,52, 2,357-364

Sasamori, T., J. London, and D. V. Hoyt, 1972: Radiation budget of the Southern Hemisphere. *Meteor. Monogr.*, **13**, No. 35, 9–23.

Schwarzkopf, M. D., and S. B. Fels, 1985: Improvements to the algorithm for computing CO2 transmissivities and cooling rates. *J. Geophys. Res.*, **90** (ND6), 541–550.

Schwarzkopf, M. D., and S. B. Fels, 1991: The simplified exchange method revisited-An accurate, rapid method for computation of infrared cooling rates and fluxes. *J. Geophys. Res.*, **96** (D5), 9075–9096.

Singh, C., Mohapatra, M., Bandyopadhyay, B.K. and Tyagi, A., 2011. Thunderstorm climatology over northeast and adjoining east India. *Mausam*, *62*(2), 163-170

Skamarock W. C. and J. B. Klemp, 1992: The Stability of Time-Split Numerical Methods for the Hydrostatic and the Nonhydrostatic Elastic Equations, *Mon. Wea. Rev.*: **120**, 2109–2127.

Skamarock W. C. and M. L. Weisman, 2009: The impact of positive-definite moisture transport on NWP precipitation forecasts, *Mon. Wea. Rev.* **137**(1), .488-494.

Skamarock, W.C., Klemp, J.B., Dudhia, J., Gill, D.O., Barker, D.M., Wang, W. and Powers, J.G., 2008. A description of the Advanced Research WRF version 3. NCAR Technical note-475+ STR.

Smirnova, T. G., J. M. Brown, and S. G. Benjamin, 1997: Performance of different soil model configurations in simulating ground surface temperature and surface fluxes. *Mon. Wea. Rev.*, **125**, 1870–1884.

Smirnova, T. G., J. M. Brown, S. G. Benjamin, and D. Kim, 2000: Parameterization of cold- season processes in the MAPS land-surface scheme. *J. Geophys. Res.*, **105** (D3), 4077–4086.

Soni, M., Payra, S., Sinha, P and Verma, S, 2014: A performance evaluation of WRF model using different physical parameterization scheme during winter season over a semi-arid region, India. *International Journal of Earth and Atmospheric Science*, ***1*(3)**, 104-114.

Stephens, G. L., 1978: Radiation profiles in extended water clouds. Part II: Parameterization schemes, *J. Atmos. Sci.*, **35**, 2123–2132.

Tao, W.-K., and J. Simpson, 1993: The Goddard cumulus ensemble model. Part I: Model description. *Terr. Atmos. Oceanic Sci.*, **4**, 35–72.

Tao, W.-K., J. Simpson, and M. McCumber 1989: An ice-water saturation adjustment, *Mon. Wea. Rev.*, **117**, 231–235.

Thompson, G., R. M. Rasmussen, and K. Manning, 2004: Explicit forecasts of winter precipita- tion using an improved bulk microphysics scheme. Part I: Description and sensitivity analysis. *Mon. Wea. Rev.*, **132**, 519–542.

Tyagi, A., 2007. Thunderstorm climatology over Indian region. *Mausam*, **58**(2), 189.

Tyagi, A., Sikka, D.R., Goyal, S. and Bhowmick, M., 2012. A satellite based study of pre-monsoon thunderstorms (Nor'westers) over eastern India and their organization into mesoscale convective complexes. *Mausam*, **63**(1), 29-54.

Vishwanathan, T.R. and Faria, J.F., 1962. A climatological study of thunderstorms at Bombay airport. *Indian J. Met. Geophys*, **13**(3), pp.377-383.

Webb, E. K., 1970: Profile relationships: The log-linear range, and extension to strong stability, *Quart. J. Roy. Meteor. Soc.*, **96**, 67–90

Wicker, L. J. and W. C. Skamarock, 2002: Time splitting methods for elastic models using forward time schemes, *Mon. Wea. Rev.*, **130**, 2088–2097. Thompson, G., R. M. Rasmussen, and K. Manning, 2004: Explicit forecasts of winter precipita- tion using an improved bulk microphysics scheme. Part I: Description and sensitivity analysis. *Mon. Wea. Rev.*, **132**, 519–542.

World Meteorological Organization. Secretariat, 1956. World Distribution of Thunderstorm Days: Tables of marine data and world maps (No. 21). World Meteorological Organization.

Xiu, A. and J. E. Pleim, 2001: Development of a land surface model part I: Application in a mesoscale meteorology model. *J. Appl. Meteor.*, **40**, 192–209

Zilitinkevich, S. S., 1995: Non-local turbulent transport: pollution dispersion aspects of coher- ent structure of convective flows, *Air Pollution III* — Volume I. Air Pollution Theory and Simulation, Eds. H. Power, N. Moussiopoulos and C.A. Brebbia. Computational Mechanics Publications, Southampton Boston, 53–60.